

Diss. ETH No. 24652

Development of a new technology to generate low-calorie food systems with dispersed solid, fluid and gas fractions and tailored properties

A dissertation submitted to attain the degree of

DOCTOR OF SCIENCES of ETH ZURICH

(Dr. sc. ETH Zürich)

presented by

Pascal Jonas Guillet

MSc Food Science ETH Zurich

born 30th July 1986

citizen of Switzerland

accepted on the recommendation of

Prof. Dr. Erich J. Windhab, Examiner

Prof. Dr. Alejandro G. Marangoni, Co-Examiner

Dr. Heiko Spitzbarth, Co-Examiner

2017

Copyright © 2017 Pascal Jonas Guillet
Laboratory of Food Process Engineering (ETH Zurich)
All rights reserved.

**Development of a new technology to generate low-calorie food systems
with dispersed solid, fluid and gas fractions and tailored properties**

ISBN: 978-3-905609-78-3

Food Process Engineering series no. 70

Published and distributed by:

Laboratory of Food Process Engineering
Institute of Food, Nutrition and Health
ETH Zurich
ETH Zentrum, LFO
8092 Zurich
Switzerland
<http://www.fpe.ethz.ch/>

Printed in Switzerland by:

ETH Reprintzentrale Hönggerberg
HIL C45
8093 Zurich
Switzerland

Shut up, legs!

Acknowledgements

An erster Stelle Prof. Dr.-Ing. Erich J. Windhab für sein Vertrauen in mich, zunächst während meiner Masterarbeit und dann vor Allem während der gesamten Dauer meines Doktorats danken. Durch seine vielen Ideen und seiner ganzheitlichen, visionären Betrachtungsweise schaffte er es oft, meinen von Zeit zu Zeit durch die vielen Bäume im Wald etwas eingeschränkten Horizont zu erweitern. Zudem waren die vielen wissenschaftlichen Inputs essenziell für das Gelingen meiner Doktorarbeit. Zudem habe ich auch die gewährten Freiräume sehr geschätzt - diese ermöglichten eine sehr selbständige Arbeitsweise und dadurch verbunden auch die, speziell in der Forschung, sehr wichtige Entstehung neuartiger, innovativer Ideen.

Desweiteren möchte ich Prof. Alejandro G. Marangoni für die Ko-Exmamination meiner Arbeit danken. Als einer der weltweit führenden Spezialisten auf dem Gebiet der (Lebensmittel-)Fette ist er für mich die ideale Person, meine Arbeit objektiv und kritisch zu Beurteilen.

Ein grosser Dank für die Übernahme der Ko-Examination geht desweiteren an Dr. Heiko Spitzbarth. Danke, dass du im Rahmen deiner Doktorarbeit in der Gruppe für Lebensmittelverfahrenstechnik als mein direkter Vorgänger solide Grundlagen geschaffen hast, welche essentiell für das Gelingen meines Projektes waren. Natürlich war es auch immer sehr fördernd, mit dir in regelmässigen Meetings den Verlauf des Projektes zu besprechen; deine Tipps haben mir auf meinem Weg immer sehr geholfen.

Während meinem Doktorat, welchem ein Projekt in Kollaboration mit der Industrie zugrunde liegt, konnte ich zudem immer auf zuverlässige Mithilfe und Ideen von Seiten meiner Industriepartner zählen - die Zusammenarbeit hat mir (meist :) Spass gemacht. Allen voran möchte ich mich bei Dirk Zwanzig (MIFA AG) und Dr. Heiko Spitzbarth (MIFA AG) für ihr stets konstruktiven aber oft auch kritischen Inputs aus der angewandteren Sichtweise der Industrie danken. Desweiteren waren die flinken Hände und das grosse Können und Wissen des Bäckermeisters Peter Guckenberger (MIFA AG) essentiell bei der Umsetzung der angewandten Backversuche im Rahmen dieser Arbeit. Desweiteren stand mir René Baumann (Florin AG) immer zur Seite und hat mich durch sein Wissen im Bereich der Fette unterstützt und die Rohstoffversorgung gesichert.

Acknowledgements

Zudem wäre die Umsetzung dieser Arbeit unmöglich gewesen ohne die tatkräftige Unterstützung unserer Techniker. Peter Bigler war Zentral beim Aufbau des Sprühprozesses - bei dieser Gelegenheit möchte ich mich auch für das omniprésente Fett im ganzen Pilot Plant während der letzten vier Jahre entschuldigen; Fett ist nun halt nicht ganz einfach zu Reinigen... Desweiteren möchte ich mich bei Daniel Kiechl, Bruno Pfister und Jan Corsano für die versierte Unterstützung bei konstruktiven und elektrischen Problemen und Fragen sowie bei Dr. Bernhard Koller fürs lösen allgegenwärtiger IT Probleme bedanken.

Natürlich hätte die Umsetzung dieser Arbeit ohne die tatkräftige Unterstützung meiner Studentinnen und Studenten etwa doppelt so lange gedauert. Vielen Dank an Silvana Bachmann, Lilian Fehlmann, Lucas Grob, Alessandra Kessler, Isabelle Koch und Lukas Schlumpf für die Zusammenarbeit, die Inputs und die (manchmal :)) lustigen Stunden und Tage am Sprühturm.

Dass ich im Laufe meiner Masterarbeit am Labor für Lebensmittelverfahrenstechnik ein Doktorat in ebendieser Gruppe in Betracht gezogen habe, verdanke ich neben meinem grossen Interesse an der Forschung vor allem der guten Atmosphäre dieser Gruppe. Auch während den dunkelsten Stunden der letzten vier Jahre, konnte ich mich immer rege (fachlich sowie auch persönlich) mit meinen Kollegen austauschen. Allen voran möchte ich bei Lea, Lucie, Stefan, Nati, Judith, Lucas, Bertsch, Socrates und Gene für fachlichen Diskussionen, aber vor allem auch an die vielen unvergesslichen Momente an der ETH, am Oktoberfest, in Krakau oder in der Science Week danken. Ihr seid nicht mehr "nur" Kollegen, sondern gute Freunde fürs Leben.

Zu guter Letzt möchte ich mich bei meiner Familie für die Schaffung eines geeigneten Nährbodens für 10 Jahre an der ETH danken. Ohne eure Geduld im Studium und vor allem während dem Doktorat wäre mir manche Entscheidung in den letzten Jahren viel schwerer gefallen.

Zürich, September 2017

Contents

Acknowledgements	v
Notation	xi
Summary	xvii
Zusammenfassung	xix
1. Introduction	1
2. Background	3
2.1. Crystallization	3
2.1.1. Polymorphism	5
2.2. Emulsions	7
2.2.1. Rotor-stator emulsification	7
2.2.2. Rotating membrane emulsification	8
2.2.3. Emulsifiers	10
2.2.4. Emulsion stability & destabilization	11
2.3. Conventional fat systems	12
2.3.1. Microstructure of conventional fat systems	14
2.4. Powder fat systems	15
2.4.1. Spray chilling	15
2.4.2. Microstructure of powder fat systems	18
2.5. Laminated dough systems	20
2.5.1. Lamination	20
2.5.2. Leavening	21
2.5.3. Limitations	21
2.5.4. Impact of the novel powder fat system	22
2.6. Bulk and confinement rheology	22
2.6.1. Bulk rheology	22
2.6.2. Confinement rheology	24
2.7. Thermogelation of methylcellulose	24

3. Materials, Processes and Methods	27
3.1. Materials	27
3.1.1. Vegetable Fat Fractions	27
3.1.2. Emulsifiers	28
3.1.3. Thickening Agents	28
3.2. Processes	28
3.2.1. Emulsification	28
3.2.2. Spray Chilling	30
3.3. Methods	31
3.3.1. Differential Scanning Calorimetry	31
3.3.2. Thermo Gravimetric Analysis	31
3.3.3. X-Ray Crystallography	32
3.3.4. Laser Particle Size Analysis	33
3.3.5. Confocal Laser Scanning Microscopy (CLSM)	33
3.3.6. Cryo Scanning Electron Microscopy	34
3.3.7. Karl-Fischer Titration	35
3.3.8. Sinterface PAT-1 Tensiometer	35
4. Short-term Emulsion Stability	37
4.1. Method	37
4.1.1. Sampling	37
4.1.2. Image acquisition and analysis	39
4.2. Results	41
4.2.1. Identifying suitable emulsifiers	41
4.2.2. Microscopic observation of jammed emulsions	42
4.2.3. Short-term emulsion stability	43
4.2.4. Interfacial Tension	45
4.2.5. Rheology	47
4.3. Conclusions	47
5. Simultaneous Spray-Chilling	51
5.1. Designing the process: Three-Stage solidification model	51
5.1.1. Solidification model assumptions	53
5.1.2. Stage I	53
5.1.3. Stage II	54
5.1.4. Stage III	55
5.1.5. Adaptation of the model: Non constant droplet-gas velocity v_r	55
5.2. Application to simultaneous spray-chilling	56
5.3. Spray particle size	57
5.4. Mass Conservation	59
5.5. Particle Morphology	59
5.6. Polymorphism	60

5.7. Conclusions	60
6. Rheology	63
6.1. Materials	64
6.2. Methods	64
6.2.1. Bulk rheology	64
6.2.2. Micro rheology	65
6.3. Bulk rheology and melting properties of powdered fat	69
6.4. The influence of particle size on the rheological properties	70
6.5. The influence of different fat melting properties on rheology	72
6.6. Emulsion based fat particles: The impact of increased intra-particle disperse water mass fractions Φ_E	73
6.7. Emulsion based fat particles: The impact of temperature	76
6.8. Significance for Puff Pastry Dough Systems	79
6.9. Conclusions	79
7. Mimicking the Baking Process	81
7.1. Materials and methods	82
7.1.1. Thermogelling agents	82
7.1.2. Baking	83
7.1.3. Differential Scanning Calorimetry (DSC) and Thermogravimetry Analysis (TGA)	83
7.2. Contribution of water contained in dough and fat towards total lift force	84
7.3. Thermal stability of emulsion based systems	85
7.4. Evaporation kinetics of emulsion based systems	86
7.5. Modulating the evaporation of water during baking	87
7.5.1. The impact of the methyl cellulose concentration	90
7.5.2. The evaporation kinetics of HPMC based systems	90
7.5.3. The evaporation kinetics of MC based systems	91
7.5.4. The impact on low temperature gelling agents (sodium alginate)	93
7.6. Significance for Puff Pastry Dough Systems	93
7.7. Conclusions	94
8. Application of powdered fat systems in laminated dough	97
8.1. Materials and Methods	97
8.1.1. Dough	97
8.1.2. Conventional puff pastry fat	98
8.1.3. Preparation of the puff pastry dough samples	99
8.1.4. Analysis of puff pastry dough structure by CLSM	100
8.1.5. Volume measurement of the baked puff pastries by 3D scanning	102
8.2. The micro- and macrostructure of conventional puff pastry products .	102

8.3. The micro- and macrostructure of puff pastry products produced with powder fat at different powder in oil disperse ratios Φ_P	104
8.4. Impact of the powder fat particle size and layering	106
8.5. The influence of an increased number of layers	109
8.6. The impact of elevated water contents	110
8.7. Influencing the consistency and baking volume of puff pastry dough with $m_{w,tot} \geq 40\%$	112
8.8. The influence of thickening agents	113
8.9. Conclusions	115
9. Concluding remarks and outlook	117
Bibliography	119
Appendix	127
A. First appendix: Short-term emulsion stability	129
B. Second appendix: Simultaneous Spray-Chilling	131
C. Third appendix: Rheology	133

Notation

Latin Letters

Symbol	Unit	Meaning
A	m^2	projected droplet area
C_{gamma}	$\frac{J}{K}$	semisolid droplet heat capacity
C_l	$\frac{J}{K}$	droplet liquid heat capacity
C_p	$\frac{J}{K}$	heat capacity
C_s	$\frac{J}{K}$	solid droplet heat capacity
c_w	$[-]$	droplet drag coefficient
d_N	m	nozzle diameter
d_p	m	crystal plane distance according to Bragg's law
d_{pore}	m	pore size (diameter)
d_s	μm	shear gap
$D_{50,3}$	μm	average mean droplet diameter
F_B	N	buoyancy force
F_D	N	drag force
F_I	N	inertia force
F_L	N	dynamic lift force
F_σ	N	interfacial tension force
F_{SP}	N	static pressure difference force
G	$Pa \cdot m$	elastic modulus
G^*	$Pa \cdot m$	dynamic complex shear modulus
G'	$Pa \cdot m$	storage modulus
G''	$Pa \cdot m$	loss modulus
H_{min}	m	minimal shear gap SSHE
h_i	m	injection height of the second fat phase (B) into the spraying tower
h_0	$[-]$	heat transfer coefficient
k	$[-]$	Herschel-Bulkley consistency factor
K_d	$\frac{W}{K \cdot m}$	droplet heat conductivity
K_g	$\frac{W}{K \cdot m}$	ambient gas heat conductivity

continued on next page

Notation

Symbol (cont.)	Unit (cont.)	Meaning (cont.)
L_c	$[-]$	characteristic length used for calculation of the Biot number
L_f	$\frac{kJ}{kg}$	latent heat of crystallization
n	$[-]$	integer n linked to the order of reflection (Bragg's law)
n_H	$[-]$	Herschel-Bulkley flow index
p_k	Pa	capillary pressure
q_h	$\frac{W}{m^2}$	heat flux
R	μm	emulsion droplet radius
r_{crit}	m	critical nucleus radius of crystallization
r_n	m	nucleus radius
R_i	m	radius of the rotating SSHE barrel
R_0	m	radius of the chilled SSHE jacket
S	m^2	nucleus surface
S_d	m^2	droplet surface
T_d	$^{\circ}C$	droplet temperature
$T_{drip.,stearin}$	$^{\circ}C$	dripping point of stearin
$T_{drip.,super-stearin}$	$^{\circ}C$	dripping point of super-stearin
$T_{drip.,mid-fraction}$	$^{\circ}C$	dripping point of palm mid-fraction
T_f	$^{\circ}C$	freezing temperature
T_g	$^{\circ}C$	ambient gas temperature
T_m	$^{\circ}C$	melt temperature
V	m^3	nucleus volume
V_d	m^3	droplet volume
V_f	m^3	frozen droplet volume
v_r	$\frac{m}{s}$	relative droplet ambient gas velocity
V_m	m^3	molar crystal cluster volume
v_{∞}	$\frac{m}{s}$	maximum droplet-gas velocity
v_0	$\frac{m}{s}$	initial droplet-gas velocity at nozzle
W_{min}	J	minimum energy for surface generation
W_c	J	total confinement work
$W_{total,forcepeaks}$	J	total confinement work
$x_{50,3}$	μm	mean particle diameter

Greek Letters

Symbol	Unit	Meaning
γ	$N \cdot m^{-1}$	surface tension
γ_{freeze}	[—]	freezing process variable
γ_L	$N \cdot m^{-1}$	liquid surface tension
γ_0	%	oscillatory shear rheometry amplitude
$\dot{\gamma}$	s^{-1}	shear rate
$\dot{\gamma}_i$	s^{-1}	shear rate at the rotating SSHE shaft surface
δ	[—]	oscillatory rheometry phase shift
ΔA	m^2	interfacial area generated
ΔG	J	Gibbs free energy
ΔG_{crit}	J	critical Gibbs free energy of nucleation
ΔG_f	J	Gibbs free energy of fusion
ΔG_S	J	Gibbs free energy of surface formation
ΔH	J	free enthalpy
ΔH_m	J	free melting enthalpy
ΔT	$^{\circ}C$	degree of supercooling
η	$Pa \cdot s$	viscosity
η_B	$Pa \cdot s$	SCR viscosity
η_c	$Pa \cdot s$	continuous phase viscosity
η_d	$Pa \cdot s$	disperse phase viscosity
$\eta_e(\dot{\gamma})$	$Pa \cdot s$	viscosity at applied shear rates $\dot{\gamma}$
η_g	$Pa \cdot s$	ambient gas viscosity
η_L	$Pa \cdot s$	liquid viscosity
η^*	$Pa \cdot s$	complex viscosity
θ	$^{\circ}$	x-ray incident angle during XRD measurements
$\theta_{D_{50,3}}$	[—]	standard deviation of $D_{50,3}$
λ	[—]	viscosity ratio of disperse (η_d) and continuous (η_c) phase
λ_w	nm	x-ray beam wavelength for XRD measurements
ρ_c	$\frac{kg}{m^3}$	continuous phase density
ρ_d	$\frac{kg}{m^3}$	droplet density
ρ_F	$\frac{kg}{m^3}$	fluid density
ρ_g	$\frac{kg}{m^3}$	ambient gas density
σ	$N \cdot m^{-1}$	interfacial tension
	Pa	shear stress
n	N	SCR normal force
Φ_E	[—]	emulsion disperse mass fraction

continued on next page

Notation

Symbol (cont.)	Unit (cont.)	Meaning (cont.)
Φ_P	[–]	fat particle disperse mass fraction
ω	Hz	oscillatory shear rheometry angular frequency
ω_{rel}	m/s	relative velocity spray filament to ambient gas

Dimensionless Numbers

Symbol	Meaning
Bi	Biot number
Ca	Capillary number
Ca_{crit}	critical Capillary number for droplet breakup
Ca_{detach}	critical Capillary number for droplet detachment from ROME membrane
Nu	Nusselt number
Oh	Ohnesorge number
Pr_d	droplet Prandtl number
Re	Reynolds number
Re_d	droplet Reynolds number
Ru	Rupture number
We	Weber number

Abbreviations

Abbreviation	Meaning
ADI	acceptable daily intake
CLSM	confocal laser scanning microscopy
CPPF	conventional puff pastry fat
cryo SEM	cryo scanning electron microscopy
DSC	differential scanning calorimetry
D.S.	degree of substitution
GRAS	generally recognized as safe
HFB	hard fat blend

continued on next page

Abbreviation (cont.)	Meaning (cont.)
HLB	hydrophilic-lipophilic balance
HPMC	hydroxypropyl methylcellulose
MC	methylcellulose
Methocel	trade name of methylcellulose and hydroxypropyl methylcellulose manufactured by Dow Chemical Company, USA
NPF	novel powder fat
OTR	oscillatory thermo rheology
O/W	oil-in-water
PGPR	polyglycerol polyricinoleate
PAT-1	Sinterface PAT-1 tensiometer
ROME	rotating membrane emulsification
SCR	shear confinement rheology
SSHE	scraped-surface heat exchanger
TAG	triacylglyceride
TGA	thermogravimetric analysis
W/O	water-in-oil
XRD	x-ray diffraction

Summary

With over 2 billion people affected, overweight has reached epidemic proportions globally. This has driven the development of calorie reduced food products. However, obtaining low-calorie food products with premium sensory and techno-functional properties has remained challenging. Especially the application of low fat spreads in laminated dough systems investigated during this thesis remains difficult; due to intense shear and elongational forces applied during the lamination process and fluctuating temperatures, mechanically stable fat systems with predictable and controllable flow properties decoupled from the sample temperature are essential.

During this thesis, a novel composite powder based fat system, consisting of solid, emulsion based fat particles suspended in a liquid oil phase, was developed. By simultaneous spray-chilling, polymorphically stable (β dominant polymorphism) emulsion based hard fat particles (average particle size $x_{50,3} = 32\mu m$) can be homogeneously blended with a second, liquid oil phase effectively generating a concentrated suspension type system in a single process. The W/O emulsion based substructure of the fat powder enables the incorporation of high water volume fractions, leading to the replacement of fat by water and thus a significant calorie reduction (total fat contents of as low as 45%). Furthermore, the composite, two phase substructure of the fat system leads to an elimination of eutectic effects, in opposite to conventional fat systems, and thereby more predictable, less temperature dependent flow properties. Bulk rheology measurements performed by oscillatory thermo rheology (OTR) confirmed, that the novel powder based fat system shows a less pronounced temperature dependency (more stable viscosity over a larger temperature range), which will allow for a broader range of temperatures during processing and manufacture of food products. Moreover it could be shown, that bulk rheology and flowing behavior of particulate, concentrated suspension type fat systems can be primarily controlled by the powder in oil suspension ratio Φ_P .

Micro rheology measurements (shear confinement rheology) allowed a quantification of normal forces exhibited by particulate fat systems and thereby an estimation of forces acting on dough layers during confinement induced by the lamination process. It was concluded, that small fat particles with an average particle size $x_{50,3} = 32\mu m$ should be favored, as they exhibit smallest normal forces upon confinement. Powder fat systems with high particle disperse fractions $\Phi_E > 0.3$ exhibited elevated normal

forces, which potentially adversely affect fine dough layers in laminated dough. Confinement measurements performed at elevated temperatures significantly decreased normal forces exhibited by high Φ_E fat particles; therefore, processing laminated dough using powder fat at elevated temperatures will reduce microstructural damage (ruptured layers) caused by high normal forces exhibited by fat particles.

Furthermore, thermal analysis by differential scanning calorimetry (DSC) and thermogravimetric analysis (TGA) were applied in order to simulate oven baking and estimate leavening forces exhibited by dough and fat layers in laminated dough. Leavening forces in laminated dough and thus oven rise originates from the evaporation of water during baking, in opposite to yeast leavened dough, where carbon dioxide generated by yeast is the main driving force for oven rise. Therefore, the evaporation of water from dough and fat layers were individually assessed. It was shown, that elevated water contents can be linked to a substantially increased evaporation and thereby increased potential for oven rise during baking. Suspending methylcellulose and hydroxypropyl-methylcellulose in the water phase of the W/O emulsions could be linked to a more controlled release of water during a longer time frame.

During application trials performed in the last step of this thesis, findings from rheometric and thermal analysis could be correlated with oven rise obtained after baking puff pastry dough samples using different powder fat systems. A good correlation with findings from rheology (small fat particles performed better than large fat particles, working at a powder in oil suspension ratio $\Phi_P = 0.675$ was found to be optimal) and thermal analysis (higher oven rise due to elevated rising force exhibited by increased steam pressures of high Φ_E fat particles) was found and further important processing factors (such as layer number, resting time between lamination steps) for generating premium, low calorie laminated dough products were identified.

Zusammenfassung

Übergewicht ist ein Problem globaler Dimension mit über 2 Milliarden betroffenen Personen weltweit. In den letzten Dekaden war diese globale Epidemie verantwortlich für die Entwicklung immer neuer Strategien zur Senkung der Kaloriendichte von Nahrungsmitteln. Die industrielle Produktion hochwertiger, kalorienreduzierter Lebensmittelprodukte mit guten techno-funktionellen Eigenschaften stellt aber nach wie vor hohe Anforderungen an die Lebensmittelindustrie. Im Speziellen bleibt auch der Einsatz von kalorienreduzierten Fettsystemen in laminiertem Teig (Blätterteig) schwierig. Durch die hohen Scher- und Elongationskräfte und Temperaturfluktuationen, welche während dem Laminieren von Blätterteig auftreten, werden Fettsysteme von hoher mechanischer Stabilität mit möglichst temperaturunabhängigen Fliesseigenschaften benötigt.

Im Rahmen dieser Dissertation wurde ein neuartiges, zweiphasiges Pulverfettsystem, bestehend aus emulsionbasierten Festfettpartikel ($x_{50,3} = 32\mu m$) suspendiert in einer flüssigen Ölphase entwickelt. In einem neuartigen, simultanen Gefriersprühprozess können stabile (β dominierter Polymorphismus) emulsionsbasierte Festfettpartikel erzeugt und homogen mit einer sekundären, flüssigen Ölphase gemischt und effizient in einem Prozessschritt ein mehrphasiges, auf einer konzentrierten Suspension basierendes Fettsystem, erzeugt werden. Die auf einer W/O Emulsion basierende Substruktur des Fettpulvers ermöglicht den Einsatz von grossen Wasser Volumenanteilen und dadurch eine signifikante Kalorienreduktion (Gesamtfettanteile von bis zu unter 45%). Desweiteren ermöglicht die zweiphasige Zusammensetzung des neuartigen Pulverfettsystems die Vermeidung eutektischer Effekte im Gegensatz zu konventionellen Fettsystemen, welche aus einer Mischung aus ≥ 2 Phasen bestehen, was zu besser abschätzbaren Fliesseigenschaften verglichen mit konventionellen Systemen führt. Mithilfe von Oszillations-Thermorheologie Messungen konnte die verringerte Temperaturabhängigkeit (stabilere Viskosität in einem breiteren Temperaturbereich) des neuartigen, Pulverbasierten Fettsystems verglichen mit konventionellen Systemen bestätigt werden. Dies ermöglicht den Einsatz des Pulverfettes bei stabilen Eigenschaften in einem breiteren Temperaturbereich, wodurch die konstante Verarbeitungstemperatur weniger kritisch ist als beim Einsatz konventioneller Fettsysteme. Zudem konnte gezeigt werden, dass die Fliesseigenschaften des neuartigen, auf einer konzentrierten Suspension bestehenden, Pulverfettsystemes vorwiegend durch das Pulver in Öl Mischungsverhältnis Φ_P gesteuert werden kann.

Mikro-rheologische Messungen (shear confinement Rheologie) ermöglichte die Quantifizierung der vom Pulverfett ausgeübten Normalkräfte, wodurch die während der Spaltverengung im laminierprozess vom Pulverfett auf die Teigschichten ausgeübten Kräfte abgeschätzt werden konnten. Die Messung der auftretenden Kräfte im verengten Spalt besätigte, dass möglichst kleine Fettpartikel ($x_{50,3} = 32\mu m$) bevorzugt werden sollten, da diese im Vergleich mit grossen Fettpartikeln die kleinsten Normalkräfte ausüben. Fettpartikel mit erhöhten Dispersphasenanteilen $\Phi_P > 0.3$ erzeugten zudem erhöhte Normalkräfte im verengten Spalt, was eine vermehrte Schädigung der feinen Teigschichten in laminiertem Teig nach sich ziehen kann. Die erhöhten Normalkräfte, welche durch grosse Partikel und erhöhte Dispersphasenanteile ausgeübt werden, konnten durch gezielte Temperaturerhöhungen reduziert und kontrolliert werden. Es ist davon auszugehen, dass erhöhte Verarbeitungstemperaturen während dem Laminierprozess, vor allem bei unvorteilhaften Partikeleigenschaften (grosse Partikel, hohe Dispersphasenanteile), die Beschädigung und den Bruch von Teigschichten reduzieren und kontrollieren kann.

Thermische Analysen wie Differenzkalorimetrie und thermogravimetrische Analyse erlaubten eine Simulation des Backvorganges im Ofen im kontrollierten, miniaturisierten Massstab, wodurch die Triebkraft von Fett- und Teigschichten abgeschätzt werden konnte. Im Gegensatz zu Hefenteig, in welchem dertrieb während dem Backen durch das während der Gärung erzeugte Kohlendioxid (biologische Lockerung) erzeugt wird, wird dertrieb in Blätterteig durch die Verdampfung von Wasser (physikalische Lockerung) erzeugt. Es konnte gezeigt werden, dass der Backprozess durch thermische Analysen nachempfunden werden kann; erhöhte Wassergehalte führen zu einem signifikanten Anstieg der durch die Verdunstung von Wasser erzeugte Triebkraft, wodurch ein von einer starken Erhöhung des Triebpotentials ausgegangen werden kann. Suspension von Methylcellulose und Hydroxypropyl-Methylcellulose in der Wasserphase der Emulsionsbasierten Partikeln führte zu einer kontrollierteren Freisetzung von Wasser in einem breiteren Temperaturbereich.

Abschliessende Anwendungsversuche in Blätterteig zeigten eine gute Korrelation zu den theoretischen Resultaten aus den rheometrischen und thermischen Analysen. Wie bereits in den rheologischen Versuchen beschrieben, funktionierten Pulverfettssysteme mit kleinen Partikelgrössen bei einem Pulver in Öl Mischungsverhältnis $\Phi_P = 0.675$ am besten und erzeugten die grössten Gebäckvolumen und die besten Schichtungen. In den thermischen Versuchen wurde eine erhöhte Triebkraft beim Einsatz von Fettpartikel mit erhöhten Dispersphasenanteilen und ein positiver Effekt der durch Zellulose kontrollierte Evaporation von Wasser erwartet, was in den Backversuchen von Blätterteig besätigt werden konnte. Zudem konnten weitere, für den Laminierprozess wichtige Parameter, wie die Anzahl Teigschichten und die Ruhezeit zwischen den Ausrollschritten identifiziert werden.

1. Introduction

Lipids are ubiquitous in food products such as confectionery, baking, ice cream, emulsions, sauces, shortenings and margarine and are responsible for a wide range of techno-functional (structuring and stabilizing) and sensory (enhancing sensory perception by influencing microstructures and acting as carriers for flavor compounds) properties in food. As fat is responsible for many positive attributes in food products such as creaminess, good mouthfeel and and aroma release, dietary preferences seem to be linked to food products with higher fat contents.

Lately, different approaches have been undertaken in order to reduce the fat content of food products; often, high levels of additives such as emulsifiers and thickeners were applied, in order to achieve low fat products with properties comparable to conventional, high fat products. This approach however, did not always lead to the desired product properties, as the applied additives adversely impacted techno-functional and sensory properties.

Therefore, a process focused approach to generate novel, low calorie fat products was pursued during this thesis. A novel, composite powder based fat system (PF) was developed. The PF consists of fat particles substructured by highly concentrated W/O emulsions, which can lead to a significant calorie reduction. In opposite to conventional fat systems, which are produced by direct crystallization of a W/O emulsions consisting of a complex blend of water, different lipid fractions, emulsifiers and thickeners, the novel PF system microstructure is binary. High melting, W/O based fat particles are suspended in a lower melting oil phase, which allows a significant reduction of additives such as emulsifiers and thickeners. Additionally, this binary nature of the PF system prevents eutectic effects as observed in conventional fat systems leading improved melting properties (higher solid fat content (SFC) over a larger temperature range) of PF compared to conventional fat systems, which are linked to improved techno-functional properties.

The novel PF was developed for application in complex, laminated dough systems, which consist of alternating dough and fat layers. Due to the high mechanical (shear and elongation) forces exhibited by the lamination process during production of laminated dough, mechanically highly stable fat is needed in order to avoid adverse effects during processing. Conventionally produced low fat laminating fats are mechanically unstable leading to challenging or impossible processing. PF is, due to its particulate

binary substructure, very stable during processing of laminated dough where high forces are being applied.

In chapter 4, the stability of W/O emulsions at reduced additive concentrations was investigated. Chapter 5 summarizes the novel simultaneous spray-chilling process developed for production of the novel powder fat system consisting of emulsions based fat particles suspended in liquid oil. Important rheologic parameters and their effect on the lamination process for production of laminated dough, such as the thermorheologic bulk flow behavior and confinement rheology of particle based fat systems have been investigated in chapter 6.

The elevated water content of the novel PF systems was expected to majorly impact the physical leavening of laminated dough (driven by evaporation), therefore, the baking process was mimicked by thermal analysis (by DSC and TGA as described in chapter 7) in order to simulate baking and estimate the leavening forces generated by PF.

In a last step of this thesis, results were validated during application trials as described in chapter 8.

2. Background

2.1. Crystallization

Crystallization is the transformation from liquid melt to solid crystallized state⁴⁴. Garti and Sato and Himawan *et al.* summarized the influence of processing and storage conditions on crystallized fat system obtained. Figure 2.1 summarizes the crystallization of liquid fat melts and illustrates the obtained microstructure.

The formation of crystal nuclei from triacylglyceride (TAG) molecules contained in the liquid melt (I) is the first stage of solid phase formation (II). Classic nucleation theory describes the event of nucleation using the Gibbs free energy of the system, as discussed by Turnbull and Fisher; Turnbull. Assuming homogeneous nucleation, the total change in Gibbs free energy ΔG of the system depends on the decrease of Gibbs free energy per unit volume based on the enthalpy of fusion $-\Delta G_f$ and the increase of surface energy due to the increase in surface tension ΔG_s . For spherical nuclei, the equation can be simplified as shown in 2.1. ΔG increases with the radius of the nucleus until a critical radius r_{crit} is reached. Crystal clusters formed from crystal nuclei grow into crystals once this critical radius is exceeded.

$$\Delta G = -\Delta G_f V + \Delta G_s S = -\frac{4}{3}\pi r_n^3 \Delta G_f + 4\pi r_n^2 \sigma \quad (2.1)$$

ΔG_f can be estimated as $\Delta G_f = -\Delta H(\Delta T/T_m V_m)$ where V_m is the molar volume of the clusters and $\Delta T = T_m - T$ is the supercooling⁴⁷. Using these terms, the critical free energy ΔG_{crit} , which is the energy barrier for crystallization from a liquid melt, can be estimated using equation 2.2. Only cluster with a size greater than r_{crit} at a Gibbs free energy ΔG_{crit} will be able to grow into stable crystals.

$$\Delta G_{crit} = \frac{16}{3} \frac{\pi \sigma^3 V_m^2 T_m^2}{(\Delta H_m \Delta T)^2} \quad (2.2)$$

These stable crystals formed during phase I and II of crystallization, will subsequently grow (III) into complex fat crystal networks and over time transit during further

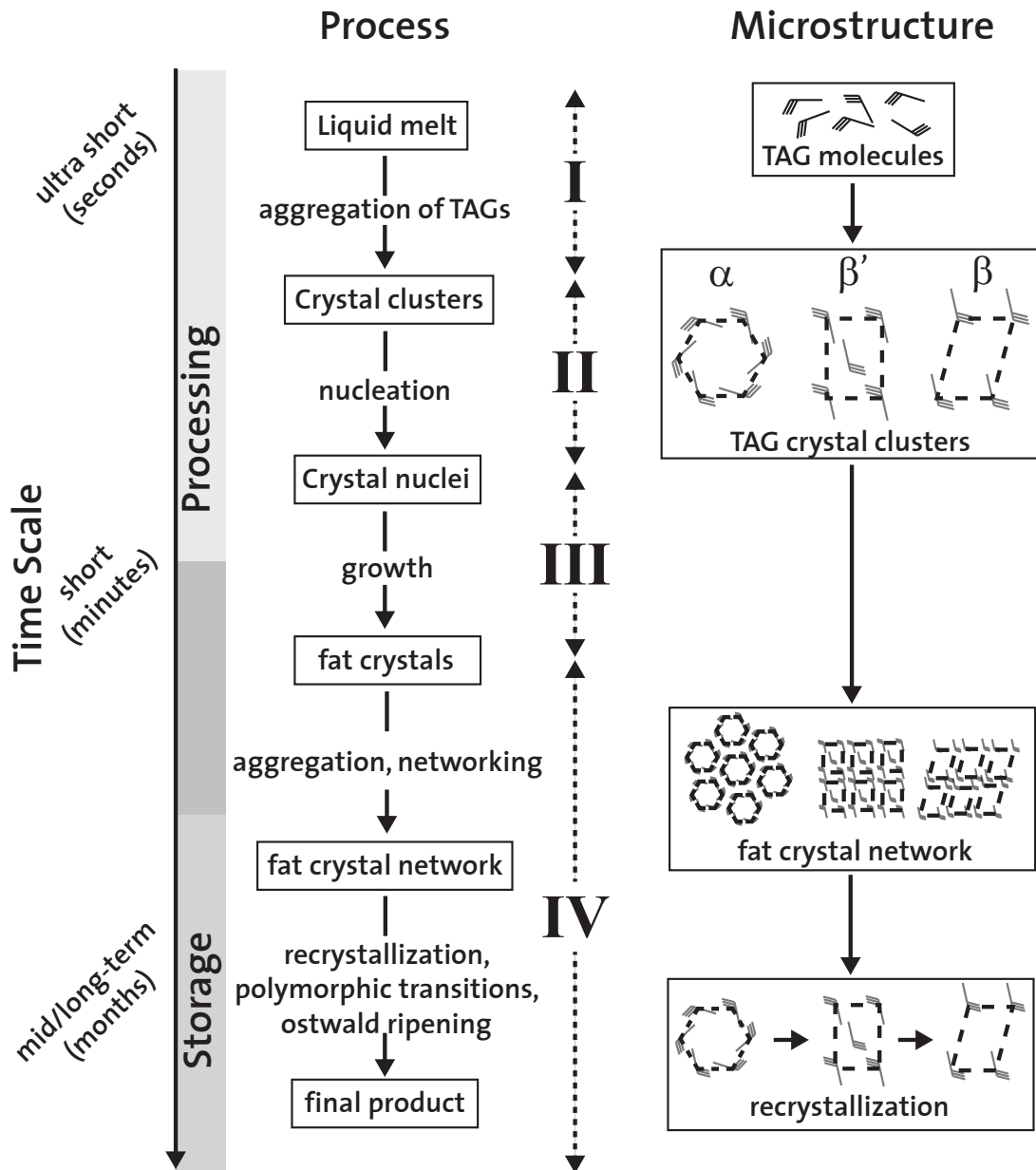


Figure 2.1.: Microstructure of fat crystal networks.^{61;78;47}

processing and storage to a final product consisting of only the most stable crystal polymorphs.

2.1.1. Polymorphism

The microstructure and polymorphism obtained during nucleation (I and II) from the liquid melt, depends on a large range of process and product parameters. Garti noted, that nucleation in real solutions usually is accelerated as it originates from heterogeneous nucleation sites present in the solution such as the wall of the vessel, impellers and impurities such as mono-diglycerides and dust particles.

As described by equation 2.2, the formation of nuclei depends on the critical radius of the crystal clusters as well as the degree of supercooling of the melt and in addition can be significantly accelerated by the presence of heterogeneous nucleation as discussed earlier. Therefore, upon supercooling, TAG molecules start to agglomerate and form crystal nuclei which then can form crystal clusters once a critical radius is exceeded.

Due to their thermodynamic instability, α -polymorphs are only meta-stable and only exist during the initial stages of production of palm fat based fat systems. Therefore, only more stable β and β' polymorphs can be detected in the final product, which can be explained Gibbs free energy of the different polymorphs. Figure 2.2 shows a comparison of the increase of energy due to surface tension (ΔG_S) and the decrease of energy due to the release of enthalpy of fusion (ΔG_f) for α , β' and β polymorphs. The Gibbs free energy of stable β polymorphs is lower than the lesser stable β' and α crystals^{78;47}. In opposite thereto, the activation energy (increase in energy due to the surface tension) is higher for the more stable polymorphic forms. Therefore, lesser stable α and β' polymorphs usually arise first during thermodynamically controlled crystallization from liquid melt. As discussed by Lawler and others, this can be explained by a lower surface tension of less stable polymorphs due to a looser microstructure.

Therefore, on short-term, lesser stable α and β' crystals are favoured due to the lower interfacial tension. However, in the mid-long term, the lower energy state of β crystals is favoured, leading to strongly β dominated fat blends.

Figure 2.3 illustrates the stability of the three polymorphic modifications as introduced by Sato. α crystals exhibit a disordered aliphatic chain conformation, β' crystals an intermediate packing and most dense packing is observed in β polymorphs. Thus, the Gibbs free energy as shown in figure 2.2 is highest for α polymorphs and decreases for β' reaching a lowest level for β polymorphs.

α polymorphs dominate at high degrees of supercooling and fast cooling rates^{50;73;15}. In opposite thereto, more stable β' and β polymorphs are generally observed at lower degrees of supercooling and slow cooling rates. α crystals formed upon chilling of a liquid melt with high cooling rates and high degrees of supercooling, usually recrystallize into more stable β' and β modifications over time.

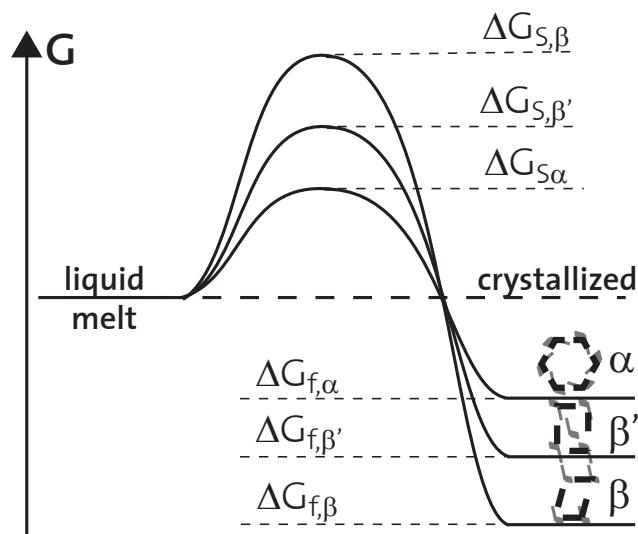


Figure 2.2.: Change in Gibbs free energy during nucleation of different fat polymorphs. ΔG_S is the increase of energy due to surface tension, ΔG_f the decrease of energy due to the release of enthalpy of fusion⁴⁴.

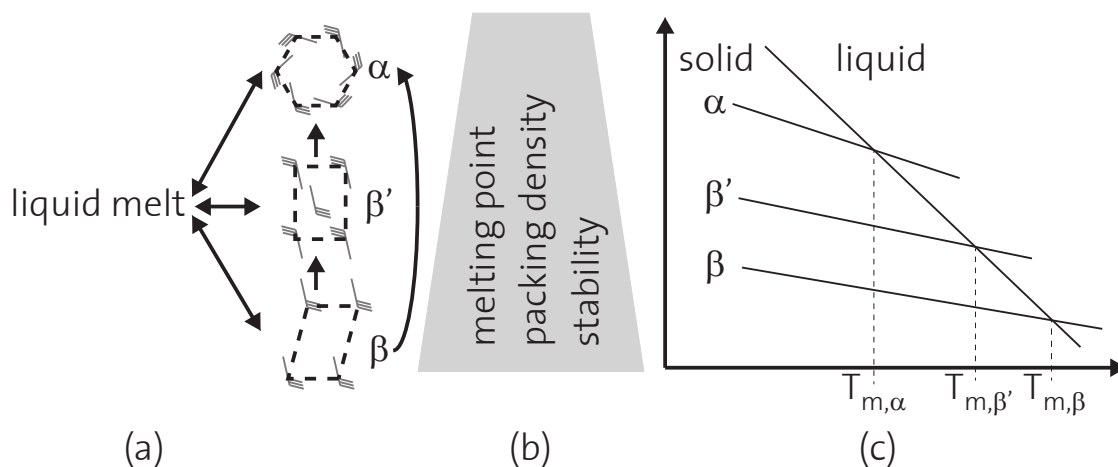


Figure 2.3.: Polymorphic modifications found in palm fat used during this thesis and their stability^{37;69;60}.

Polymorphic forms can be determined based on their melting point by DSC or based on their crystal lattice short spacing by x-ray diffraction (XRD).²⁴ described the application of XRD for analysis of polymorphs contained in a fat blend. α polymorphs were correlated with a short spacing of $0.415nm$, β' with a short spacing of $0.38nm$ and $0.42nm$ and β polymorphs with a more complex scattering pattern with an additional peak at $0.46nm$.

Palm fat applied during this thesis shows a predominantly β stable system, which was also confirmed by others^{103;9;38}.

2.2. Emulsions

Emulsions consist of two immiscible phases (oil and water)⁴⁶. As the interfacial tension σ between two immiscible phases is always greater than zero, surfactants are needed to stabilize the additional interface generated by energy input during emulsification processing.

Two immiscible phases are always trying to reduce the interface and therefore demix as this is the energetically favored state where the Gibbs free energy is at a minimum. Thus, additional interfacial area generated when droplets are obtained by emulsification processing, always leads to a substantial increase in the Gibbs free energy. The energy required to create additional surface area during emulsification can be calculated using equation 2.3, where W_{min} is the minimum energy required for the generation of additional interface, ΔA the interfacial area generated and σ the interfacial tension.

$$W_{min} = \Delta A \sigma \quad (2.3)$$

Emulsions therefore are thermodynamically not favored and will always strive towards the lowest energetic state of the two separate phases where the interfacial area is minimal⁴. Surfactants have two different modes of action leading to a stabilization of emulsions. Firstly, they are used to decrease the interfacial tension and thereby have a direct impact on the energy required for the generation of total interfacial area as shown in equation 2.3. Secondly, surfactants can alter the viscoelastic properties of the interface and thereby sterically hinder coalescence of emulsion droplets. Emulsion stability and destabilization mechanisms have been described in detail^{19;77}.

2.2.1. Rotor-stator emulsification

Rotor-stator mixers consist of a high-speed rotor (driven mixing element) in close proximity to a stator (fix mixing element) with typical rotor speeds of 10 – 50m/s. Rotor-stator mixers are also called high-shear devices as local energy dissipation and shear rates are much higher than in conventionally mechanically stirred vessels; shear rate ranges of 20000 – 100000s⁻¹ have been observed³.

2. Background

In dispersion processing, structural forces are competing against flow forces. The structural forces present in emulsions can be described by the capillary pressure p_k as shown in equation 2.4, where d is the droplet diameter.

$$p_k = \frac{4\sigma}{d} \quad (2.4)$$

During emulsification processing, disruptive forces greater than these interfacial forces have to be present. The dimensionless Capillary number Ca (equation 2.5) describes the ratio between these forces for a spherical droplet in laminar flow⁷⁹, with the emulsions viscosity at applied shear rates of $\eta_e(\dot{\gamma})$, the shear rate $\dot{\gamma}$ and the droplet diameter d .

$$Ca = \frac{\eta_e(\dot{\gamma})\dot{\gamma}d}{\sigma} = \frac{\text{viscous stress}}{\text{surface forces}} \quad (2.5)$$

The critical Capillary number Ca_{crit} for breakup of emulsion droplet is reached, once disruptive forces are strong enough to cause droplet breakup. If $Ca > Ca_{crit}$, a droplet breaks up into two smaller droplets, and if $Ca \gg Ca_{crit}$ breakup into more than two droplets can occur⁵¹. Additionally, Ca_{crit} is a function of the viscosity ratio $\lambda = \frac{\eta_d}{\eta_c}$ of disperse (η_d) and continuous (η_c) phase⁴¹. The grace curve as shown in figure 2.4 illustrates this dependency for pure elongational and shear flow.

In pure shear flow, breakup is only possible for $\lambda < 4$, while for pure elongational forces no critical limit of λ could be found.

2.2.2. Rotating membrane emulsification

Membrane emulsification is known to generate smaller and narrower droplet size distributions compared to rotor-stator emulsification⁷⁵. The rotating membrane process (ROME) developed at the lab of food process engineering at ETH Zürich was described in detail⁴⁰.

In general two types of forces have to be considered in ROME emulsification: forces retaining a droplet at a pore and forces leading to detachment of droplets. Figure 2.5 summarized the forces acting at a droplet detaching from a membrane pore. Forces retaining the droplet at the pore consist of the interfacial tension force F_σ , the static pressure difference force F_{SP} and the inertia force F_I . Detaching forces are the viscous drag force F_D , the buoyancy force F_B and the dynamic lift force F_L .

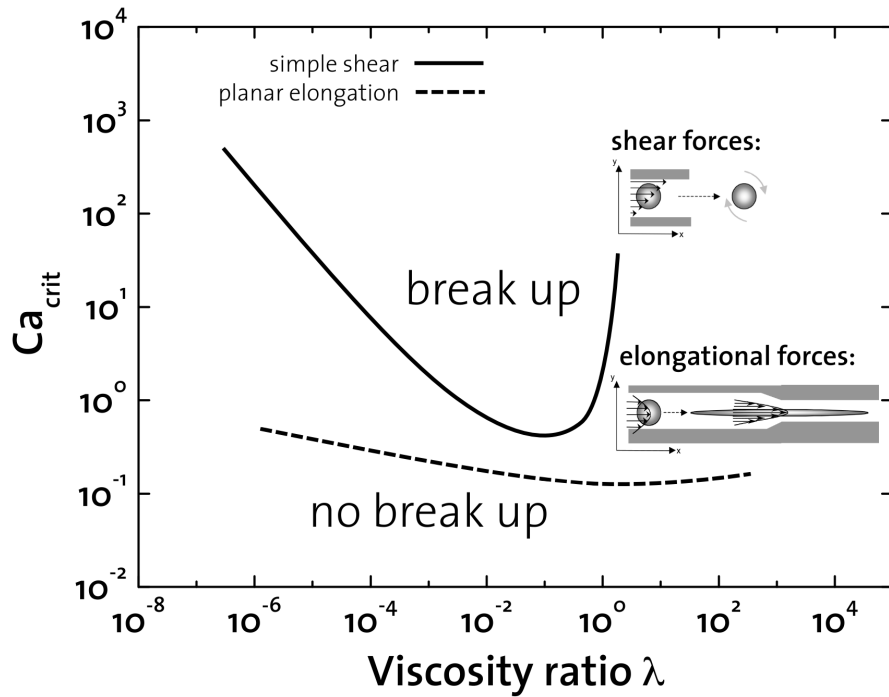


Figure 2.4.: Grace curve linking the critical Capillary number Ca_{crit} and the viscosity ratio λ for pure shear and pure elongational flow^{41;83}.

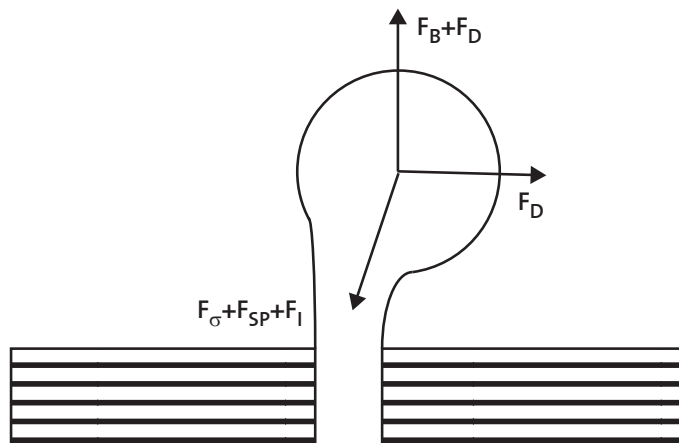


Figure 2.5.: Forces acting at an emulsion droplet detaching from a membrane pore⁴⁰.

As previously discussed for rotor-stator processing, a Capillary number for detachment of droplets from a membrane pore Ca_{detach} can be defined, which is defined as the ratio of retaining and detaching forces as shown in equation 2.6.

$$Ca_{detach} = \frac{F_L + F_{SP} + F_D}{F_\sigma} \quad (2.6)$$

This leads to equation 2.7²⁸, where d_{pore} is the pore diameter, d the droplet diameter, η_c the continuous phase viscosity, ρ_c the continuous phase density, τ_W the wall shear stress.

$$Ca_{detach} = \frac{d}{d_{pore}} + \frac{d}{d_{pore}} \frac{\tau_W d}{\sigma} \left(1 + \frac{\sqrt{\tau_W \rho_c d}}{\eta_c \pi}\right) \quad (2.7)$$

2.2.3. Emulsifiers

Emulsifiers stabilize emulsions by adsorbing at the interface between oil and water phase and thus are also known as surface-active agents or surfactants. Surfactants can alter surface and interfacial free energies. Interfaces are the boundary layers between two immiscible phases as for example between oil and water, whereas surfaces define the interface of one phase towards a gas phase⁷⁶. Non-ionic emulsifiers are most effective for stabilizing W/O or O/W emulsions. Choosing the optimum emulsifiers is crucial for the emulsification process and temporal stability of an emulsion⁹⁰.

Rules for choosing the optimum emulsifier for an emulsion have been defined by Rosen:

- High surface activity linked to low interfacial tensions
- Stable interfacial film, with laterally interacting hydrophilic groups for W/O emulsions
- Fast migration to the interface in order to ensure reduction of the interfacial tension in the time-frame of emulsification in order to ensure proper action
- Surfactant should be oil soluble for W/O emulsions
- Application of a combination of water and oil soluble surfactants are most efficient
- More polar oil phases require more hydrophilic emulsifiers

The HLB concept is frequently used in order to classify emulsions⁴². HLB stands for the hydrophilic-lipophilic balance of a surfactant; as emulsifiers are amphiphilic and therefore possess hydrophilic and lipophilic parts, the balance between those two parts determines the functionality of the emulsifier in an emulsion.

HLB is used to quantify the relative solubilities of the hydrophilic and lipophilic parts of an emulsifier and is calculated according to equation 2.8. An emulsifier with a high HLB value possesses a high level of hydrophilic groups, whereas a low

HLB emulsifier is highly lipophilic¹⁰⁴. Figure 2.6 shows the HLB values of selected functional groups.

$$\text{HLB value} = \sum(\text{hydrophilic value}) - \sum(\text{lipophilic values}) + 7 \quad (2.8)$$

	Groups number
Hydrophilic groups	
SO ₄ Na	38.7
—COOK	21.1
—COONa	19.1
Sulfonate	c.11
—N(CH ₃) ₃	9.4
Ester	
sorbitan ring	6.8
Other	2.4
—COOH	1.9
—OH:	
sorbitan ring	0.5
Other	1.9
—(CH ₂ —CH ₂ —O)}	0.33
Lipophilic groups	
—CH—	0.475
—CH ₂ —	0.475
—CH ₃	0.475
—CH—	0.475

Figure 2.6.: Values of functional group members to determine the HLB value¹⁰⁴.

High HLB emulsifiers with values ranging from 8-18 will favor O/W emulsions, whereas low HLB emulsifiers with values of 4-6 will favor W/O emulsions⁹⁹. Table 2.1 shows the HLB values of selected emulsifiers used during this thesis and their legal limits.

Table 2.1.: HLB values for emulsifiers and its legal limits for fat spreads.

Emulsifier	HLB value	Source	Legal limits for fat spreads 107	E number
PGPR			4g for 1kg	E 476
Mono-diglycerides	3-6	67	GMP	E 471
Lecithin	2-7	13	GMP	E 322

2.2.4. Emulsion stability & destabilization

Emulsions consisting of two liquid phases are mainly kinetically stabilized. Several emulsion break down processes are known and may occur during storage of an emulsion (see figure 2.7).

1. **Sedimentation or creaming** occurs, when external forces (gravitational or centrifugal forces) exceed Brownian Motion of the droplets. The thereby forming concentration gradient leads to sedimentation or creaming of droplets.

2. Background

2. **Flocculation** occurs, when the attractive forces between droplet overcome repulsive forces, leading to aggregation of droplets.
3. **Ostwald Ripening** is a result of incremental differences in solubility between the two immiscible phases (larger solubility of smaller droplets compared to larger droplets); small droplets diffuse with time towards larger droplets leading to a shift of larger droplet size distributions.
4. **Coalescence** is the result of thinning and disruption of the liquid film between the droplets and therefore, the fusion of two or more droplets to larger ones. The driving force are the surface fluctuations, which result in close approach of the droplets whereby the van der Waals is strong and prevents their separation.
5. **Phase inversion** is the process where an exchange between disperse and continuous phase occurs⁹⁰.

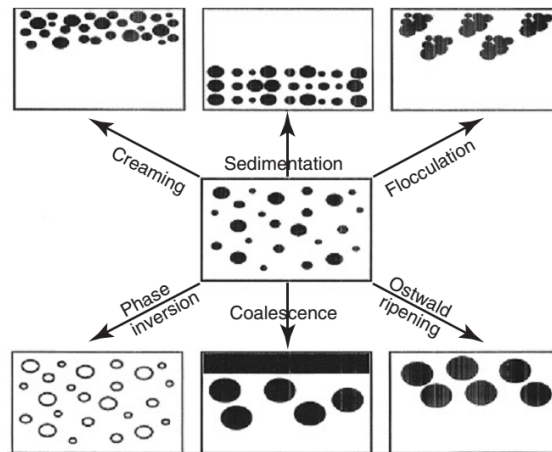


Figure 2.7.: Illustration of various breakdown processes in emulsions⁹⁰.

2.3. Conventional fat systems

In conventional processing, crystallized fat systems are mostly produced under high shear and elongational forces by scraped-surface heat exchangers (SSHE)⁵³ as illustrated in figure 2.8. The SSHE consists of a chilled outer jacket enclosing the scraper blades attached to a rotating barrel. SSHE processing allows the controlled crystallization of fat blends and emulsions while effectively preventing the formation of crystal networks by high shear forces applied.

The scraping blades rotate at high rotational speeds (up to 1000 *rpm*) leading to high shear rates. The maximum shear rates can be calculated according to¹¹ using

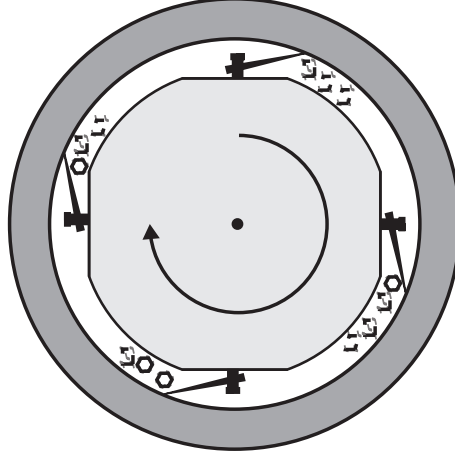


Figure 2.8.: Scraped surface heat exchanger (SSHE), where scraper blades generate local shear at the chilled jacket leading to crystallization and trigger the desired polymorphism.

equation 2.9, where $\dot{\gamma}_i(H_{min})$ is the maximum local shear rate at a minimal shear gap H_{min} , R_0 the radius of the chilled jacket, R_i the radius of the rotating barrel and $\dot{\gamma}_i$ the shear at the rotating shaft surface.

$$\dot{\gamma}_i(H_{min}) = \frac{H^2}{H_{min}^2} \dot{\gamma}_i = \frac{(R_0 R_i)^2}{H_{min}^2} \dot{\gamma}_i \quad (2.9)$$

Crystal nucleation and transformation to more stable polymorphs is favored by shear^{53;63}. The phase transition from unstable α to more stable β' and β polymorphs has been investigated in detail^{63;2}. It was concluded, that α crystals nucleate and grow from the melt. At high shear rates present in SSHE processing, α crystal cluster get separated leading to a much higher surface area in contact with the liquid melt and therefore a much higher possibility of acting as nucleation sites for β' crystals. The formation of β' crystal depends on the direct rate of nucleation from α crystals as well as on the rate of transformation from α to β' crystals in the melt. The rate of transformation is accelerated at high shear due to local super heating leading to partial melting of α crystal and favored re-crystallization as more stable β' polymorphs.

At low or no shear conditions, initially formed α crystal clusters can aggregate retarding nucleation of β' polymorphs leading to α dominated fat crystal networks.

Fat blends crystallized from melt by shear crystallization in SSHE processing will never fully crystallize, but always contain certain fractions of uncrystallized fat due to the large mechanical energy introduced by processing and thus triggered remelting of fat crystals. Additionally, the conventionally crystallized fat blend will not only

result in stable β polymorphs, but contain rather large fractions of α and β' polymorphs. The fat will only fully crystallize and reach a final state during storage, which influences the properties of the fat crystal network as it will with time facilitate recrystallization of unstable into more stable polymorphs. Thereby, the originally obtained fat crystal network by shear processing and the thereby obtained plasticity, may be adversely affected by a strengthened network and a (partial) loss of plasticity which is of crucial importance for laminating fats.

2.3.1. Microstructure of conventional fat systems

Conventionally produced fat systems are shear crystallized from fat melt by undercooling as described above. The fat melt usually consists of different melting fat fractions (high melting phase which is being crystallized during processing forming a solid fat crystal network and low melting fraction, which stays liquid) and can be supplemented by emulsified water droplets and secondary ingredients such as thickeners and functional compounds.

Crystallization from fat melt leads to a complex fat crystal network consisting of at least two different fat fractions. This complex blend of crystallized and liquid fat leads to eutectic effects⁶⁰. 'Eutectic' in greek means 'easily melted', indicating a lowered melting point of an at least binary mixture of two different fats. Eutectic effects can have catastrophic impacts in lipid applications, where a specific hardness and plasticity are required.

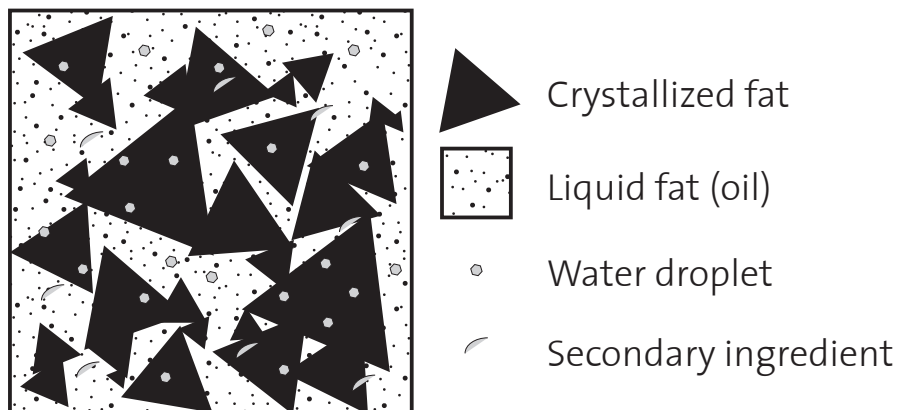


Figure 2.9.: The microstructure of conventional fat systems (produced by SSHE).

The novel, powder based fat system was invented with the aim to improve two critical, negative properties of conventional fat systems as described before:

- Not fully crystallized conventional fat systems and unstable polymorphic modifications contained in conventional fat systems lead to post- and re crystallization during storage adversely affecting the plasticity of the fat.
- Eutectic effects can lead to a reduced melting point of crystallized fat blends adversely affecting plasticity.

2.4. Powder fat systems

2.4.1. Spray chilling

'A spray is defined as a flow of individual liquid droplets evolving in a surrounding gaseous medium. Each droplet has its own diameter and velocity and may collide and coalesce with other droplets.'²⁵. The most important characteristic which is used to describe a spray is the droplet size distribution. The breakdown of the liquid jet leaving the spray nozzle originates from process and product properties. The process influences the breakdown through the large density differences between gas and liquid phase (larger than two orders of magnitude), and the velocity differences of injected jet surrounding atmosphere, and if applicable velocity of the atomizing gas in the spray nozzle. Relevant product properties are surface tension of the liquid phase as well as its shear, extensional viscosity and viscoelasticity.

Two main types of spraying can be distinguished: spray drying and spray chilling. During spray drying, mass is being removed from the sprayed droplet through evaporation leading to dried particles with a reduced mass. In opposite thereto, no mass is lost during spray chilling as droplets formed from the liquid jet at the spray nozzle are solidified during spray chilling. As spray chilling is applied during this thesis, a model for the solidification of droplets is described in chapter 5.

In the following, the theory behind the breakup of a liquid jet at the nozzle and the formation of droplets is described.

Primary and secondary breakup The droplet breakup starts once the liquid jet leaves the atomization nozzle²⁵. During primary breakup, the liquid jet forms into ligaments and other irregular liquid elements along the surface of the liquid column⁸⁷. Due to the instability of these liquid filaments which are subjected to relatively large drag forces by the surrounding gas, secondary breakup will occur as shown in figure 2.10.

The fluid can be atomized into the spraying tower using different types of atomization (pressure nozzle and air-assist two-component nozzle). During this thesis,

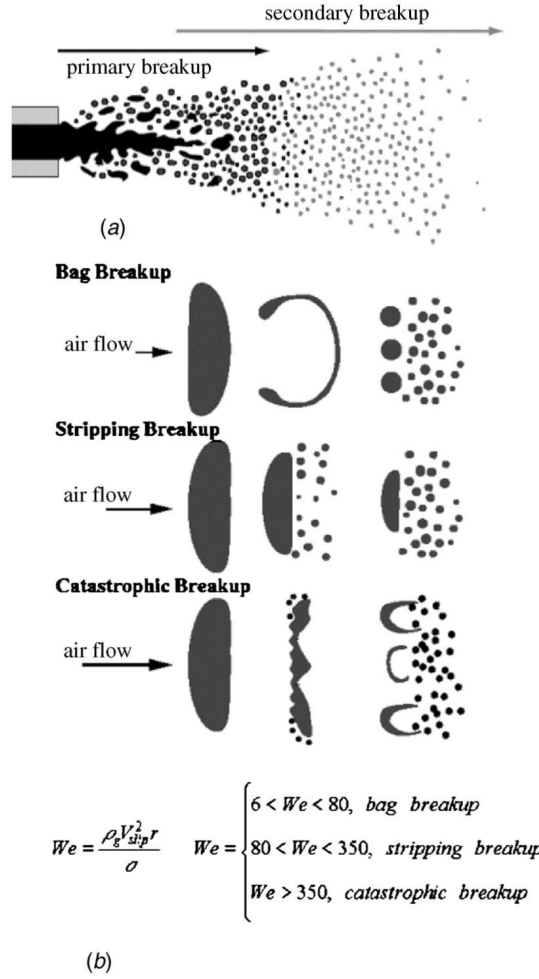


Figure 2.10.: Spray droplet breakup from liquid filament: (a) Primary and secondary breakup, (b) droplet breakup for different domains of We ⁸⁷.

air-assisted two-component atomization, where the liquid is pumped to the nozzle by a volumetric pump and atomized by pressurized air, was applied. In opposition to single-component fluid nozzles, the particle size distribution obtained does not depend only on the fluid flow rate, but mainly on the pressure of the atomization air flow. Other atomization principles, such as rotary atomizers and ultrasonic atomizers have been described in literature⁵⁵.

The liquid jet breakdown and the formation of droplets based on surface, inertia and viscous forces has been previously described⁷². The Weber number (We) (equation 2.10) is defined as the ratio of the velocity of the sprayed liquid filament relative to the ambient gas w_{rel} , the diameter of the nozzle d_N , the density of the fluid ρ_F and the surface tension of the liquid γ_L . The We number describes the ratio of inertia to

surface forces.

$$We = \frac{w_{rel}^2 d_N \rho_F}{\gamma_L} \quad (2.10)$$

Rupture of the liquid filament can be expected if $We > 8/c_d$ where c_d is the drag coefficient⁵⁵. To achieve this, the relative velocity of liquid filament and atomizing gas in the two component nozzle has to be increased.

The Reynolds number (equation 5.6) is defined as the ratio of relative velocity of the liquid, nozzle diameter, fluid density and the viscosity η_L of the liquid. The Re number takes the flow regime of the liquid leaving the nozzle into account; at laminar flow regimes, incomplete atomization can be expected, whereas a turbulent regime will lead to a catastrophic breakdown of the liquid jet and to a breakdown into fine liquid droplets.

$$Re = \frac{w_{rel} d_N \rho_F}{\eta_L} \quad (2.11)$$

Ohnesorge combined the Weber and the Reynolds number into the dimensionless Ohnesorge (equation 2.12) number eliminating w_{rel} . Figure 2.11 shows the application of the Ohnesorge Reynolds diagram for differentiation of different breakup regimes. Raleigh (dripping) breakup occurs in the laminar regime solely due to gravitational forces. In the first wind induced section, a the jet is being disrupted due to high liquid filament relative to ambient gas velocity. Droplet size is considerably smaller than droplets formed by Rayleigh breakup, however satellite droplets are formed leading to a relatively large droplet size distribution. In the second wind induced regime, the liquid jet is disrupted right at the nozzle exit exhibiting a very turbulent shape⁵⁵. The second wind regime is reached, once surrounding gas inertia forces are equal to surface tension forces.

In the atomization regime, is defined as a complete jet disruption and disintegration starting at the nozzle exit generating much smaller droplet sizes with broader size distribution due to catastrophic or fully turbulent breakup phenomena compared to the break up regimes as discussed before²⁹.

$$Oh = \frac{\sqrt{We}}{Re} = \frac{\eta_L}{\sqrt{\gamma_L \rho_F d_N}} \quad (2.12)$$

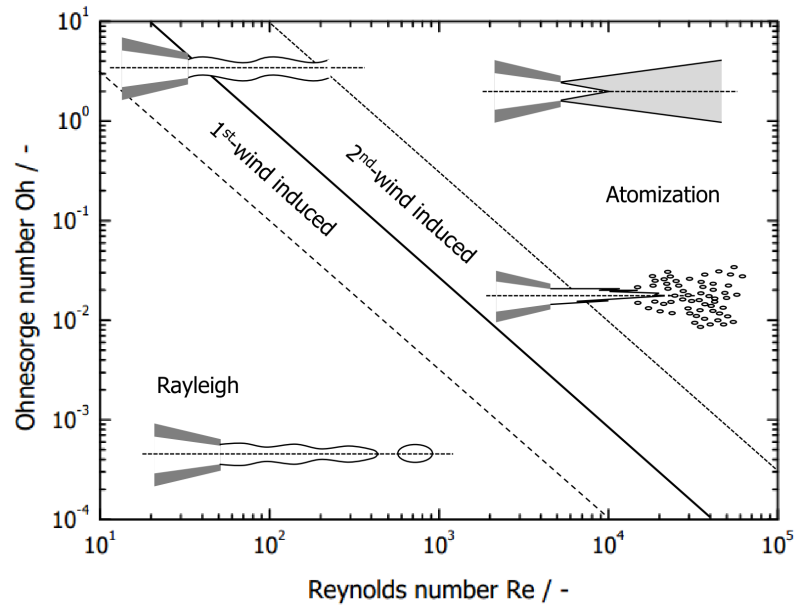


Figure 2.11.: Ohnesorge Reynolds diagram⁷².

2.4.2. Microstructure of powder fat systems

As discussed earlier, the novel, powder based fat system was invented with the aim, to improve two critical, negative properties of conventional fat systems:

- Not fully crystallized conventional fat systems and unstable polymorphic modifications contained in conventional fat systems lead to post- and re crystallization during storage adversely affecting the plasticity of the fat.
- Eutectic effects can lead to a reduced melting point of crystallized fat blends adversely affecting plasticity.

By applying a novel co-spray process, as described in detail in section 3.2.2 and thermodynamically modeled in section 5, powder fat consisting of substructured fat particles mixed with a continuous oil phase was obtained. Figure 2.12 illustrates the microstructure of the powder fat system. Fat particles are suspended at relatively high volume fractions in a continuous oil phase resulting in a highly concentrated suspension type system. Fat particles can be substructured with water or o/w emulsions resulting in a (multiple-) emulsion type system or contain air bubble inclusions resulting in a foamed microstructure. Additionally, fat particles can be enriched with functional components and / or hydrophobic & hydrophilic particles. The continuous oil can be enriched with functional particles and / or hydrophobic & hydrophilic particles as well.

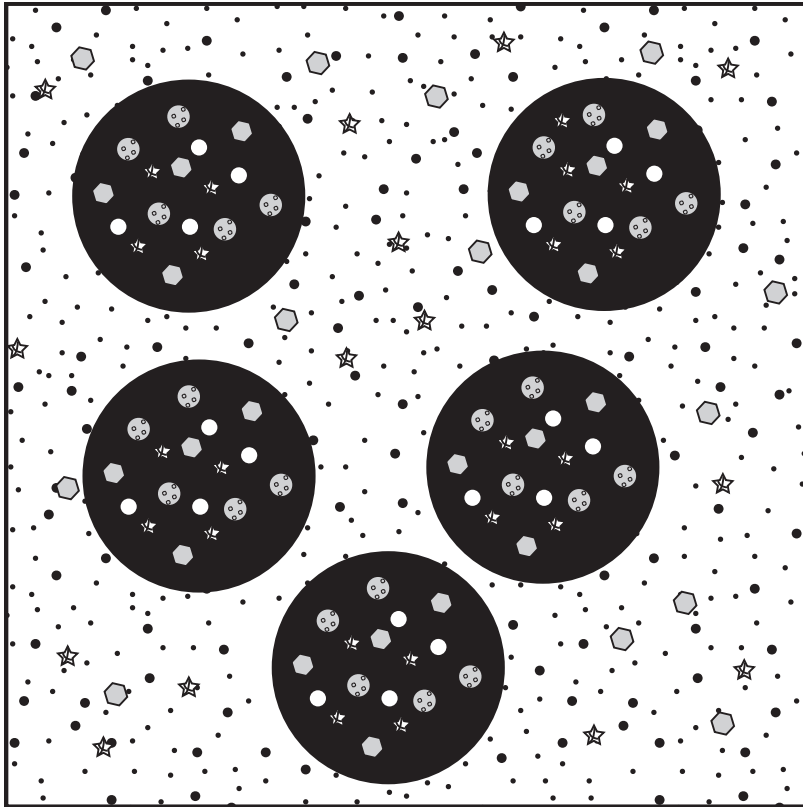


Figure 2.12.: The microstructure of powder fat systems (produced by spray chilling).

This novel microstructure results in numerous advantages over conventionally crystallized fat systems:

- Separation of high and low melting fat fractions (particles and continuous oil phase) eliminates eutectic effects and leads to a much less temperature dependent melting behavior. This is particularly important in systems such as laminated dough, where minimal temperature dependency of the fat during production is required.
- Crystallization of fat particles is completed during the spraying process leading to a fat system consisting of stable fat polymorphs where post and re crystallization are no issues.
- Calorie reduction: By incorporating water and / or air inclusions, the caloric content of the novel fat system can be effectively reduced. Due to the absent eutectic effects and the nature of the powder fat system where rheologic properties can be tailored mainly by the particle in continuous oil mixing ratio, low calorie fat systems with mostly unchanged rheologic properties are expected.

- High potential for functionalization: The nature of the powder fat system (no eutectics, fully crystallized after processing) allows the incorporation of functional compounds without influencing the technological properties.

2.5. Laminated dough systems

Laminated dough systems consist of a distinctly layered substructure. Puff pastries in particular is a nonyeasted layered product consisting of a paste of many alternating thin layers of dough separated (laminated) by alternate fat layers¹⁰⁰. Puff pastries are produced in different scales, ranging from table-top production to fully industrialized mass production lines. As the production process depends on the quantity of fat, bakers typically use a fat content varying from 50% to 100% on our basis in the recipe s and the nished pu pastry can contain 30% or more fat on a weight basis⁸⁸, and hence, it is considered to be a high fat food. It additionally has to be noted, that the fat used for puff pastry production is usually high in saturated and trans fats.

Puff pastry production has not been changed recently, therefore the general methodology as introduced by McGill is still valid.

2.5.1. Lamination

The composition of the the base dough is described in section 8.1.1. After mixing and kneading of the dough ingredients, the dough is rested before being extruded into a dough sheet. The laminating fat is extruded into a fat sheet and placed onto the dough sheet which is then folded in order to enclose the fat sheet for subsequent layering by folding and sheeting. This method is known as the german method of lamination. Other sheeting methods are described elsewhere⁶⁴.

During layering, the finely layered microstructure is built up by further sheeting and folding⁸⁴. Lamination steps (single and double tours as shown in figure 8.1 according to the german method of lamination, where fat is enclosed by dough) as listed in table 8.5 are applied. Depending on the number and combination of (single and double) tours applied to the dough, the desired number of fat layers in the composite dough can be controlled. The composite dough is usually rested for 30 minutes after lamination and rolling out steps in order to let possible tensions in the dough relax and to reassure a homogeneous pastry product.

After the last touring step, the dough is rested for 30 minutes prior to baking.

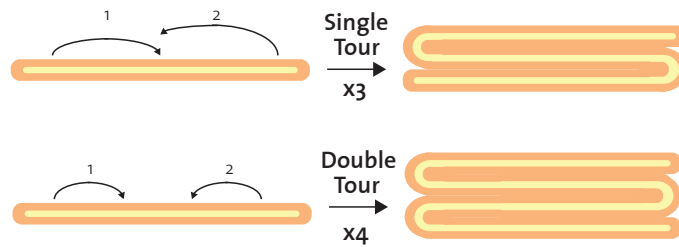


Figure 2.13.: Touring steps during lamination of puff pastry dough. Single tours result in a 3*-multiplier, double tours in a 4*-multiplier to the fat layers contained in the dough.

Table 2.2.: Number of fat layers obtained by lamination and the underlying program of lamination.

Total number of fat layers	Touring steps
27 ($3 \cdot 3 \cdot 3$)	single · single · single
48 ($3 \cdot 4 \cdot 4$)	single · double · double
144 ($3 \cdot 4 \cdot 3 \cdot 4$)	single · double · double · single
192 ($3 \cdot 4 \cdot 4 \cdot 4$)	single · double · double · double
256 ($4 \cdot 4 \cdot 4 \cdot 4$)	double · double · double · double

2.5.2. Leavening

In puff pastry dough, leavening forces originate in evaporation of water contained in the composite dough (physical leavening) in opposite to yeast leavened doughs. Conventionally, fat layers are expected to act as steam barriers, trapping steam in the layered microstructure and thus generating rise during baking¹⁰⁰. During baking, the laminating fat is absorbed by the dough giving it a soft texture and a resistance moisture gain during storage.

2.5.3. Limitations

Due to the finely layered microstructure obtained by the multi-step process of lamination, puff pastry dough production remains challenging. Resting periods between layering steps are required in order to:

1. Relax tensions caused by stresses (elongation and shear) originating from lamination and avoid catastrophic breakdown of the layered microstructure.
2. Control the temperature of the laminated dough at $4 - 8^{\circ}\text{C}$, where conventional puff pastry margarine is at the desired viscosity.

The novel powder fat system has the potential to solve these limitations through the changed microstructure and corresponding technological advantages.

2.5.4. Impact of the novel powder fat system

The properties of the novel fat system are described in section 2.4.2. Applying the novel fat system to laminated dough has the following potential advantages:

1. Temperature independent rheology: Due to a decreased temperature dependency of powder fat systems, increases in temperature arising during touring (mechanical energy impact, elevated room temperature) have a negligible impact on the dough viscosity. Therefore, no resting time in order to control the dough temperature is required.
2. Altered, suspension based rheological properties: The powder based nature of the system allows tailored rheologic properties of the fat. Therefore less tensions will arise during touring resulting in a reduction or avoiding of resting times.
3. Increased water content of powder fat: As previously discussed in section 2.5.2, moisture contained in laminated dough is responsible for leavening during baking. Emulsion based powder fat can contain very high water contents and thus significantly influence the leavening forces generated during baking.

2.6. Bulk and confinement rheology

Rheology is the science of flow and deformation of matter. During rheologic measurements, a defined force is applied to a sample while the response of the system is measured, giving insight into structural interactions in the sample. Bulk rheology is of interest in this thesis, since it allows characterization of the flowing characteristics of novel fat system, which is of crucial importance for application in laminated dough as discussed in 2.5. Additionally, confinement or micro rheology allows the measurement of normal forces exhibited by substances. This is of interest in this thesis, as normal forces exhibited by fat powders on dough layers might have a catastrophic impact on the finely layered microstructure of laminated dough.

2.6.1. Bulk rheology

In general, elongational and shear rheology can be distinguished. In elongational rheology, a material is stretched (elongated) in a shear flow. The presence of only

pure elongational flow is called dilatational rheometry and shear rheometry is defined as pure shear rheology where stress is induced by rotational or oscillatory flow.

Rotational rheometry is controlled by either shear rate $\dot{\gamma}$ or shear stress τ . The viscosity η can be calculated according to newtons law as shown in equation 2.13.

$$\eta(\dot{\gamma}) = \frac{\tau}{\dot{\gamma}(t)} \quad (2.13)$$

Using a flow curve, the viscosity can be described as a function of the shear rate. A fluid is newtonian, if the viscosity shear rate independent. In the non-Newtonian case, either shear thickening or shear thinning effects occur leading to a shear rate dependence of the viscosity.

Viscoelastic material properties can be measured by oscillatory rheometry. During oscillatory shear experiments, a defined strain of sinusoidal form $\gamma(t) = \gamma_0 \sin(\omega t)$ is applied at an amplitude γ_0 and an angular frequency ω . Thereby, a periodic material stress response $\tau(t) = \tau_0 \sin(\omega t + \delta)$ with a phase shift of δ is induced, containing both Newtonian and elastic parts.

From these stress and strain waves, the dynamic complex shear modulus $G^*(\omega)$ can be calculated (equation 2.14).

$$G^*(\omega) = \frac{\tau_0 e^{i\delta}}{\gamma_0} = \frac{\tau_0}{\gamma_0} \cos(\delta) + i \frac{\tau_0}{\gamma_0} \sin(\delta) = G'(\omega) + iG''(\omega) \quad (2.14)$$

$G'(\omega)$ is the storage modulus describing the elastic material properties and $G''(\omega)$ is the loss modulus describing the viscous properties of the material. In a purely Newtonian fluid, $G'(\omega) = 0$ and $G''(\omega) = \eta'\omega$. A purely elastic material in opposite, is in phase with the strain applied with $G' = G$ and $G'' = 0$. In real systems however, where these extreme cases do not occur, non-zero values for G' and G'' can be expected.

The complex viscosity η^* can then be calculated using equation 2.15, in relation to G^* .

$$\eta^*(\omega) = \frac{G^*(\omega)}{i\omega} = \eta' + i\eta'' \quad (2.15)$$

2.6.2. Confinement rheology

Confining of systems to thin layers can alter their flow behavior significantly from bulk rheologic properties. Brown *et al.* described the transition from flowing to jamming for densely packed non-Brownian suspensions. Shear thickening fluids are considered non-Newtonian, as their dynamic viscosity increases over some range of shear rate.

During this thesis, confinement shear rheology was used in order to measure normal forces exhibited by fat particles upon confinement, as they may be exhibiting normal forces on dough layers in laminated dough adversely impacting the fine microstructure.

2.7. Thermogelation of methylcellulose

Methylcelluloses are water-soluble gums which are derived from cellulose. They form thermally reversible gels making them highly interesting agents for food, pharmaceutical, constructional, and various other applications. They are used as thickeners, binders, film former, or water-retention agents. Additionally, they can be included as suspension aids, surfactants, lubricants, protective colloids, and emulsifiers. These cellulose ethers are nearly colorless, odorless and tasteless with no caloric value which makes it especially attractive for food products. Methylcellulose is accepted as food additive and has GRAS status (Generally Recognized As Safe). The viscosity of a formulation is easily adapted by choosing a suitable methylcellulose and varying the concentration. The viscosity range of methylcellulose reaches from 3 to 100'000 mPa·s. In bakery products, the gelation of methylcellulose increases the water retention which induces a higher volume and improved texture[?].

Two different basic structures of methylcellulose exist: Methylcellulose (MC) and hydroxypropyl methylcellulose (HPMC). MC and HPMC are built up on a repeating backbone of anhydroglucose units. In HPMC additionally, some anhydroglucose units are substituted as shown in figure 2.14. The amount of these substituent groups on the rings determines the properties of the methylcellulose and is referred to as degree of substitution (D.S.). For example, methylcellulose with a low D.S. are less water-soluble than the other with a high D.S.

Methylcellulose has a unique solubility behavior in water, as it hydrates and therefore completely dissolve at lower temperatures. Increasing temperatures decreases the solubility in the solvent up to a complete insolubility. Working at temperatures above 75 °C, the molecules are only dispersed in the solvent without a dissolution[?].

The temperature point where a methylcellulose solution gels and an increasing gel firmness can be observed is called gelation temperature. The gelation temperature

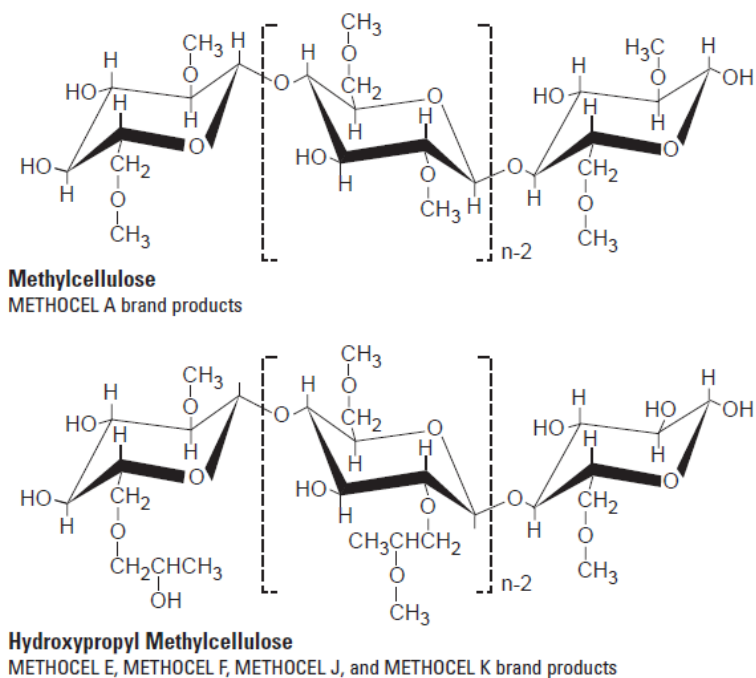


Figure 2.14.: Chemical basic structure of methylcellulose and hydroxypropyl methylcellulose¹.

2. Background

depends to a high degree on the applied heating and shear rate during measurement. Furthermore, the gelation temperature increases with decreasing degree of methyl substitution and increases with increasing hydroxypropyl substitution^{80;49}. Aggregation of MC leads to the formation of fibrillar structure, whereas HPMC, at least initially, favors more globular object⁶. Increasing the concentration of MC and HPMC, leads to a lowered gelling temperature. If the gel is cooled again after thermogelation induced by heating, the original state and viscosity are reached again. Therefore, MC and HPMC gels are completely thermoreversible⁷. Even though the gelation mechanism of methylcellulose is extensively investigated, various different mechanisms are reported. Most studies support a two-stage process for the gelation mechanism of aqueous methylcellulose solutions.

The sol-gel transition is suggested to be the first stage of the mechanism. It has been concluded, that phase separation and gelation occur simultaneously⁵⁹. Therefore, the clear methylcellulose solutions turn in into turbid gel upon gelation. This can be explained by hydrophobic interactions between molecules containing methoxyl groups⁸⁵. Advancing dehydration induce polymer-polymer interactions and the solution starts to gel.

At the second stage, the gel network formation occurs. They suggested a network formation due to disruption of the cage structure⁴³, polymer-polymer association⁸¹, or phase separation induced by hydrophobic interactions^{18;48;57}. These processes are mainly recognized by an increasing viscosity of the gels.

3. Materials, Processes and Methods

3.1. Materials

3.1.1. Vegetable Fat Fractions

Fat fractions used during this thesis are listed in table 3.1.

Table 3.1.: Confectionery Fats

	FA]	[%]	T[°C]	SFC [%]	IV	Dripping Point
Palm fat, mid-fraction	C14	<2	10	75-80	37	47-50
	C16	42-47	20	57-63		
	C18	4-6	30	34-39		
	C18:1	32-41	40	13-19		
	C18:2	5-9				
Palm fat super-stearin	C14	<2	10	85-95	21	61-63
	C16	68-78	20	85-95		
	C18	3-6	30	80-90		
	C18:1	12-18	40	75-85		
	C18:2	2-4				
Palm fat stearin	C14	<2	10	79-94	21	54-58
	C16	63-77	20	79-94		
	C18	3-8	30	62-80		
	C18:1	12-22	40	43-61		
	C18:2	2-6				
Canola oil	C16	4-6	10	0	112-117	(-10.5)-(-18.5)
	C18	1.5-2.5	20	0		
	C18:1	56-64	30	0		
	C18:2	18-26				
	C18:3	6-10				

3.1.2. Emulsifiers

Emulsifiers used during this thesis are listed in table 3.2.

Table 3.2.: Emulsifiers

	Compound	Producer	IV
Dimodan U/J Kosher	Mono- and diglycerides of fatty acids	DuPont Nutrition & Health, Denmark	105
Dimodan RT-Pel/B Kosher	Mono- and diglycerides of fatty acids	DuPont Nutrition & Health, Denmark	60
Dimodan HR Kosher	Mono- and diglycerides of fatty acids	DuPont Nutrition & Health, Denmark	<2
GRINDSTED PGPR 90 Kosher	Polyglycerol polyricinoleate	DuPont Nutrition & Health, Denmark	72-102
Leico Sun FM 580	Lecithin	Leico GmbH Hamburg,	95-100

3.1.3. Thickening Agents

Thickening agents used during this thesis are listed in table 3.3.

3.2. Processes

3.2.1. Emulsification

The theory behind rotor-stator and rotating membrane emulsification was previously described in section 2.2. For all emulsions, the fat phase was melted at a temperature of 80°C for at least 30 minutes in order to delete all crystal (-lattice) memory. Water was heated to the same temperature of 80°C . Fat and emulsifiers were blended according to recipe and the desired amount of water was added during processing and emulsified as described below for different emulsification processes.

Table 3.3.: Thickeners

	Producer	Compound
Methocel A15 Methocel A4C Methocel A15C Methocel SGA7C	Methylcellulose	Dow Chemical Company, USA
Methocel E19 Methocel F50 Methocel K99	Hydroxypropyl Methylcellulose	Dow Chemical Company, USA
Inulin	Frutafit TEX	Sensus, Netherlands
Maltodextrin	C DRY Light	Cargill Haubourdin, France
Sodium Alginate	GRINDSTED Alginate LFS 200	DuPont Nutrition & Health, Denmark

Rotor-stator emulsification

Emulsions were produced by rotor-stator emulsification at a batch size of 2000g. The fat and emulsifier blend was added to a temperature controlled container (80°C) and stirred with a rotor-stator mixer type Polytron PT 6000 (Polytron PT 6000, Kinematica AG, Switzerland) at 3000rpm for 3 min in order to reassure homogeneous mixing. The measured amount of water was added carefully while the rotational speed of the mixer was increased to 8000rpm. The emulsion was dispersed at 8000rpm for 10min.

Rotating Membrane emulsification

A continuously working rotating membrane (ROME) device (Megatron FM 1-56 SO, Kinematica AG, Switzerland) was used to produce W/O-Emulsions. The ROME device consists of a cylindrical membrane module which is mounted on a hollow shaft and enclosed by an outer cylinder. The rotating membrane module was a Poremet mesh membrane (Bopp AG, Switzerland), had a diameter of 56mm, a length of 60mm and the respective gap width between membrane and outer cylinder was 1mm. The dispersed phase (in case of a W/O-emulsion distilled water) was pumped through the hollow shaft into the membrane module and dispersed into the continuous phase (in

case of a W/O-emulsion oil) which was flowing through the gap between membrane and outer cylinder. Emulsion droplet size is determined by the most close-meshed layer of the membrane (2 pore size), rotational speed of the ROME device, disperse and continuous phase viscosities as well as flow rates of the two phases.

The temperature of the ROME device was set at 80°C . Flow rate of disperse and continuous phase were controlled by tempered eccentric screw pumps type NM 008BY03S12B (Netzsch, Germany). Ratio of dispersed to continuous fraction in the emulsions was controlled by selecting respective flowrates of the two pumps. In order to reach a fine droplet size, the rotational speed of the device was set at 8000rpm .

3.2.2. Spray Chilling

Process Setup

A cylindrical shaped spray tower as shown in figure 3.1 (inner diameter 100 cm and height 370 cm) produced by the workshop at the Laboratory of Food Process Engineering at ETH Zürich was used to manufacture the novel fat system. The spray tower temperature was controlled at 4°C by liquid nitrogen, which was atomized into the tower by six concentrically arranged nozzles from top. Liquid nitrogen flow rate was set through a feedback dosing valve (VariPak Serie 28000, PanGas, Zurich, Switzerland) operated by a control software (Spraying-Controller V100, LabVIEW 8.5, National Instruments, Austin TX, United States of America).

Two different components (A+B) can be sprayed into the spray chilling tower simultaneously. Container A was a temperature controlled, double-walled vessel, allowing tempered spraying of component A. The fat or W/O-emulsion contained in A was pumped by a tempered volumetric eccentric crew pump (Hilge GmbH Co. KG, Bodenheim, Germany) controlled by a MEGATRON[®] FM 12-50 / 2 HR (Kinematica AG, Lucerne, Switzerland). Phase A was sprayed into the tower by a temperature controlled external mixing spray nozzle (Spraying Systems Co.[®], Wheaton IL, USA) located in the center of the tower lid. The nozzle used was a two-component system type SU12 consisting of an outer atomizing air cap (type 73160) and an inner fluid cap (type 2850).

Container B was set at 20°C . Component B (canola oil) was pumped by a volumetric eccentric crew pump (Hilge GmbH Co. KG, Bodenheim, Germany) connected to an external mixing spray nozzle (Spraying Systems Co.[®], Wheaton IL, USA) located at a height of 250cm from the top of the tower at the wall of the tower, which allowed injection of component B at an angle of 45° . The nozzle used was a two-component system type SU12 consisting of an outer atomizing air cap (type 73160) and an inner fluid cap (type 2850).

Injecting two different fat based phases into the temperature controlled spray-chilling tower allowed homogenous mixing of two phases and leads to a composite fat system, consisting of a fat particle in oil suspension. No further post-processing (mixing) is required.

3.3. Methods

3.3.1. Differential Scanning Calorimetry

Differential Scanning Calorimetry (DSC) is a thermoanalytic method used to quantify heat flow to and from a sample connected to chemical reactions and physical transitions that encompass endothermic and exothermic processes or changes in heat capacity⁶². DSC measures temperatures and heat flows associated with transitions in materials in a controlled atmosphere: endothermic such as melting and dehydration and exothermic such as crystallization and nucleation.

A STAR^e system consisting of a DSC822^e module and the STAR^e software version 8.10 (Windows) (Mettler Toledo GmbH, Greifensee, Switzerland) was used to measure melting and crystallization properties of fats, emulsions and composite fat powders. Furthermore, DSC was used to quantify water released during baking from dough and fat fractions of composite dough in order to estimate leavening forces generated by individual layers. Two aluminum pans ($V_{\text{pan}}=40\mu\text{m}$), one containing the sample and an empty reference pan were placed in the DSC measurement cell, allowing simultaneous heating and cooling at a controlled rate. The temperature of the sample pan was constantly adjusted to match the temperature of the empty reference sample and the heat flow difference was measured.

The temperature of the DSC822^e module was controlled using a Peltier element. In order to reassure a controlled atmosphere in the measurement chamber, nitrogen was used as purge gas at a flow rate of $1L/min$. The device was calibrated using a sample of Indium with known melting temperature and melting enthalpy.

3.3.2. Thermo Gravimetric Analysis

Thermogravimetric Analysis (TGA) is a method, where the mass of a sample is measured as a function of temperature or time⁷. The sample was heated at a constant rate and sample mass was plotted against temperature. A STAR^e system consisting of a TGA 1 module and the STAR^e software version 8.10 (Windows) (Mettler Toledo GmbH, Greifensee, Switzerland) was used to simulate the baking process and measure

vaporization of water during baking of emulsions, composite fat powders and puff pastries.

3.3.3. X-Ray Crystallography

Fundamentals of X-Ray Diffraction techniques, their applications and measurement principles have been described in detail⁸⁶. To determine the crystal structure of a material, x-ray beams with a wavelength in the order of the atomic distances are required. The symmetry of the underlying crystal lattices determine the intensity of scattered x-ray beams.

X-ray powder diffraction measurements are based on Bragg's law, which establishes a relationship between diffraction angle (Bragg angle), wavelength and plane distance⁷⁴. As described by Bragg, diffraction from a crystalline sample can be described by a mirror reflection of the incident x-ray beam from the crystallographic planes. The scattering of x-rays results in specific diffraction patterns and depends on the crystalline subcell geometry.

Diffraction of x-ray beams from the underlying crystal structure (equally spaced crystal planes) is only possible at specific angles, which have been established by Bragg's law. Positive interference can be observed if the plane distance d_p is equivalent to a multiple of the wave length, leading to an increase in radiation intensity at respective reflection angle of the incident beam. The relationship between the scattering angle θ and the plane distance d_p is described by Bragg's law 3.1, where n is an integer and λ_w is the wavelength of the incident wavefront. The integer n is linked to the order of reflection, and as orders $n > 1$ can always be represented by first order reflections ($n = 1$), its value is taken as 1 in all calculations.

$$d_p = \frac{n * \lambda_w}{2 * \sin(\theta)} \quad (3.1)$$

Since the wavelength λ of the x-ray beams and the incident angle θ are known for all measurements, d_p -spacing in relation to the peak intensities can be calculated by Bragg's law.

Measurement principle

X-ray powder diffraction measurements of fat powder was performed using a D8 advanced X-Ray diffractometer (Bruker axs GmbH, Germany). Fat powders were filled into sample holders and a blade was used to create a planar surface of the sample.

A $Cu-K\alpha 1$ -radiation source was used ($\lambda = 0.15406nm$, $E_{beam} = 40keV$) and samples were rotated during measurement (scanned circular area with a diameter of $6mm$) for statistical reasons. In order to avoid heating of the sample during measurement, measurement time was kept short. The device was operated at a diffraction angle $\theta = 18 - 25^\circ$. Step size was 0.02° with a time per step of $0.8s$.

3.3.4. Laser Particle Size Analysis

The size and size distribution of fat particles was determined by laser diffraction analysis using a Beckman Coulter LS 13320 (Beckmann Coulter Inc., Germany/USA) equipped with a $780nm$ laser beam. Hydriol was used as a carrier substance in the sample handling module. Stirrer velocity in the sample handling module was set to 20% in order to reassure homogeneous distribution of fat powder particles throughout the liquid reservoir of the sample handling module. Measurement time was set to $90s$. For all fat powders, $5g$ of powder were pre-diluted in $20mL$ of Hydriol prior to transfer into the sample handling module.

In this work, volume based particle size distribution was used and the median $d_{50,3}$ distribution of the fat particles was determined using the Mie theory using a refractive index of 1.45 for Hydriol. All measurements were performed in triplicate.

3.3.5. Confocal Laser Scanning Microscopy (CLSM)

Microscopy has been used broadly in food science to characterize structural organization of food materials and as a tool towards a better understanding of material properties such as texture, stability and appearance³⁹. Dürrenberger *et al.* highlighted, that in opposite to conventional light microscopy, the light source is replaced by laser and a scanning unit and a pinhole in the back focal plane is added to improve the limited depth of focus in light microscopy. The main advantage of CLSM over conventional microscopy is the ability to obtain optical slices through a 3-D specimen, allowing visualization of rather thick, 3-D samples. It has to be noted as well, that samples mostly need some kind of pre-treatment prior to image acquisition. By using fluorescent dyes, selected regions in the sample can be specifically dyed and visualized using a laser operating at a corresponding wavelength.

During the experimental section of this thesis, Nile red (Sigma-Aldrich, USA) was used as a lipophilic dye and Nile blue was used to stain gluten protein contained in puff pastry dough. The dyes used during the experimental section of this thesis are listed in 3.4.

Table 3.4.: Dyes used for staining of samples for CLSM.

Dye	Absorption $\lambda_{max}[nm]$	Emission $\lambda_{max}[nm]$
Nile red in methanol	552	636
Nile blue in methanol	626	637

A Zeiss LSM 780 (Zeiss, Germany) was used for visualization of emulsion and composite dough structures. The CLSM was equipped with an Argon laser and the software Zeiss Zen Black (Zeiss, Germany) was used for image acquisition.

Images of emulsions for assessment of emulsion stability as discussed in chapter 4 were acquired using a 63x 1.4NA Oil Plan-Apochromat DIC M27 objective with $0.1 \mu m/pixel$ and a resolution of $1355 \cdot 1355$ pixels. Dough slices analyzed by CLSM were acquired using a 10x 0.3NA EC Plan-Neofluar Ph1 M27 objective.

3.3.6. Cryo Scanning Electron Microscopy

Scanning electron microscopy has been widely used to capture images of samples by scanning the surface with a focused electron beam. The emission, transmission and reflection capacity of the sample can be correlated to the surface properties resulting in a surface scan image of the sample.

For conventional SEM imaging, specimen need to be electronically conductive. Therefore, non-conducting materials are usually coated with an ultra-thin coating of electronically conducting material, such as graphite, gold, platinum or others. This generates a conductive surface layer enabling surface scanning of the specimen by the SEM electron beam.

Fat samples were analyzed by cryo SEM during this thesis. Cryo SEM was applied in order to avoid changes to the sample during analysis of the sample through radiation damage caused by the electron beam. Powdered fat samples were filled into aluminum tubes (inner diameter: $1.16mm$, wall thickness: $0.13mm$, length: $20mm$). The aluminum tubes had a predetermined breaking point, where they were ruptured prior to coating with a conductive layer. Samples were taken from the process, filled into the aluminum tubes and immediately frozen in liquid nitrogen at $-196^{\circ}C$ in order to avoid structural changes between production of the samples and sample preparation prior to SEM image acquisition.

Samples were fixed in a specially manufactured sample holder, while being continuously immersed in liquid nitrogen atmosphere reassuring constant temperature of the sample and rupture of the aluminum sample holder tube at the predetermined rupture point created a pristine sample surface. After transfer into a freeze-etching

device BAF 060 (Bal-Tec AG, Liechtenstein), the samples were freeze etched and covered with a conductive tungsten layer under vacuum conditions (10^{-6} to 10^{-7} bar and -120°C). Freeze etching was carried out at an elevated temperature of -95°C for 5 minutes in order to remove ice and contamination from the sample surface. In a next step, the sample was coated with tungsten at 1.98kV and 0.98mA . An emission rate of $0.02\text{nm} * \text{s}^{-1}$ at an emission angle of 45° was used to achieve a coating with a thickness of 3nm . A secondary coating layer was applied while changing the emission angle continuously from $45 - 90^{\circ}$ and back. The sample was then transferred to the SEM using a cryo transfer system Leica EM VCT100 (Leica Microsystems GmbH, Germany).

A cryo scanning electron microscope Zeiss Gemini 1530 FEG (Carl Zeiss AG, Germany) was used for image acquisition after the sample preparation as described above. The device was operated with the electron beam set at 2.0kV with a working distance to the sample of $4.0 - 4.5\text{mm}$ and was operated at a temperature of -120°C .

3.3.7. Karl-Fischer Titration

Karl-Fischer titration is a method introduced by³⁴ allowing quantitative determination of water content in a material. Water is titrated with Iodine in a volumetric titration device 784 KFP Titrino, 703 TiStad (Metrohm AG, Switzerland). Powder fat samples were dissolved in a solution consisting of equal parts methanol and chloroform, which lead to a dissolution of the continuous fat matrix and solution of the water contained. The obtained solution was titrated using Hydranal®-dry (Sigma-Aldrich, Switzerland) and the total water content contained was calculated. The device was calibrated prior to all measurements using a water standard provided by Sigma-Aldrich.

3.3.8. Sinterface PAT-1 Tensiometer

Pendant and sessile drop tensiometry can be used to measure static interfacial tension and surface tension. Interfacial tension of water in palm fat systems were characterized using a sessile droplet tensiometer PAT-1 (Sinterface Technologies, Germany) equipped with a needle of 1.96mm diameter. Setup and methodology was described in detail by⁵⁸.

Static, isovolumetric interfacial tension measurements of w/o emulsions using different emulsifiers in the fat phase were performed. The contour of the drop was monitored and fitted using the Young-Laplace equation and the interfacial tension σ was calculated.

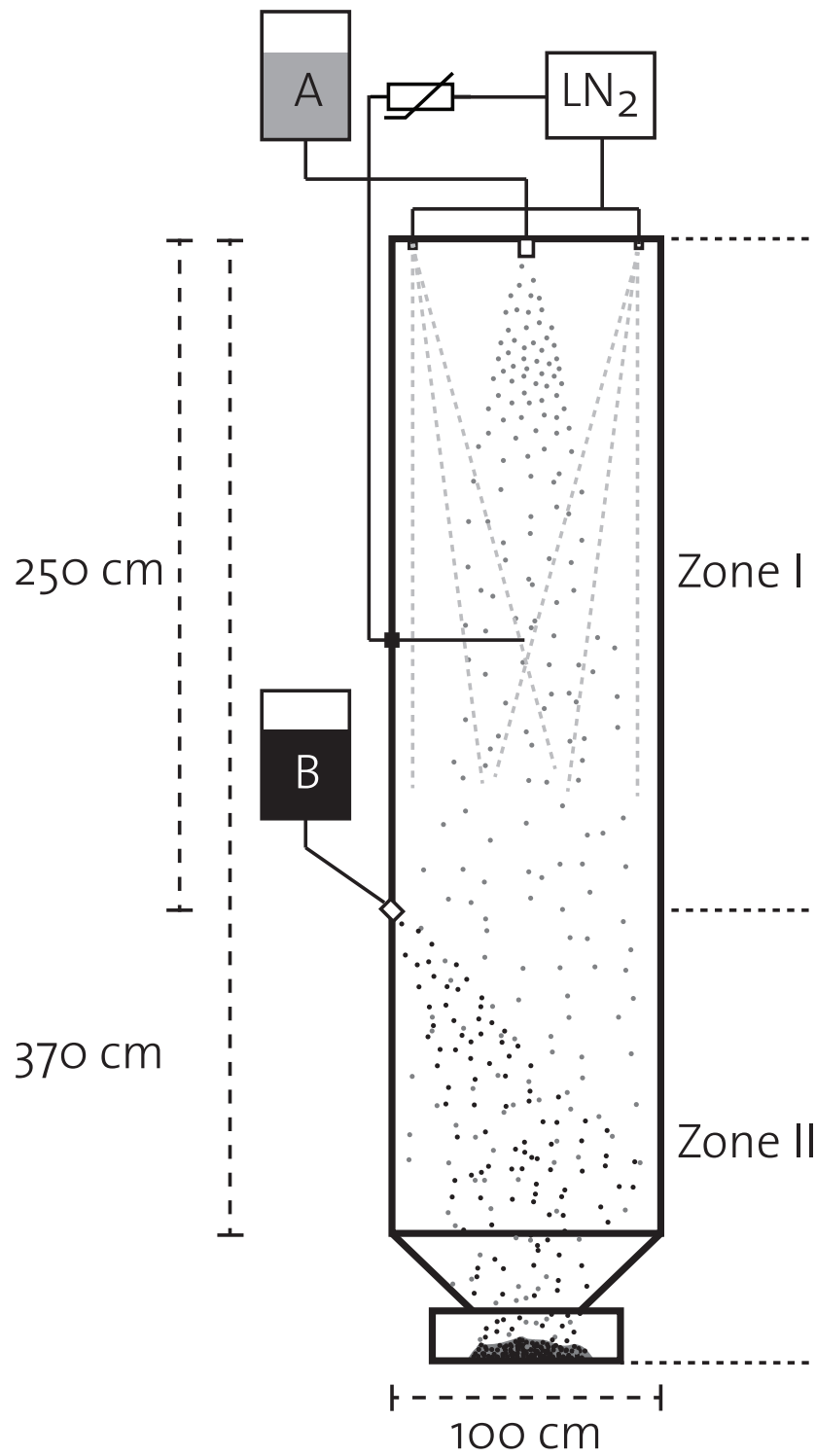


Figure 3.1.: Schematic drawing of the spray tower.

4. Short-term Emulsion Stability

A stable emulsion is a prerequisite prior to spray chilling and obtaining the powdered fat system. Spray chilling leads to emulsion-based solid fat particles, stabilized by a solid fat matrix. As the microstructure of the solid fat particles is determined by the droplet size distribution of the underlying emulsion, (meta-)stable and finely dispersed W/O emulsions are essential. In literature, short-term stability assessment of emulsions has been described. However, the term 'short-term' referred to the stability of emulsions in a time-frame of hours to days^{93;35;94}.

During the production of powder fats, temporal stability within a frame of $T_r = 240s$ (depicted green in figure 4.1), while being pumped from the emulsification vessel to the spraying nozzle and being stabilized by the solid matrix of the individual fat particle, is required. In order to meet these requirements, process (rotor-stator and rotating membrane emulsification), materials (disperse phase fractions, stabilizers used) and respective combinations and synergies thereof were investigated and optimized.

4.1. Method

Ultra short-term emulsion stability assessment requires an exact, high temporal resolution measurement method. It had to be ensured, that emulsion samples could be taken at discrete time steps, while conserving the microstructure for analysis. A novel sampling method for emulsion samples was developed and analysis thereof was performed by confocal laser scanning microscopy. Quantitative parameters were extracted by image analysis.

4.1.1. Sampling

Emulsions were obtained as described in section 3.2.1. The fat phase was stained with Nile red (Sigma-Aldrich, USA) before emulsification. Samples were taken at time steps T_r after stopping the emulsification. T_r describes the discrete time after completion of the emulsification process, at which samples were taken. The emulsions were instantly chilled on microscopic slides chilled at 0°C, leading to instant crystallization of the

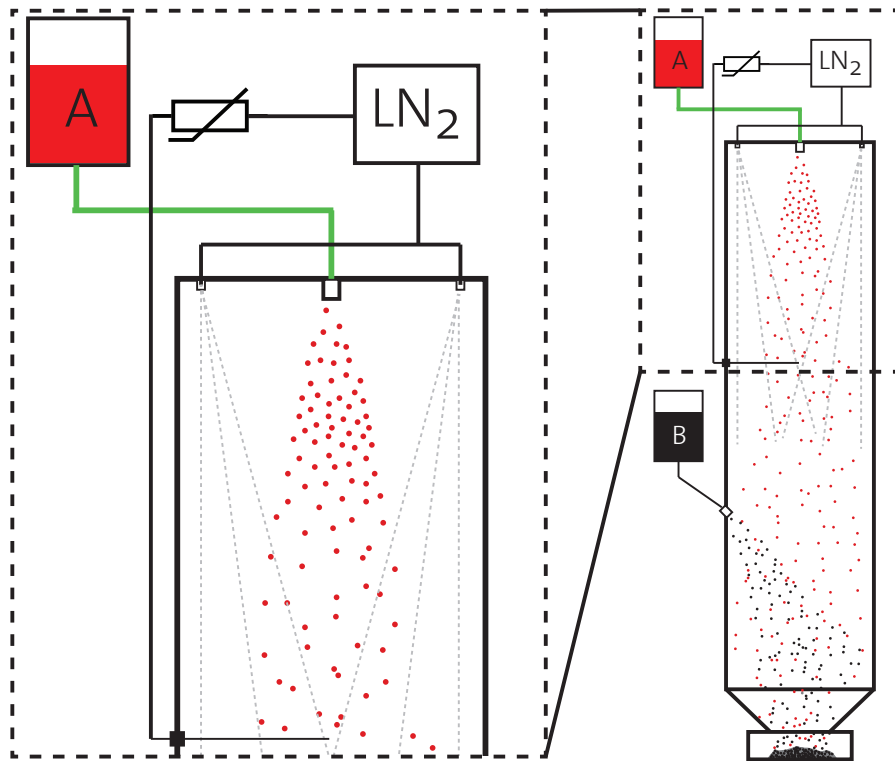


Figure 4.1.: Schematic drawing of the spray tower. Crucial time for emulsion stability in green.

fat while avoiding any phase changes of the water phase. Emulsion sampling was performed as shown in figure 4.2.

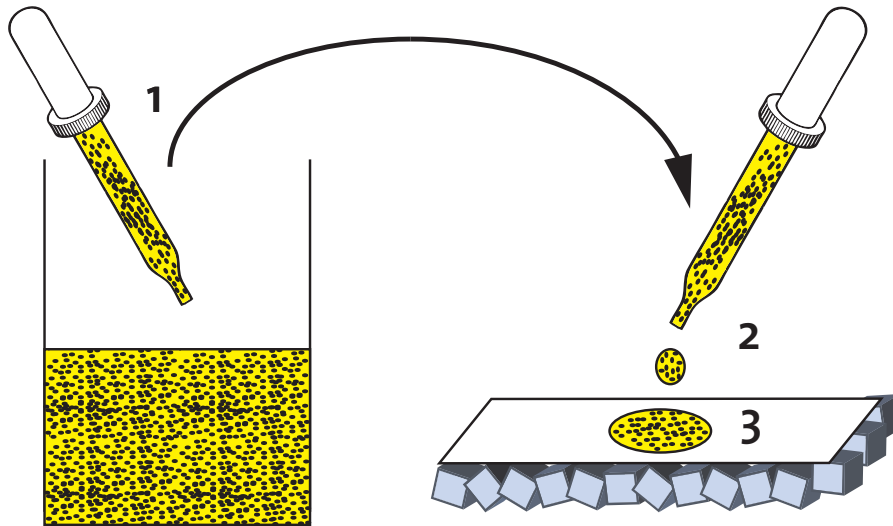


Figure 4.2.: Sampling of Emulsions: (1) Samples taken at time $T_r = 0s, 20s, 40s, 60s, 90s, 120s, 180s, 240s$ after stopping the emulsification process, (2) samples pipetted onto chilled microscopic slide at $T = 0^\circ C$, (3) emulsion droplet instantly solidified and stabilized for subsequent CLSM image acquisition.

4.1.2. Image acquisition and analysis

Images of emulsions were acquired using a Zeiss LSM 780 (Zeiss, Gernymn) equipped with a 63x 1.4 Oil Plan-Apochromat DIC M27 objective. Resolution was 0.1/pixel at an image size of 1355 x 1355 pixels. For each sampled emulsion, at least three pictures were acquired at random locations.

Image analysis was performed by an ImageJ (National Institutes of Health, USA) macro as shown in figure 4.3. The macro consisted of the following image processing steps:

1. Step 1: The original CLSM picture 4.3a was thresholded and inverted resulting in 4.3b.
2. Step 2: The output of step 1 4.3b was segmented by applying an adjustable watershed operation with a tolerance set at 15 resulting in 4.3c.

4. Short-term Emulsion Stability

3. Step 3: The output of step 2 4.3c was analyzed by the function "Analyze Particles" using the settings "size=1-200, show=Ellipses" resulting in graphic output as shown in 4.3d and numeric output of droplet sizes and droplet size distributions.

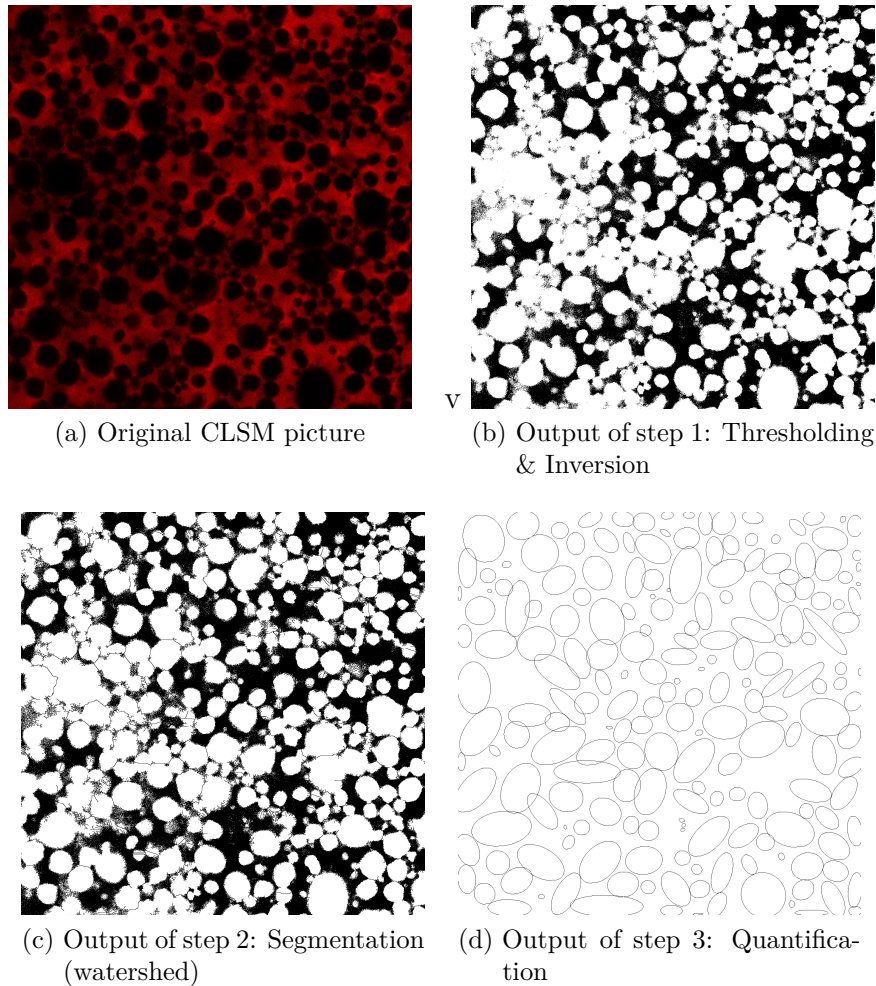


Figure 4.3.: Image processing of emulsion CLSM pictures

From these droplet size distributions, the median droplet size $d_{50,3}$ for each emulsion was calculated. Median droplet size values are always based on measurements in triplicates.

4.2. Results

4.2.1. Identifying suitable emulsifiers

Visual observation of emulsions and CLSM imaging were used to identify suitable emulsifiers from the broad range of surfactants currently used in food fat industry. PGPR was the only single emulsifier able to sufficiently stabilize highly concentrated ($\Phi_E > 0.7$) W/O emulsions. PGPR in combination with other emulsifiers was used, to identify possible synergistic effects between emulsifiers.

Figure 4.4 illustrates the macrostructure and stability of emulsions using different emulsifier and emulsifier combinations. PGPR (0.3%) used as single emulsifier (4.4a) lead to a stable emulsion. Combining PGPR with 0.3% or 1% Lecithin (4.4b + 4.4c) or 0.3% Dimodan U/J (4.4d) lead to stable emulsions with finely dispersed droplets. Using 0.3% Dimodan RT-Pel in combination with 0.3% PGPR can be linked to a clustered emulsion substructure and partial phase inversion (4.4e). A combination of 0.3% Dimodan HR and 0.3% PGPR did lead to phase inversion and did not result in a stable emulsion.

These findings can be explained with the microstructure and the underlying interfacial properties of the used emulsifiers. The iodine value (IV) is a measure for the degree of unsaturation of the fatty acids. High IV values are linked to a high degree of unsaturation. As previously discussed⁴⁵, unsaturated mono-diglycerides (high IV values) are used for low fat spreads and low fat W/O emulsions. This can be explained by the higher surface tension reducing activity of unsaturated mono-diglycerides compared to saturated mono-diglycerides. Less emulsifier molecules are necessary to stabilize water droplets in the oil phase²⁷. Also, unsaturated mono-diglycerides might structure water through cubic phases³⁷.

As all stable emulsions shown in figure 4.4a-4.4d (produced with PGPR, Lecithin and Dimodan U/J as emulsifiers) possess high IV values in the range of 72 to 105 (listed in table 4.1) and are highly unsaturated. This explains, why these emulsions are stable opposite to the emulsions produced with Dimodan RT-Pel and Dimodan HR with significantly lower IV values and higher degrees of saturation.

PGPR was identified as a highly efficient single emulsifier. Visual observations point to possible synergistic interactions when combining PGPR with unsaturated monodiglyceride emulsifiers (Dimodan U/J) and lecithin. Therefore, emulsion stability (droplet size distribution and evolution over time) using different emulsifier combinations and concentrations and different disperse phase fractions was investigated.

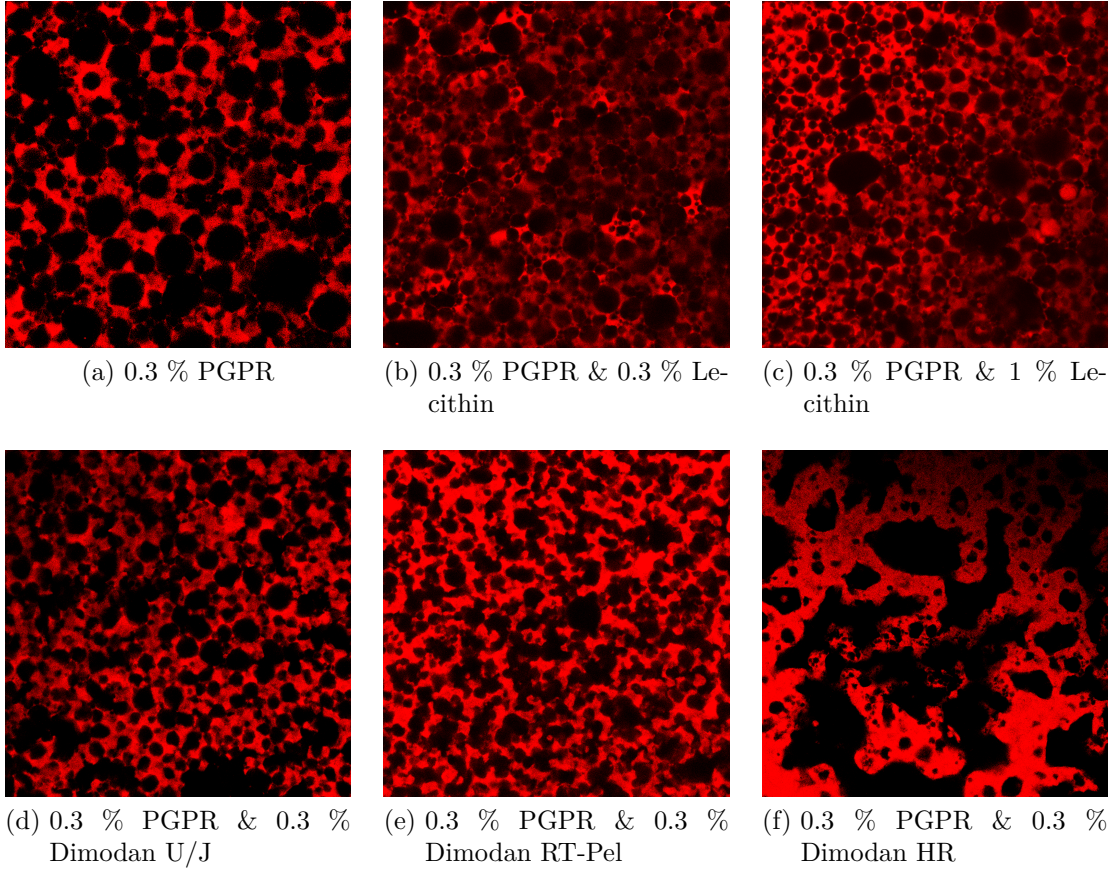


Figure 4.4.: CLSM: Effect of different emulsifiers on emulsion macrostructure and stability of emulsions with a disperse fraction $\Phi_E = 0.7$

4.2.2. Microscopic observation of jammed emulsions

Random packing of spheres has been discussed to a large extent in literature^{95;22}. However, little is known about polydisperse packings of spheres. A granocentric model for random packing has been applied in literature¹⁷, which initially forms a set of neighbors, followed by the creation of contacts. The model was in accordance with confocal laser scanning microscopy images. The calculated global maximum packing fraction Φ_E was within 0.5% of the experimentally measured value $\Phi_E = 0.664$, and slightly higher than $\Phi_E = 0.64$ for monodisperse systems. Recent publications support these findings and also discuss advanced models to calculate Φ_E for jammed systems^{105;21}.

By proper processing, high disperse phase fraction (jammed) emulsions $\Phi_E = 0.9$ were obtained. Microscopic images (4.5) were acquired in order to understand and explain the microstructure of jammed emulsions.

Table 4.1.: Iodine Values (IV) of emulsifiers.

Emulsifier	Iodine Value (IV)
PGPR	72-103
Lecithin	85-95
Dimodan U/J	105
Dimodan RT-Pel	60
Dimodan HR	<2

Figure 4.5 supports the theoretical basics as discussed above. Figure 4.5a shows a micrograph of a relatively unjammed system at $\Phi_E \sim 0.7$. Water droplets are spherical and intact. In a jammed system ($\Phi_E \sim 0.9$, 4.5b) in opposition, water droplets appear deformed. Deformation of water droplets explains the theoretically, for rigid spheres unreachable $\Phi_E \sim 0.9$. Deformation of spheres leads to a much more dense packing and thereby a much higher concentrated emulsion system.

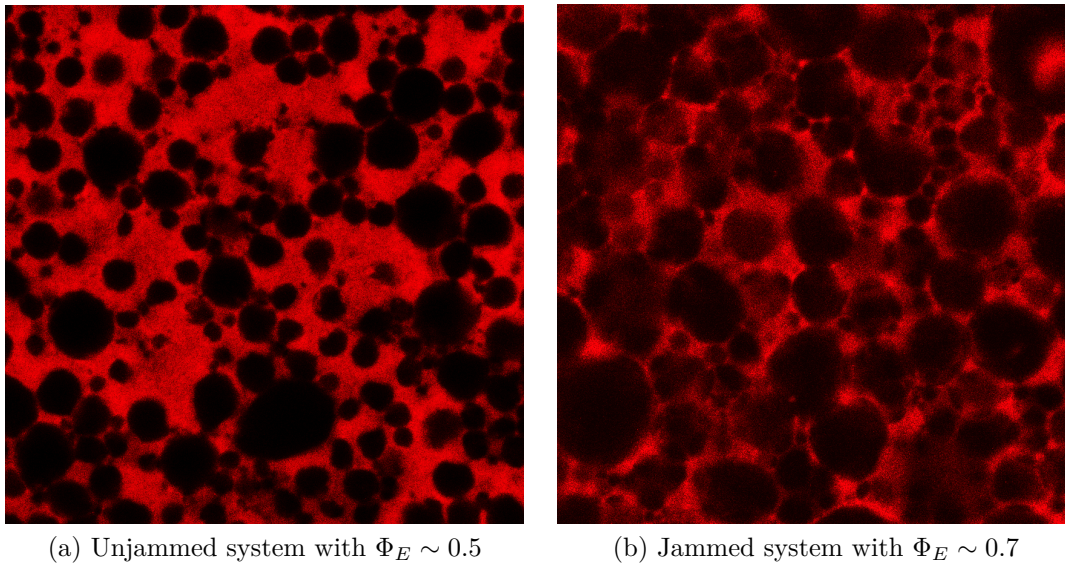


Figure 4.5.: Jammed emulsions: Visualization by CLSM

4.2.3. Short-term emulsion stability

Emulsions were produced by rotor-stator or rotating membrane emulsification (3.2.1) and short-term stability ($T_r = 0 - 240s$) was assessed by confocal laser scanning microscopy (CLSM) and subsequent image analysis as described in 4.1.

4. Short-term Emulsion Stability

Figure 4.6-4.7 illustrate the average mean diameter $D_{50,3}$ of emulsions at different disperse phase concentrations Φ_E and emulsifiers used. Underlying temporal stability is plotted in A. The displayed value $D_{50,3}$ stands for the average mean diameter during a time frame of 0 – 240s for a specific emulsion (with a defined emulsifier and disperse phase fraction). The y-error bar is the standard deviation $\theta_{D_{50,3}}$ of $D_{50,3}$, which can be interpreted as the change in droplet size between $T_r = 0 - 240$ and thereby the destabilization of the emulsion.

Emulsions produced by rotor-stator are listed in figure 4.6. For all used emulsifiers and emulsifier combinations, an increased disperse phase fraction Φ_E can be linked to a larger droplet size. A combination of 0.3% PGPR & 0.3% Dimodan U/J leads to most stable emulsions with smallest droplet size. Exact numeric values are listed in table A.1.

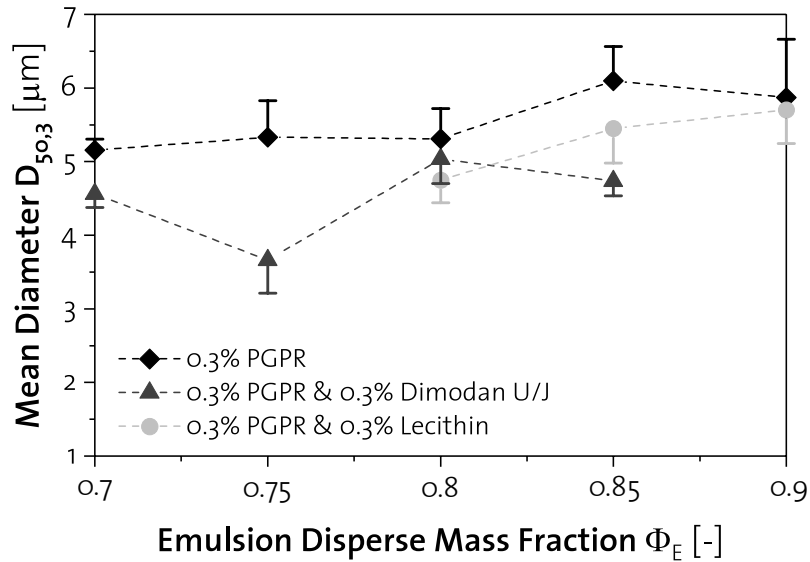


Figure 4.6.: Stability of emulsions produced by Rotor-Stator emulsification.

Applying a rotating membrane emulsification process using a metal laminated Poremet mesh membrane (Bopp AG, Switzerland) consisting of five woven wire mesh layers of different pore size (nominal pore size of $2\mu\text{m}$) leads to a significant decrease in emulsion droplet size. A combination of 0.3% PGPR and 0.3% Dimodan U/J is still the most efficient emulsifier combination as shown in figure 4.7 and leads to finely dispersed water droplets with $D_{50,3} = 3.0 - 4.0\mu\text{m}$. As already observed for rotor-stator emulsification, an increase in emulsion disperse mass fraction is linked to a larger droplet size. However, this trend is less pronounced than for emulsions produced by rotor-stator.

Figure 4.7 shows, that $\theta_{D_{50,3}}$ is significantly larger for emulsions produced by ROME, compared to emulsions produced by rotor-stator. This may be explained by equation

4.1, where σ is the interfacial tension, R is the droplet radius and p_k is the Laplace pressure. The Laplace pressure is a measure for the pressure difference between the inside and the outside of a curved surface.

$$p_k = 2\sigma/R \quad (4.1)$$

As evident from equation 4.1, the lower stability of the smaller droplet size emulsion produced by ROME may be explained by:

1. Interfacial tension increase: Increase in interfacial area when the droplet size is decreased. As a constant amount of emulsifier was added to all emulsions to stay within the legal limits (0.3% of the total emulsion weight m_{tot}), emulsions with a smaller disperse phase droplet size and therefore a larger total interface area, were stabilized by a lower local emulsifier concentration per unit surface area. A lower interfacial emulsifier concentration is proportional to a higher interfacial tension leading to a lower stability of emulsion droplets.
2. Reduction of the droplet radius itself leads to lower stability of smaller droplets.

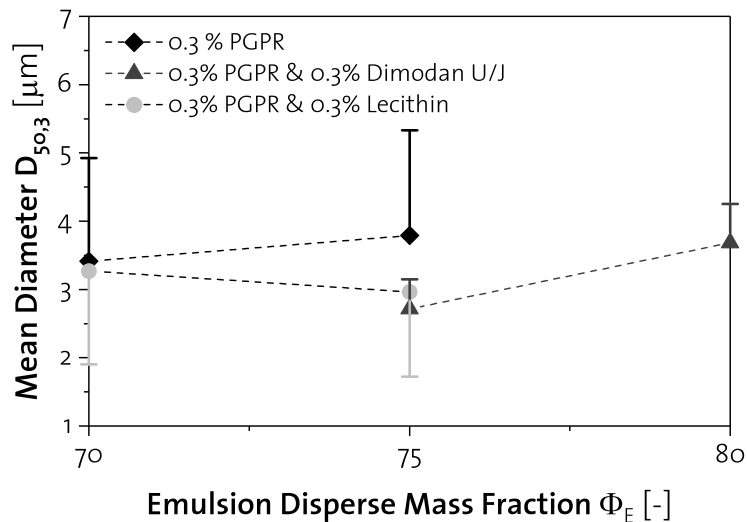


Figure 4.7.: Stability of emulsions produced by rotating membrane emulsification.

4.2.4. Interfacial Tension

Interfacial tension σ of a water droplet enclosed by palm fat was measured by pendant drop tensiometry as described in section 3.3.8.

4. Short-term Emulsion Stability

The fat phase contained either no emulsifier or PGPR, Dimodan U/J or a combination thereof at a concentration of 0.3% (concentration limit set by the swiss food law). In figure 4.8, the respective interfacial tension kinetics are shown.

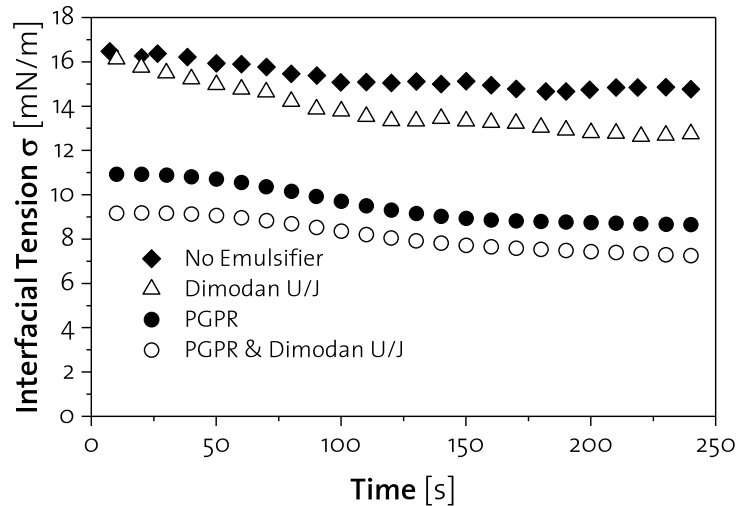


Figure 4.8.: Interfacial tension of W/O systems as a function of time for different emulsifiers.

The interfacial tension measured for water droplet in pure palm fat after a waiting time of 240s was at a stable value of $\sigma = 14.5mN/m$. This value is comparable to values shown in literature for pure water in palm fat systems²³. Using distilled monodiglyceride type emulsifiers Dimodan U/J lead to a lower interfacial tension of $\sigma = 13.5mN/m$.

PGPR in opposite, is known to be a very efficient emulsifier for W/O type emulsions, leading to a significantly lower interfacial tension of $\sigma = 13.5mN/m$ compared to distilled monodiglycerides type emulsifiers. Furthermore, an even lower interfacial tension was found when combining PGPR and Dimodan U/J at equal concentrations of 0.3%.

These results are in line with the assessment of short-term emulsions stability in section 4.2.1-4.2.3 and confirm, that a combination of PGPR & Dimodan U/J is a more efficient emulsifier combination compared to using PGPR or Dimodan U/J as single emulsifier in the continuous phase.

4.2.5. Rheology

Figure 4.9 illustrates flow curves measured for W/O emulsions with different emulsion disperse mass fractions $\Phi_E = 0.7, 0.75, 0.8, 0.85$ at 80°C using either 0.3% PGPR or a combination of 0.3% PGPR + 0.3% Dimodan U/J.

The flow curves were fitted using a Herschel-Bulkley model (equation 4.2), where τ stands for the shear stress, τ_0 is the yield stress, k a consistency factor, $\dot{\gamma}$ the shear rate and n_H is the flow index (power law exponent). The Herschel-Bulkley fitting parameters are listed in table 4.2.

$$\tau = \tau_0 + k \cdot \dot{\gamma}^{n_H} \quad (4.2)$$

All emulsions exhibit shear thinning behavior, which is further supported by the flow index n_H . For 0.3% PGPR, n_H is closest to Newtonian behavior with $n_H = 0.71$ at relatively low emulsion disperse mass fractions Φ_E of 0.7. With increasing Φ_E , n_H decreases to a value of as low as $n_H = 0.51$ for $\Phi_E = 0.85$ as listed in table 4.2. The same trend is valid for a combination of 0.3% PGPR and 0.3% Dimodan U/J.

From figure 4.9 it is obvious, that higher disperse phase concentrations Φ_E lead to higher viscosities. This is further supported by an increasing Herschel-Bulkley yield stress τ_0 for higher Φ_E values. Emulsions containing 0.3% PGPR and 0.3% Dimodan U/J as emulsifier show higher yield stresses than emulsions containing only 0.3% PGPR as emulsifier at the same Φ_E values. Low disperse phase fraction $\Phi_E = 0.7$ emulsions have a yield stress of 0, whereas highly concentrated emulsions at $\Phi_E = 0.85$ exhibit τ_0 values of 15.4 and 35.3 respectively. This increase in yield stress τ_0 and viscosity for higher Φ_E values can be explained by a higher number of water droplets dispersed at higher Φ_E leading to more possible interactions between water droplets. It can also be observed, that a combination of PGPR and Dimodan U/J, in comparison to PGPR as a sole emulsifier, consistently for all Φ_E leads to higher τ_0 and lower n_H values. This can be explained with a more efficient stabilization of emulsion droplets, when an emulsifier blend is used leading to smaller droplets compared to PGPR as single emulsifier.

4.3. Conclusions

In this section, short-time stability of W/O emulsions was assessed. The ultra short-time stability of emulsions while being pumped from the emulsification vessel to the spraying nozzle was of particular interest. Upon atomization in the spray-chilling

4. Short-term Emulsion Stability

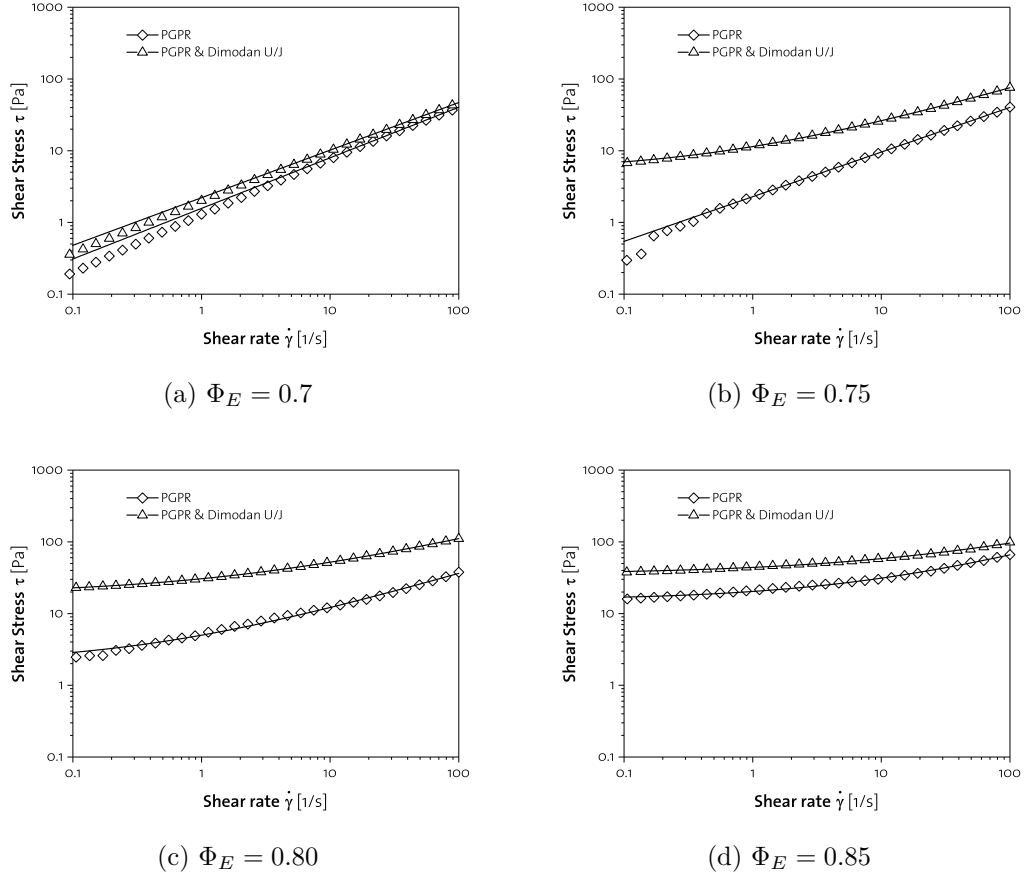


Figure 4.9.: Flow curves for different W/O emulsions at different disperse phase fractions Φ_E . \blacksquare = 0.3%PGPR, \square = 0.3%PGPR+0.3%Dimodan U/J

tower, a solid fat crystal network forms leading to steric stabilization of the emulsion.

Confocal Scanning Laser Microscopy (CLSM) was identified as a favourable method for indirect quantitative investigation of the ultra short-term stability of emulsions. The most important property of an emulsion on the macro-scale is the droplet size distribution. In general, increasing disperse phase concentrations in emulsions lead to destabilizing effects. These destabilizing effects can be delayed by suitable emulsifiers (surfactants).

Therefore, emulsion droplet size distributions and droplet morphology of highly concentrated emulsions were assessed by CSLM. The influence of different emulsifiers and emulsifier combinations were analyzed. Applying only PGPR as sole emulsifying agent lead to small water droplet size distributions, but insufficient temporal

Table 4.2.: Herschel-Bulkley fitting parameters derived for various emulsion disperse mass fractions Φ_E and emulsifier combinations (■ = 0.3%PGPR, □ = 0.3%PGPR+0.3%Dimodan U/J) from figure 4.9.

Φ_E	Emulsifier	τ_0	k	n_H	R^2
0.7	■	0	1.57	0.71	0.999
	□	0	2.21	0.66	0.999
0.75	■	0	2.28	0.62	0.999
	□	5.08	6.34	0.52	0.999
0.8	■	1.98	3.01	0.53	0.997
	□	18.38	12.21	0.44	0.999
0.85	■	15.4	4.93	0.51	0.997
	□	35.3	8.75	0.42	0.997

stability. Combining PGPR with Dimodan U/J and Lecithin lead to an improved temporal stability. Apparent droplet size distributions using a combination of PGPR and Dimodan U/J was small, compared to larger droplet size distributions observed when a combination of PGPR and Lecithin was used.

The impact of different emulsifying processes on the droplet size distributions and temporal stability was assessed. Rotor-stator processing lead to larger mean droplet sizes and broader droplet size distributions compared to continuous rotating membrane (ROME) processing, where small and more narrowly distributed droplets were observed.

Rotating membrane processing is the favorable method for obtaining small and narrowly distributed emulsion droplets with high temporal stability. Using a combination of PGPR and Dimodan U/J as a binary emulsifier system, lead to smallest and most stable emulsion droplets and is the most promising emulsifier system for application in highly concentrated, ultra short-term stable emulsions.

5. Simultaneous Spray-Chilling

In order to homogeneously mix solid fat particles (component A) with the liquid oil (component B) and to obtain the composite fat system described in 3.2.2, a novel process for simultaneous spray-chilling was applied. Component A consists of a high melting palm fat based W/O emulsion (dripping point $T_d = 330K$), which forms solid fat particles after atomization in the spray-chilling tower. Component B consists of a liquid oil phase, which stays liquid at spraying conditions and through the entire process (dripping point $T_d = 262K$). The injection location for B (as shown in figure 5.1) had to be selected in such a way, that homogeneous coating of the fat particles (A) with oil (B) was ensured, while avoiding possible blending of the two phases A and B in the spraying tower. Blending of A and B could occur, if the surface of the fat particles (A) was not completely solidified upon first contact with the coating oil (B).

5.1. Designing the process: Three-Stage solidification model

The optimum injection location for the oil phase (B) was determined using a three-stage solidification model as introduced by Srinivasan, S and Tanner, F X and Feigl T O and Althaus, T O and Windhab and described in detail by others^{91;92} based on⁶⁶.

The solidification model used is applied to polymorphous fats, which do not undergo supercooling and recoalescence. Therefore the solidification can be described in three stages⁹². In the first stage, the cooling of a droplet is modeled in a convective heat transfer process. As soon as the solidification temperature is reached, crystallization is induced through nucleation and crystal growth. Stage three consists of the cooling of completely solidified particles and can be again described using a convective heat transfer equation. Tanner *et al.* validated the model for a single cocoa butter droplet. As the palm fat fractions used in the course of this thesis exhibit crystallization kinetics comparable to cocoa butter^{69;78}, the application of the three-stage solidification model is seen appropriate.

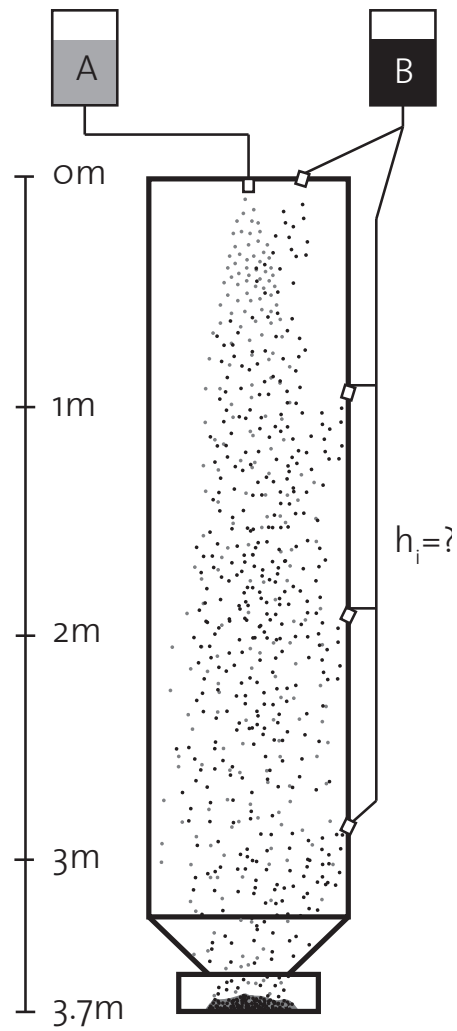


Figure 5.1.: Simultaneous spray-chilling: Finding the optimum injection location for component B

5.1.1. Solidification model assumptions

The following assumptions were made justifying the implementation of a three-stage solidification model:

- The material has a uniform initial temperature
- Constant temperature in the spray tower
- Heat transfer is controlled by conduction (within the material) and a constant uniform surface heat transfer coefficient
- Constant thermophysical properties of the material in solid and liquid state
- No mass transfer from and to the droplet
- Uniform temperature in the droplet as conduction inside the droplet is much more pronounced than convection. This can be described by the Biot number (Bi) 5.1, where h_0 is the heat transfer coefficient, L_c is the characteristic length (ratio of volume and surface area) and K_d is the heat conductivity inside the droplet. A typical palm fat droplet with a diameter of $32\mu m$ has a $Bi \approx 0.003$.

$$Bi = h_0 * L_c / K_d < 0.1 \quad (5.1)$$

5.1.2. Stage I

The first stage of the cooling process, where the droplet temperature T_d is larger than the freezing temperature T_f , is described by equation 5.2, governed by convective heat transfer. Whereas ρ_d is the droplet density, V_d the droplet volume, C_l the specific heat capacity of the liquid droplet, h_0 is the heat transfer coefficient, S_d is the droplet surface, T_d the droplet temperature and T_g is the gas temperature.

$$\rho_d V_d C_l \frac{dT_d}{dt} = -h_0 (T_d - T_g) S_d \quad (5.2)$$

Equation 5.2 relates the rate of change of the droplet temperature to the heat transferred between droplet and ambient gas. The heat transfer coefficient is related to the heat flux q_h by equation 5.3.

$$q_h = h_0 (T_d - T_s) \quad (5.3)$$

The heat transfer from a spherical droplet has been modeled using the Ranz-Marshall correlation 5.4, whereas Nu is the Nusselt number, d is the droplet diameter, K_g is

the thermal conductivity of the ambient gas, Pr_d the Prandtl and Re_d the Reynolds number of the droplet.

$$Nu = \frac{h_0 * d}{K_g} = 2 + 0.6Pr_d^{1/3} * Re_d^{1/2} \quad (5.4)$$

The Prandtl and the Reynolds number are given by equations 5.5 and 5.6, whereas ρ_g is the ambient gas density, v_r the relative droplet - gas velocity and μ_g the viscosity of the surrounding gas.

$$Pr_d = \frac{C_l \mu_g}{K_g} \quad (5.5)$$

$$Re_d = \frac{\rho_g v_r d}{\mu_g} \quad (5.6)$$

5.1.3. Stage II

After the droplet reaches the solidification temperature T_f (T_{fd}), crystallization is initiated. For assumed negligible supercooling, the release of latent heat during crystallization contributes to heating of the droplet, leading to equation 5.7, where C_γ is the heat capacity of the semisolid droplet, V_f is the solidified volume of the droplet and L_f is the averaged latent heat of crystallization.

$$\rho_d V_d C_\gamma \frac{dT_d}{dt} = -h_o(T_d - T_g)S_d + L_f \rho_d \frac{dV_f}{dt} \quad (5.7)$$

The volumetric solidification rate $\frac{V_f}{dt}$ is determined by the rate of enthalpy change due to heat convection away from the droplet ($h_o(T_d - T_g)S_d$) and the rate of enthalpy change due to latent heat release ($L_f \rho_d \frac{V_f}{dt}$) as described in equation 5.8, with k as a material and process dependent variable $0 \leq k \leq 1$.

$$L_f \rho_d \frac{V_f}{dt} = k h_o(T_d - T_g)S_d \quad (5.8)$$

Substitution of equation 5.8 into 5.7 leads to equation 5.9 for the temperature dependent volumetric solidification rate of the droplet.

$$\frac{dV_f}{dT} = -\frac{k}{1-k} \frac{V_d C_\gamma}{L_f} \quad (5.9)$$

Introducing the freezing process variable $\gamma = V_f/V_d$ with $0 < \gamma \leq 1$, the semisolid heat capacity can be expressed with equation 5.10, whereas C_s is the specific heat capacity of the solid droplet.

$$C_\gamma = (1 - k)C_l + \gamma \cdot C_s \quad (5.10)$$

Therefore, the solidification (stage II) of the spray-chilling process can be described with 5.11.

$$\rho_d V_d C_\gamma \frac{dT_d}{dt} = -h_o S_d (T_d - T_g)(1 - k) \quad (5.11)$$

In this thesis, k was taken as approximately constant, making the rate of latent heat release constant to the heat convected away from the droplet.

5.1.4. Stage III

After the droplet is completely solidified (stage II completed), the cooling process continues as described in stage I (equation 5.2), with liquid properties replaced by solid properties.

5.1.5. Adaptation of the model: Non constant droplet-gas velocity v_r

As a spraying droplet is in a non-steady state after being sprayed with a droplet-gas relative velocity at the nozzle tip of $v_0 = 1\text{m/s}$, the relative droplet-gas velocity v_r was calculated according to the equation of motion. The maximum droplet-gas velocity v_∞ was calculated using equations 5.12 and 5.13, where m is the mass of the droplet, c_w denotes the drag coefficient of the droplet and A the projected area into the flow direction of the droplet.

$$v_\infty = v(t \rightarrow \infty) = -\sqrt{\frac{mg}{r}} \quad (5.12)$$

$$r = 0.5c_w A \quad (5.13)$$

Using time dependent droplet-gas velocity v_r was calculated according to equation 5.14.

$$v(t) = -v_{\infty} \tanh\left(\frac{gt}{v_{\infty}} - \operatorname{artanh}\left(\frac{v_0}{v_{\infty}}\right)\right) \quad (5.14)$$

5.2. Application to simultaneous spray-chilling

Simultaneous spray-chilling of the hard-fat fraction (A) based on the three-stage solidification model was simulated using Matlab (MathWorks, USA), parameters are listed in the appendix in table B.1. As described in section 5, the high melting fat droplets (A) are always injected into the spray-chilling tower from the tower top. Subsequently, they are chilled in the spraying tower, which has been numerically simulated using a modified three-stage solidification approach. Prior to radial injection of fraction B and in-tower mixing, the fat particles (A) need to be solidified to such an extent, that blending and thereby formation of eutectic mixtures of fraction A and B is inhibited.

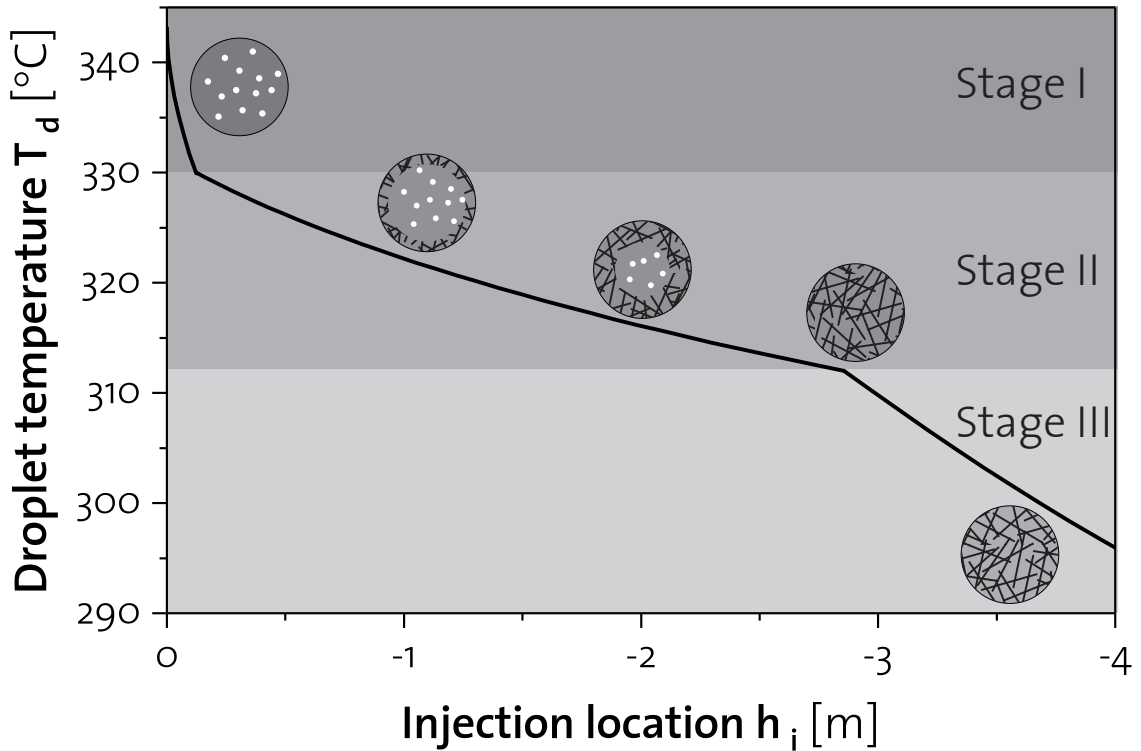


Figure 5.2.: Three-stage solidification model: Development of droplet temperature T_d in relation to the falling height (injection location h_i) of the droplet in the spray-chilling tower. Droplets with a diameter $x_{50,3} = 32\mu\text{m}$ were chilled at a spray tower temperature of $T_g = 277\text{K}$.

If fraction A and B are injected at a height of $h_i = 0m$ into the spray chilling tower, undesired blending of the two phases has to be expected due to the liquid nature of both phases. As shown in figure 5.2, stage I (cooling of a high-melting fat droplet with a diameter of $x_{50,3} = 32\mu m$ at a spray tower temperature of $T_g = 277K$ to solidification temperature T_f) is completed after a falling height $h_i = 0.12m$. After a short crystallization time (stage II, crystallization and further cooling of the droplet), a solid shell will be enclosing the droplet, effectively inhibiting mixing of fraction A and B. Therefore, radial injection of fraction B (see 5) is possible after a falling height of approximately $h_i \gtrsim 0.2m$.

To reassure, that also larger droplets of fraction A and B will not be blended during simultaneous spray-chilling, an injection height $h_i = 2m$ was selected. Microscopic observation showed, that fat particles (A) stay completely intact if the liquid oil phase (B) is injected at a height $h_i = 2m$.

5.3. Spray particle size

Particle size distributions of hard fat particles (obtained by spraying the hard-fat fraction A) in dependence of the main process parameters (atomizing pressure, liquid flow rate) produced by simultaneous spray-chilling were obtained from laser diffraction particle size analysis. Due to the negligible (immeasurable) impact of the spray tower chilling temperature on the measured particle size distribution, particle size distributions in relation to the spray chilling temperature are not shown here.

Figure 5.3 illustrates the particle size distributions obtained after atomizing at 3 bar using different fluid flow rates u . Higher fluid flow rates resulted in larger mean particle sizes $x_{50,3}$ and an amplification of the bimodality of the particle size distribution. Applying an atomizing pressure of 6 bar as shown in 5.4, lead to slightly decreased mean droplet sizes $x_{50,3}$. As already observed at 3 bar atomizing pressure, the bimodality of the particle size distributions at 6 bar also increased at higher flow rates at 6 bar.

Working at the highest possible atomizing pressure of 6 bar and the lowest possible flow rate of 4.8 kg/h, lead to monomodal particle size distribution and the smallest mean particle size of 31.98 μm .

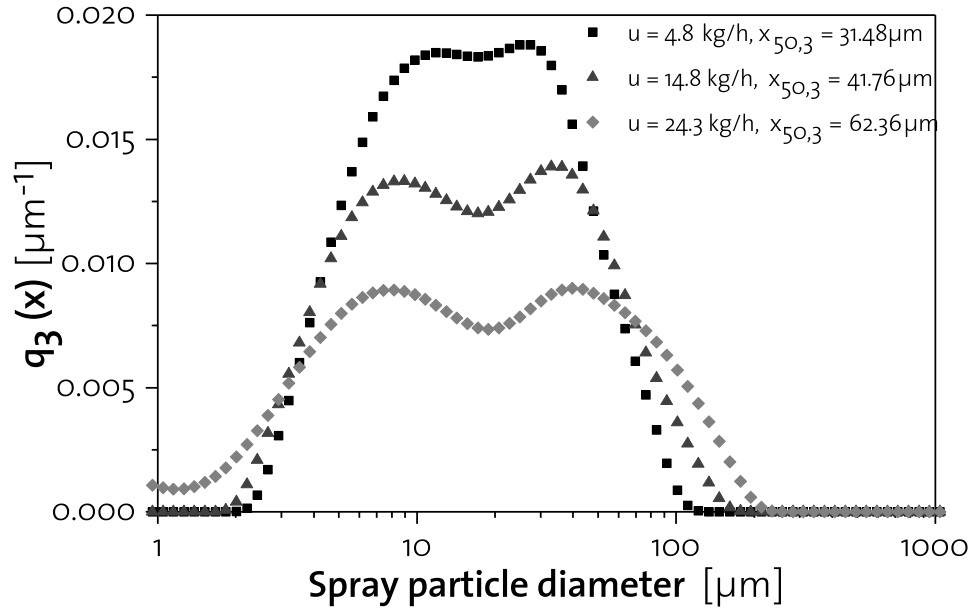


Figure 5.3.: Volumetric frequency distribution $q_3(x)$ of emulsions atomized at 3 bar atomization pressure.

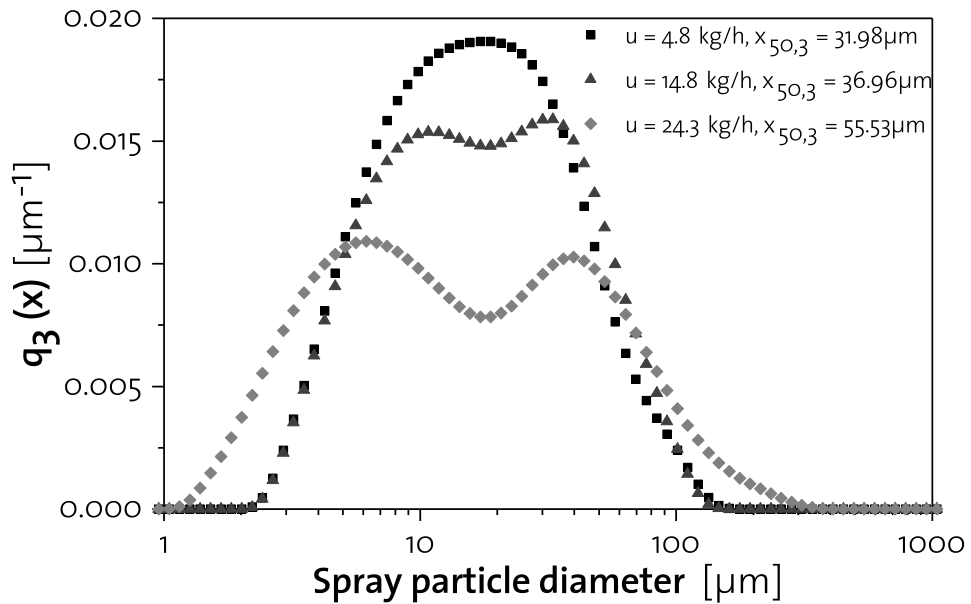


Figure 5.4.: Volumetric frequency distribution $q_3(x)$ of emulsions atomized at 6 bar atomization pressure.

5.4. Mass Conservation

Disperse water mass fractions of W/O emulsions (Φ_E) before spraying and in the sprayed fat particles (Φ_P) were measured and compared, to confirm the preservation of the entrapped disperse water load in the final product. Figure 5.5 confirms a linear correlation between Φ_E and Φ_P . Therefore mass conservation through the whole process is fulfilled which also proves the emulsion structure preservation.

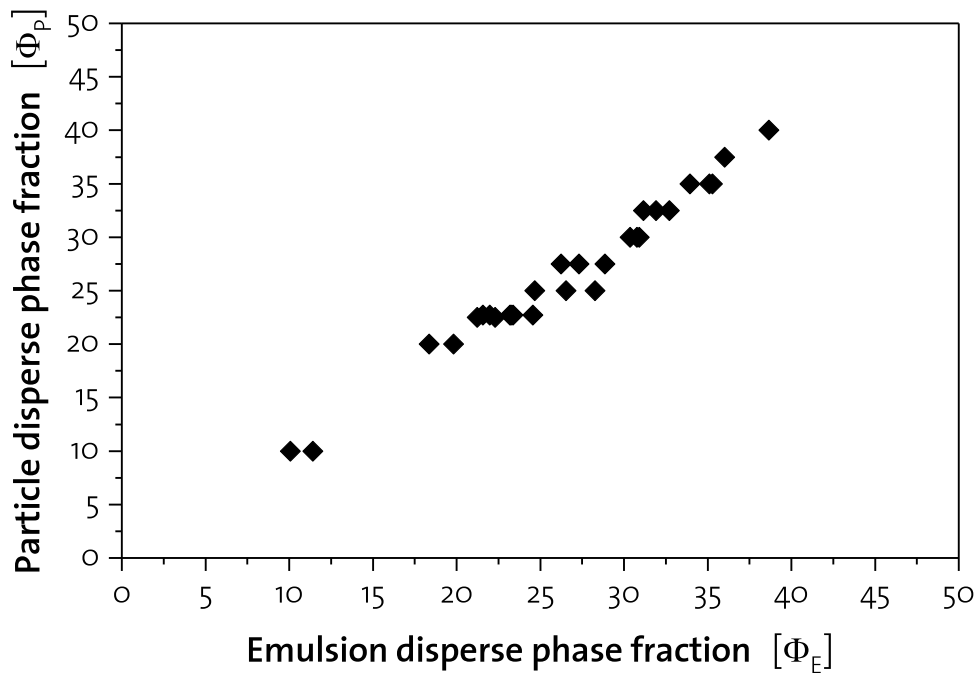


Figure 5.5.: Mass conservation during spray-chilling of W/O emulsions at an atomization pressure of 6 bar at a liquid flow rate of 4.8kg/h for fat droplets with a diameter $x_{50,3} = 32\mu\text{m}$ were chilled at a spray tower temperature of $T_g = 277\text{K}$.

5.5. Particle Morphology

The fat particles produced by spray chilling fraction A were overall spherical (figure 5.6a) with a smooth surface. Cryo-fracturing such fat particles reveals the emulsion based substructure. In figure 5.6b, some water droplets are indicated by red arrows. The substructure illustrated by SEM is in line with the emulsion substructure as described in chapter 4.

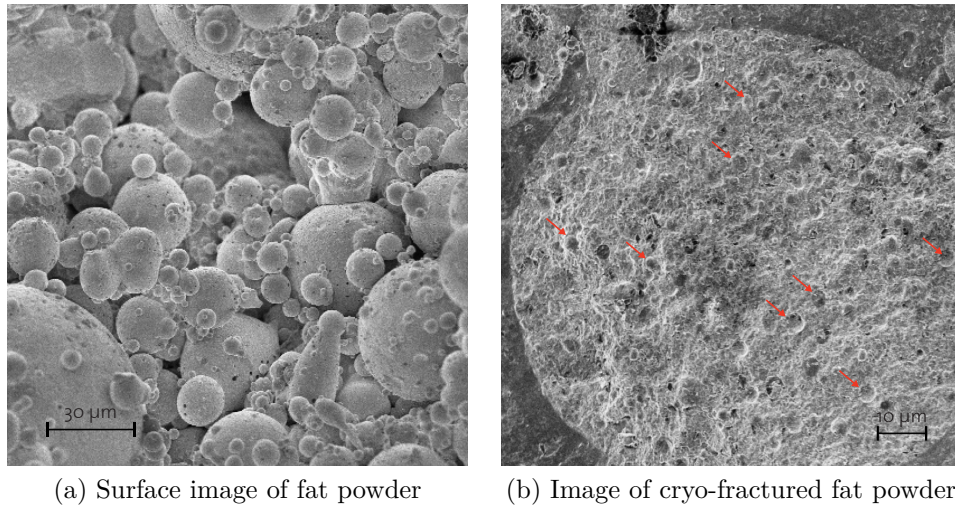


Figure 5.6.: SEM images of fat particles obtained by spraying fraction A.

5.6. Polymorphism

Polymorphism of palm fat spray chilled at gas temperatures T_g of 10, 0, -10, -20, -30 and -40°C was investigated in this section. Figure 5.7 shows the x-ray diffraction patterns measured directly after spraying. Equation 5.2 and 5.7 shows the linear impact of the difference of droplet and ambient temperature $T_d - T_g$ on the freezing rate of the droplet. As discussed in section 2.1.1, high degrees of supercooling and high cooling rates favour the formation of α and β' polymorphs, whereas low cooling rates lead to crystallization dominated by β crystals. Figure 5.7 illustrates this for different gas temperatures. Lower gas temperatures are linked to a higher degree of supercooling and therefore high cooling rates leading to lesser stable α and/or β' crystals. Increasing the gas temperature T_g up to 10°C leads to a continuously increasing β peak. Therefore, higher gas temperatures in the spray chilling tower are favored due to the formation of more stable polymorphs.

During all further spray chilling trials performed within this thesis, a spray tower gas temperature of 4°C was applied, in order to reassure the formation of β dominated fat polymorphs.

5.7. Conclusions

Using the novel simultaneous spray-chilling process, intact, emulsion based fat particles could be produced and homogeneously mix-coated with a lower melting oil phase in

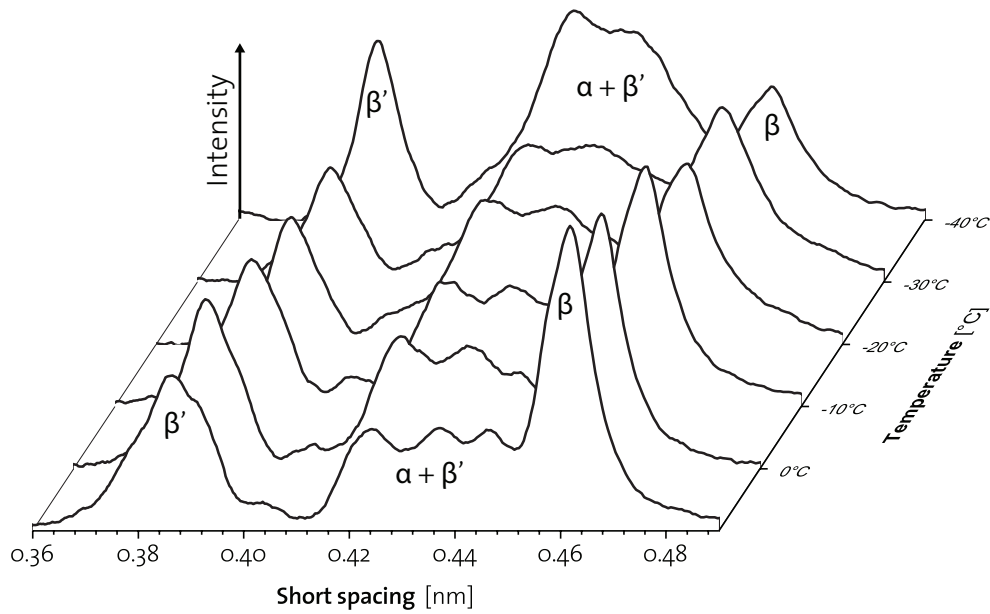


Figure 5.7.: Polymorphism obtained by spray-chilling of hard-fat fraction A at different temperatures T_g of 10, 0, -10, -20, -30 and -40°C at an atomization pressure of 6 bar and a liquid flow rate of 4.8kg/h for fat droplets with a diameter $x_{50,3} = 32\mu m$.

one process. Careful adjustment of the axial injection point in the spray-chilling tower of the low melting oil phase (fraction B) fixed according to the three-stage solidification model allowed the implementation of a one-step process for production of novel, concentrated multiphase composite fat systems.

The fat systems produced consist of fat particles with a tailored particle microstructure and particle size distribution as shown in sections 5.5 and 5.3. It was demonstrated, that disperse water mass conservation during the spray-chilling process is valid meaning that no water is lost during processing and spraying (section 5.4).

Analysis of the polymorphism obtained, when spray chilling composite fat systems at different spray tower temperatures, showed, that most stable β dominated systems are obtained at spray tower temperatures of 0 to 10°C. Lower temperatures of -10 to -40°C resulted in lesser stable, progressively more α and β' dominated fat systems. As described in section 2.1.1, this can be explained with the higher degree of supercooling at lower spray temperatures and thereby faster cooling rates applied to the fat particles, which lead to faster crystallization resulting in lower stable α and β' polymorphs, compared to lower degrees of supercooling which favor more stable β polymorphs as confirmed by measurements performed in this thesis and shown in figure 5.7.

Selecting the right spray chilling tower temperature and the proper injecting location for the two components A and B allows the production of a highly stable, novel, W/O-suspension-emulsion based fat system. This system will, due to the stable polymorphism and avoidance of eutectic effect, be extremely shelf stable during storage and have improved properties during application.

6. Rheology

As described in 2.4, the new fat system can be described as a substructured, multi-phase fatty mass with less temperature dependent consistency and stability compared to a conventional fat system with similar fat composition but without structurally separated high and low melting fat fractions and with additionally techno-functional or nutritionally physiological relevant encapsulation characteristics.

Conventionally produced margarine (as described in section 2.3) is a partially crystallized W/O-emulsion, consisting of multiple fat fractions with discrete melting temperature ranges. During manufacturing, shear and undercooling are applied to such a blend leading to crystallization of the higher melting fat fractions and formation of a fat continuous suspension-emulsion system. Fat crystal (-cluster) size and interconnectivity depend on process and storage parameters, and are of crucial importance for the thermo-rheological properties of such a fat system. The novel powder fat system designed and investigated during this thesis, has the same composition as a conventionally produced fat-continuous systems. However, the spray-chilling process applied, leads to a different microstructure: As high-melting W/O based fat particles dispersed in a low-melting oil are obtained by the specific spray-chilling and thereby (i) eutectic mixtures of the two fat phases and (ii) related post crystallization leading to inter connected fat crystal networks and (iii) further related destabilization of the W/O emulsion structure can be effectively avoided.

As described in chapter 2.4, the novel fat system was developed and optimized with focus towards laminated pastry systems. Industrial pastry production generally depends on two properties of the fat system applied:

1. **Bulk rheology:** Important during handling and processing of bulk fat and the initial steps of lamination where layer thickness is $> 100\mu m$. To characterize bulk rheology, oscillatory thermo rheometry (OTR) measurements were performed.
2. **Thin layer rheology:** Important during the later stages of the lamination process, where the fat layers reach a thickness below $> 25\mu m$ and the confined space and increased fat dough interaction impact on the fat rheology. To better understand the fat flow on such a micro scale, thin layer rotational rheology measurements were performed.

6.1. Materials

6.2. Methods

6.2.1. Bulk rheology

Rotational rheometry

Bulk rotational rheometry of emulsions was performed using a rotational rheometer (Physica MCR 300, Anton Paar, Austria) equipped with a coaxial cylinder geometry (CC27). Viscosity was derived from rotational experiments (in the shear rate range from $\dot{\gamma} = 10s^{-1}$ to $100s^{-1}$ of relevance for the lamination process) and respective flow curves were plotted.

Oscillatory thermo rheology (OTR)

The small deformation amplitudes applied during the oscillatory thermo rheometry (OTR) trials in this thesis, lead to negligible shear-induced changes in the fat-system sample. Therefore oscillatory rheometry is a well suited method for the characterization of highly viscous structured fat systems^{102;71}. As discussed in 6.3, storage (G') and loss (G'') moduli can be extracted from such oscillatory shear measurements. OTR is a sensitive method suited well for understanding changes in microstructure during flow and thermal treatment.

OTR measurements were carried out using also a Physica MCR 300 (Anton Paar, Austria) equipped with a PP25 parallel plate measuring geometry with profiled plates¹⁰¹. Temperature was controlled using a peltier controlled system of the type TEK 150PA-C (Anton Paar, Austria). The measurement gap was set to $1mm$ and the dynamic moduli were derived. An OTR temperature sweep test was performed continuously increasing the temperature from 4 to 70°C at a heating rate of $10^{\circ}C/min$ at constant deformation of $\gamma = 0.02$ and constant angular frequency of $\omega = 100rad/s$ we characterized the temperature dependent (complex) viscosity, linked to the structural changes during melting of a fat sample.

Figure 6.1 shows OTR curves for two fat systems with the same composition and an emulsified total water content of 16%. System 1 was a conventional fat system (fat crystal network) produced by scraped surface heat exchanger and pin-mixer and will be labeled as CF (conventional fat system) in this thesis. System 2 was a novel, powder based fat system produced by simultaneous spray-chilling and will be labeled as PF (powder fat) in this thesis. Therefore, all differences observed by

thermo-rheological measurements are caused by the differences in microstructure. The complex viscosity of powder margarine stays at a higher level with a less steep slope with increasing temperature compared to conventionally produced puff pastry margarine. Using the powder based novel fat system, eutectic interactions between the fat fractions are avoided, leading to the increased temperature stability in the thermo-rheometric test.

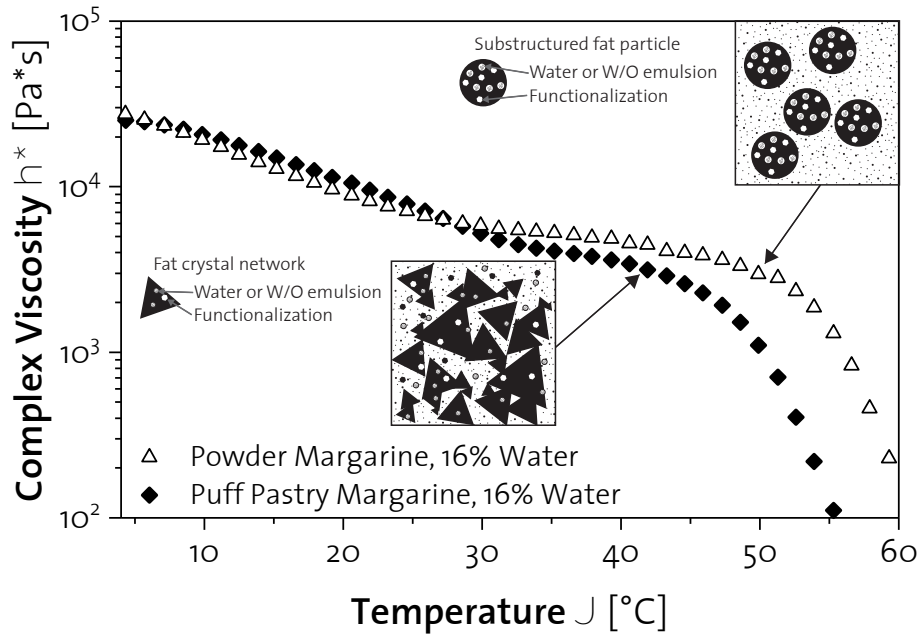


Figure 6.1.: Rheometric comparison of the conventional (CF) and powder fat (PF) system.

6.2.2. Micro rheology

Shear confinement rheology (SCR)

Confinement of fluids in thin layers can change their rheological behavior compared to their bulk rheological characteristics, which is of crucial importance in the context of this thesis.

As previously discussed¹⁰, thin layer flow behavior is an issue of considerable importance in situations ranging from molecular lubrication films where it can induce increased friction to macroscopic granular materials flowing out of a narrow hopper opening and where the particles can jam into rigid structures. Thin layer mechanics is of crucial importance during the late stage of lamination of pastry products, where

typically thin layer thicknesses of $100 - 12.5\mu m$ occur which goes below the hard fat particle mean diameter of $x_{50,3} = 32\mu m$.

Brown *et al.* previously investigated confined shear thickening suspensions for which the sample thickness is comparable to the particle dimensions. Rheometry measurements are presented for densely packed suspensions of spheres. By varying the suspension layer thickness at constant shear rate, pronounced oscillations in the stress were found¹². These oscillations became stronger as the confinement gap (distance of confinement d_s decreased), and the stress was minimized when the sample thickness became commensurate with an integer number of particle layers.

Thin layer mechanics were investigated by Shear Confinement Rheology (SCR) using a Physica MCR 300 (Anton Paar, Austria) rotational rheometer equipped with a PP25 parallel plate measuring geometry allowing continuous variation of the sample thickness d_s between the plates. Sample thickness can be set with a resolution of $1\mu m$ and with a parallelity of $3\mu m$ ¹². The plate surfaces are smooth and the tool stainless steel. Measurements were performed at controlled plate temperature.

Transition from fluid to jammed states were measured at a constant shear rate $\dot{\gamma} = 25s^{-1}$ while reducing the gap size from $d_s = 200\mu m$ to $d_s = 20\mu m$ at a confinement rate of $0.45\mu m/s$. Viscosity η_B and normal force τ_N were monitored during superimposed confinement and shear¹².

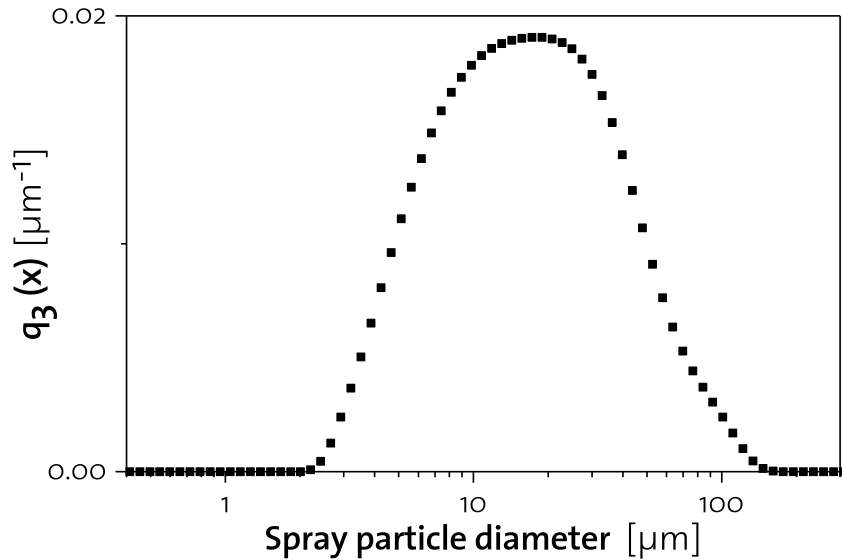


Figure 6.2.: Volumetric frequency distribution of the $x_{50,3} = 32\mu m$ particles applied in the measurement described in figure 6.3.

Figure 6.3 shows an exemplary shear confinement rheology measurement and its underlying mechanics. Particles with a mean average particle size of $x_{50,3} = 32\mu m$ and a volumetric frequency size distribution illustrated in figure 6.2 were used during this measurement.

Viscosity and normal force increase linearly (are quasi constant) until a confined gap size of approximately $80\mu m$ is reached. This is in line with previous observations¹², where constant values for normal force and viscosity were observed for larger confinement gaps d_s . The oscillations in normal force and viscosity upon confinement are also in line with previous observations¹². Brown *et al.* observed strong confinement induced oscillations in normal force for confinement gaps of up to three times the particle size and weaker oscillations of approximately 10% of the measured normal force at larger gaps of around six to seven times the particle size. In figure 6.3, small oscillations in normal force and viscosity can be observed up to a confinement gap of approximately $d_s = 80\mu m$ (confinement zone A, where $d = 2.5 * x_{50,3}$). Starting at confinement gaps $d < 2.5 * x_{50,3}$ (confinement zone B), larger oscillations combined with a non-linear increase in normal force and viscosity were observed.

As illustrated in figure 6.3 (a)-(c), confinement progresses through the measurement from (a) to (b). Subfigure (c) illustrates the starting compression, rupture and deformation of particles in confinement zone B, which leads to the largely increased oscillations in normal force.

Normal force and viscosity data in general show compatible trends during confinement measurements. However, as normal force data is a more direct means of quantifying direct forces acting from fat particles on rupture prone dough layers, normal force data will be preferably used in the following subsections.

Figure 6.4 shows a normal force measurement as described above for fat powder containing a dispersed mass fraction $\Phi_P = 0.1$ water. The normal force measured were here distinguished into two different characteristics (a) and (b). (a) denotes the baseline normal force measured, while (b) describes the normal force peaks measured. It is concluded, that (a) is integrally exhibited by the whole sample during confinement, while (b) stands for the confined fat particle response. Once fat particles rupture, the normal force measured falls back to the baseline (a).

Numeric information was extracted by integration of normal force baseline (a) and peaks (b) in order to quantitatively compare normal forces exerted by different fat particle systems.

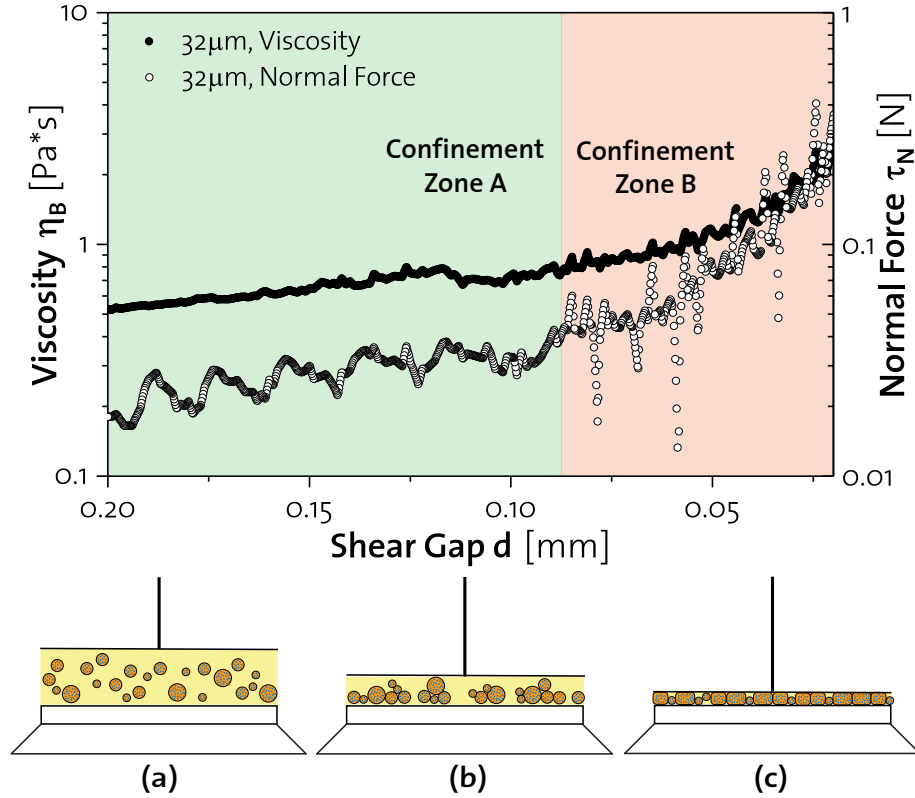


Figure 6.3.: Confinement measurement at a for fat particles with a particle size $x_{50,3} = 32\mu m$ at a constant shear rate $\dot{\gamma} = 25s^{-1}$ while reducing the gap size from $d_s = 200\mu m$ to $d_s = 20\mu m$ at a confinement rate of $0.45\mu m/s$. Viscosity η_B and normal force τ_N were monitored during superimposed confinement and shear.

Oscillatory confinement rheology (OCR)

The same basic methodology as previously described for SCR measurements applies for OCR measurements. As discussed in 6.3, storage (G') and loss (G'') moduli can be extracted from oscillatory measurements. Therefore, OCR is a sensitive method which was used supplementary to SCR measurements in order to extract information about storage and loss properties of fat particles.

SCR measurements were carried out using a Physica MCR 300 (Anton Paar, Austria) equipped with a PP25 parallel plate measuring geometry. The measurement gap was set to $1mm$ and the dynamic moduli were extracted. A constant deformation of $\gamma = 0.02$ at a constant angular frequency $\omega = 100rad/s$ was applied to characterize the viscous and elastic behavior of the material.

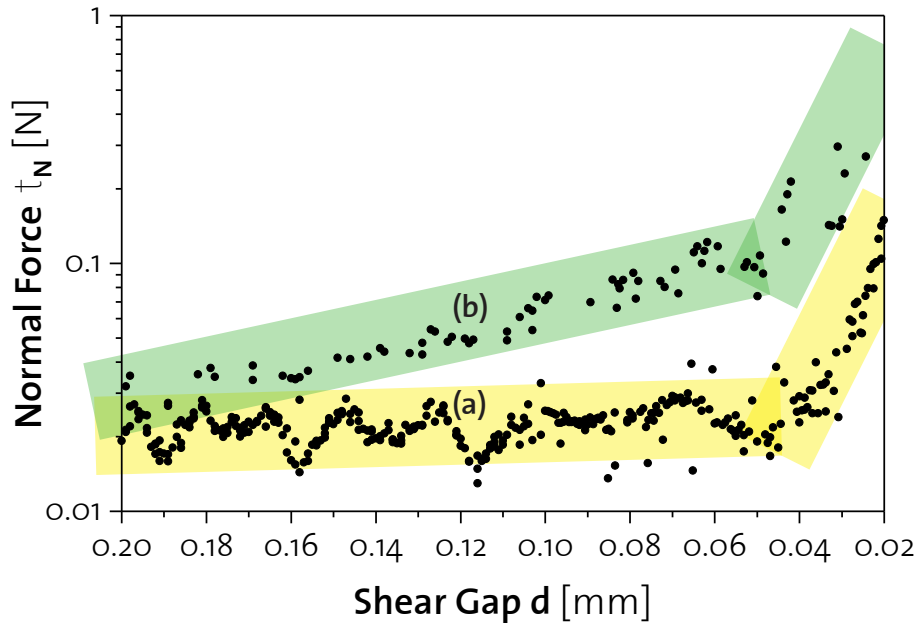


Figure 6.4.: SCR measurement for fat powder containing a dispersed mass fraction $\Phi = 0.1$ water. (a) denotes the baseline normal force, (b) the normal force peaks measured.

6.3. Bulk rheology and melting properties of powdered fat

For identification of a powder fat system closely matching the thermorheologic properties of conventional (non-powder based), optimized fat systems used in puff pastry, OTR measurements were performed using different fat fractions, powder to oil disperse phase ratios Φ_P and particle disperse phase concentrations Φ_E as shown in figure 6.5.

Figure 6.5a shows OTR curves for stearin particles dispersed at different Φ_P fractions with canola oil compared to conventional pastry margarine. Powdered fats show lower slopes of the curve compared to pastry margarine, and thus are less temperature dependent. Increasing Φ_P results in a more concentrated suspension and thereby to an increased complex viscosity of the fat systems, which is in line with general suspension rheology. Due to the lower slope of the powdered systems, stearin powder mixed with canola oil at a fraction of $\Phi_P = 0.75$ matches the complex viscosity of conventional pastry margarine at high temperatures (40 – 60°C). However, as pastry dough usually is processed at lower temperatures in the range of 4 – 10°C, different fat systems were investigated.

Using super-stearin particles leads to a significantly higher complex viscosity and melting behavior as illustrated by figure 6.5b. As previously described for stearin based fat particles, a more flat curve linked to a lowered temperature dependency compared to conventional pastry margarine could be observed. Super-stearin powder in canola oil fraction of $\Phi_P = 0.65$ matches the complex viscosity of pastry margarine well at lower temperatures in the range of 4 – 40°C.

From 6.5a and 6.5b it can be concluded, that the fat fraction and their underlying melting behavior as well as the powder in oil mass fraction Φ_P have a major influence on the rheology of the novel powder based fat system. Matching the thermorheometric properties of conventional pastry margarine thus requires careful selection of the blend of fat fractions used and optimization of Φ_P .

In figure 6.5c, a fat blend for the powder margarine with the same melting behavior as conventional puff pastry margarine (consisting of 36.4% super-stearin, 57.8% stearin and 5.8% mid-fraction) was combined with an optimum powder to oil ratio $\Phi_P = 0.675$. The complex viscosity of these optimized powder margarines at powder disperse water fractions of $\Phi_E = 0.2$ and 0.3 respectively matched the thermorheologic properties of conventional pastry margarine with a water content of 16% very closely with a lower temperature dependency in the typical processing temperature range of such fats of 4 – 30°C as described previously.

Therefore, an optimum fat blend consisting of 36.4% super-stearin, 57.8% stearin and 5.8% mid-fraction and a powder to oil ratio of $\Phi_P = 0.675$ were used for all application trials focused on pastry products as described in chapter 8 of this thesis.

6.4. The influence of particle size on the rheological properties

Figure 6.6 illustrates the influence of particle size of the stearin fat powder on the rheological properties of the novel powder fat composite system. Powder margarine systems consisting of 75% stearin powder and 25% oil fraction (6.6a) show, that the particle size distribution has a negligible influence on the melting properties measured by shear rheometry (bulk rheology measured by OTR) of the novel powder fat composite system.

However, a different tendency is apparent in micro rheological measurements performed by SCR measurements as illustrated by figure 6.6b. Larger fat particles show a steeper increase in normal force and in general a much higher normal force over the whole range of confinement. This could be quantified by integration of the normal force resulting in the total work needed carried out for the systems with different

6.4. The influence of particle size on the rheological properties

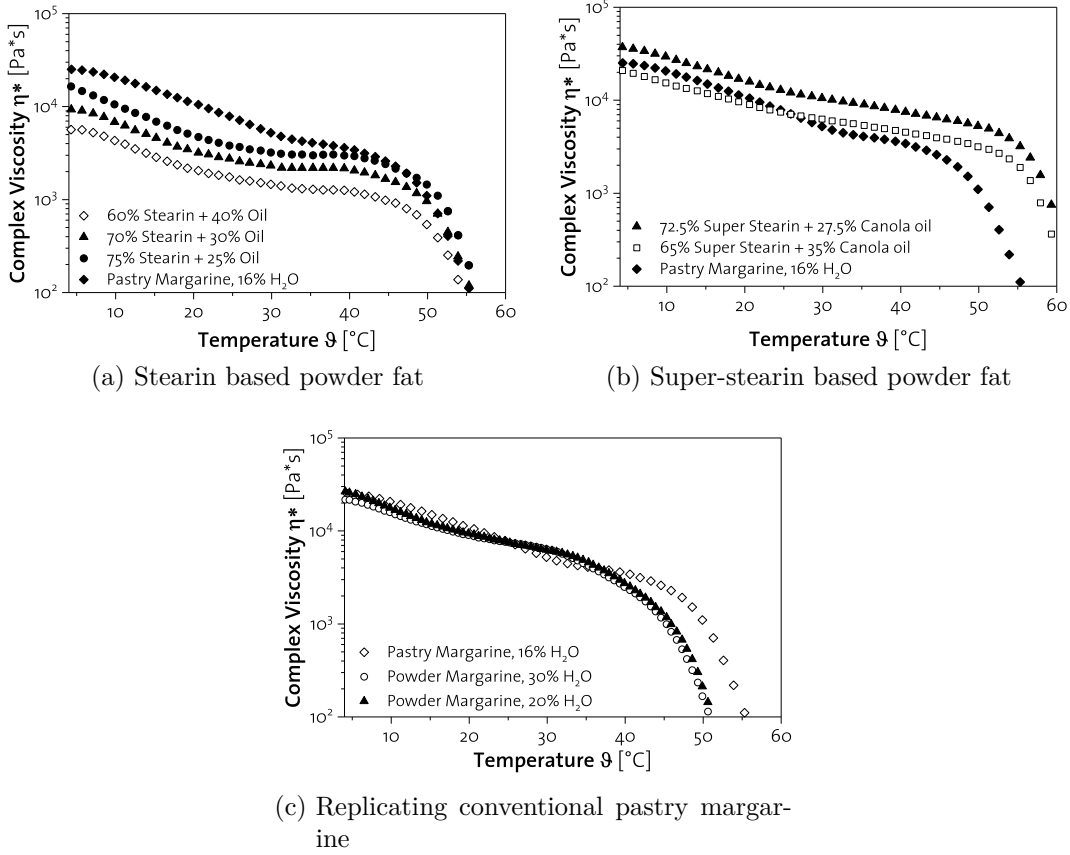


Figure 6.5.: Bulk rheology for powder fat systems consisting of different fat blends, powder to oil ratios Φ_P and emulsion based particle disperse phase concentrations Φ_E compared to conventional pastry margarine and low fat margarine.

mean average particle sizes $x_{50,3} = 100\mu m$ and $x_{50,3} = 32\mu m$ (see equation 6.2) 6.6b. Confinement of the larger particles $x_{50,3} = 100\mu m$ required a total confinement work $W_c = 0.09121J$, whereas the small particles $x_{50,3} = 32\mu m$ required a significantly, approximately 10 fold lower confinement work $W_c = 0.0095J$.

$$W_c = \int_{200\mu m}^{20\mu m} \tau_N(d_s) dd_s \quad (6.1)$$

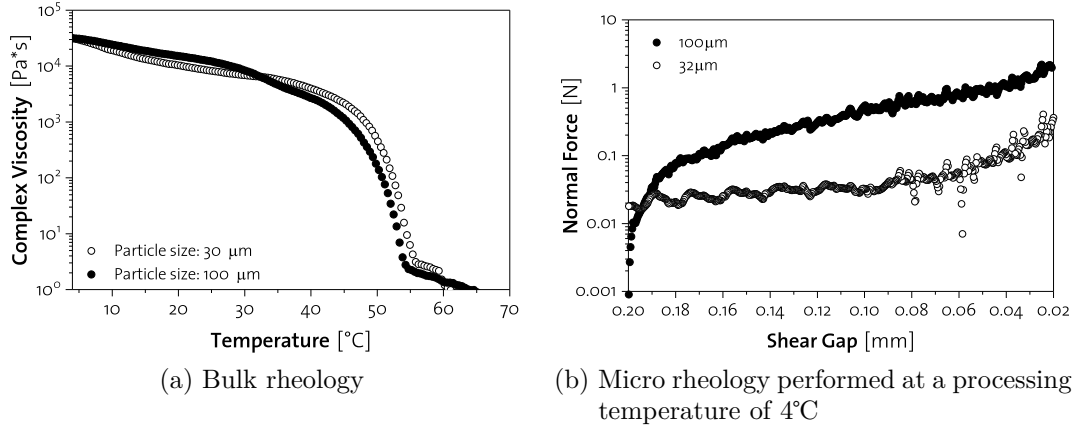


Figure 6.6.: Rheologic measurement of particle fat systems with two different mean average particle sizes of $x_{50,3} = 32\mu\text{m}$ and $x_{50,3} = 100\mu\text{m}$. Hard fat particles consisted of palm stearin and were mixed with canola oil at a ratio $\Phi_P = 0.675$.

6.5. The influence of different fat melting properties on rheology

In figure 6.7, bulk and micro rheology measurements for different powdered fat systems composed of fat particles consisting of different fat fractions (dripping point for stearin $T_{drip.,stearin} = 54^\circ\text{C}$, $T_{drip.,super-stearin} = 61^\circ\text{C}$ and $T_{drip.,mid-fraction} = 47^\circ\text{C}$) are shown. As depicted in figure 6.7a, different fat fractions have a large impact on bulk rheology and thereby melting properties of the fat systems. Bulk rheology and related temperature dependent melting properties of the novel powder fat composite system can be tailored by the combination of hard fat fractions used.

Figure 6.7b illustrates a different behavior on the macro scale. The fat fraction used has a minor influence on the normal force generated by the fat particles upon confinement, as no significant difference between stearin or super-stearin hard fat particles can be observed from the normal force measurements. Integration proves the small differences observed; the lowest melting mid-fraction requires the total confinement work $W_c = 0.00799J$, while stearin and super-stearin absorb slightly higher W_c of $0.00851J$ and $0.00924J$ respectively. This slight but significant difference in total confinement work required can be explained by the differences in melting point and thereby mechanic strength of fat particles produced using these three different fat fractions.

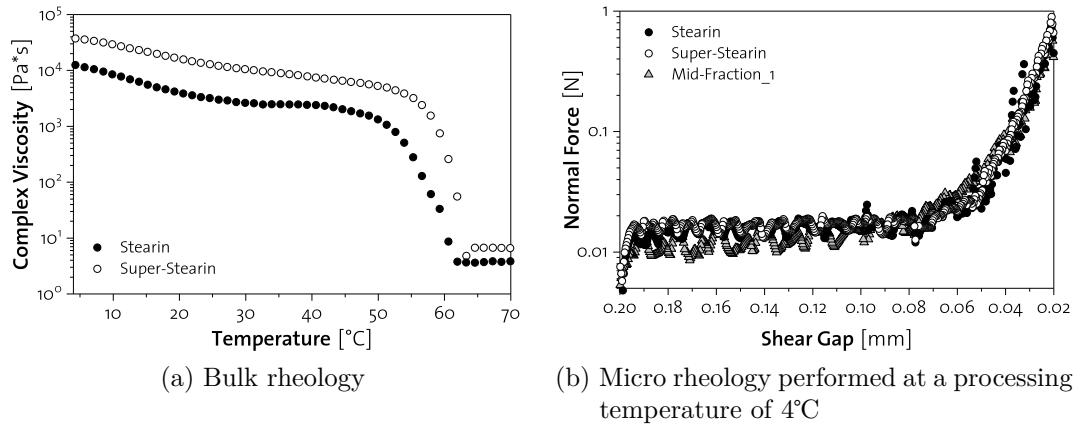


Figure 6.7.: Rheologic measurement of stearin and super stearin based particle fat systems.

6.6. Emulsion based fat particles: The impact of increased intra-particle disperse water mass fractions Φ_E

Figure 6.8 shows shear confinement rheology (SCR) measurements of fat particles substructured with a particle disperse fraction Φ_E of 0.1 – 0.7 at temperature of 4°C. The normal force exerted by the particles substantially increases with increasing Φ_E . At a $\Phi_E = 0.1$ (6.8a), the normal force stays at a constant baseline value of approximately $\tau_N = 0.02$ up to a confinement gap of $d_s = 40\mu m$, after which the normal force increases with a steep slope (confinement zone depicted in red). If we proceeded to higher intra-particle disperse water fractions $\Phi_E = 0.3$, $\Phi_E = 0.5$ and $\Phi_E = 0.7$ (figure 6.8b-6.8d), the confinement zone where the normal force deviates from the baseline value of $\tau_N = 0.02$ shifts to a progressively larger confinement gap. At $\Phi_E = 0.3$ (6.8b), confinement already occurs at a confinement gap of $d_s = 70\mu m$. Increasing Φ_E to 0.5 and 0.7 leads to even earlier onset of confinement (deviation from baseline) at confinement gaps of $d_s = 120\mu m$ and $d_s = 160\mu m$ respectively.

This strong increasing trend at large disperse intra-particle disperse mass fractions Φ_E can be explained the particle size distributions and mean particle sizes of powder fat containing increased intra-particle disperse mass fractions Φ_E .

The flow curves of the underlying emulsions, as shown in figure 6.10 containing elevated disperse water fractions Φ_E , exhibit significantly larger viscosities demonstrated by flow curves measured with rotational rheometry at a temperature of 70°C as described in section 6.2.1. The increasing trend in emulsion viscosities at increasing

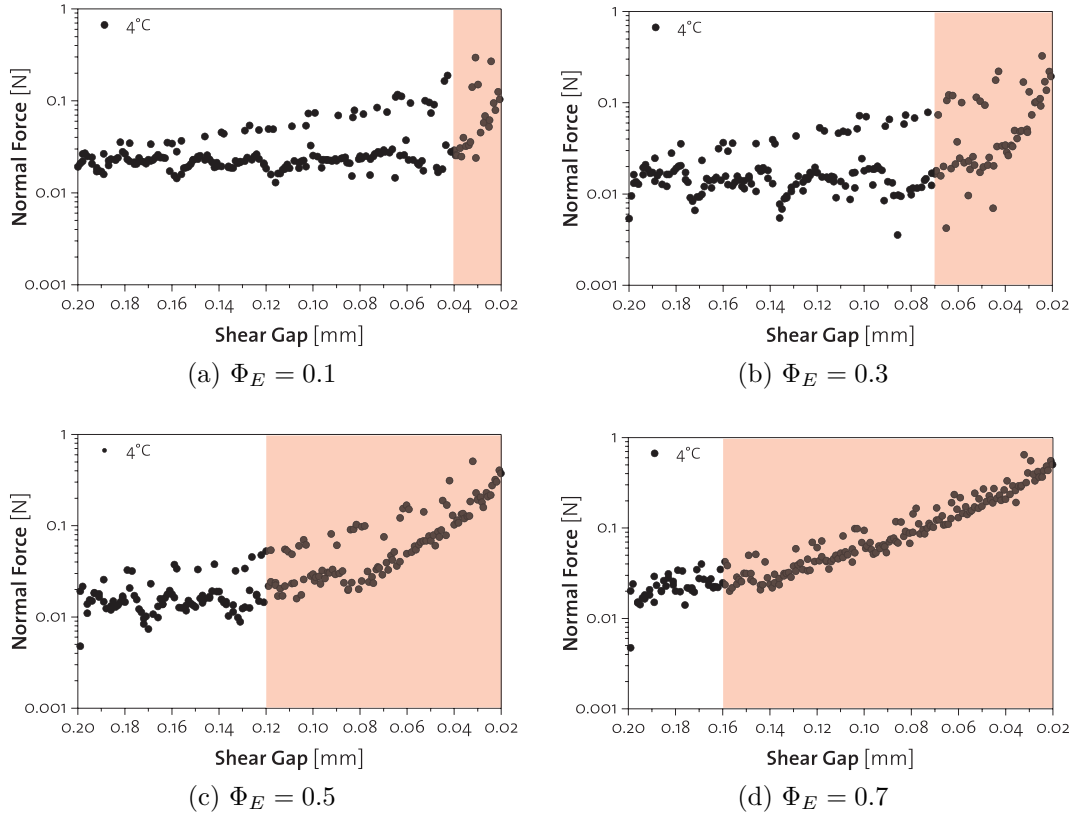


Figure 6.8.: The impact of an increased particle disperse fraction Φ_E on the micro rheology of powder fat. Confinement zone depicted in red. Micro rheology performed at a temperature of 4°C

disperse mass fractions Φ_E has a large impact on the droplet atomization when producing powder fat by simultaneous spray chilling as described in chapter 5. The particle size distributions of powder fat produced from emulsions containing elevated disperse mass fractions Φ_E is described in figure 6.9 and the underlying mean particle sizes $x_{50,3}$ of powders are summarized in table 6.1.

Additionally, as a second metric, integration of the normal force resulting in the total work ΔW_{total} needed was carried out for the systems with different particle disperse fraction (see equation 6.2). $W_{total,forcepeaks}$, $W_{total,baseline}$ as well as $\Delta W_{total} = W_{total,forcepeaks} - W_{total,baseline}$ were calculated.

$$W = \int_{200\mu m}^{20\mu m} \tau_N(d_s) dd_s \quad (6.2)$$

In figure 6.11, $W_{total,forcepeaks}$, $W_{total,baseline}$ and ΔW_{total} are plotted. $W_{total,forcepeaks}$

6.6. Emulsion based fat particles: The impact of increased intra-particle disperse water mass fractions Φ_E

Table 6.1.: Mean particle sizes $x_{50,3}$ of particles produced with different intra-particle disperse mass fractions Φ_E .

Φ_E	$x_{50,3}$ [μm]
0	31.59
0.1	32.26
0.2	31.51
0.3	32.50
0.4	38.88
0.5	46.72
0.6	56.88
0.7	68.08

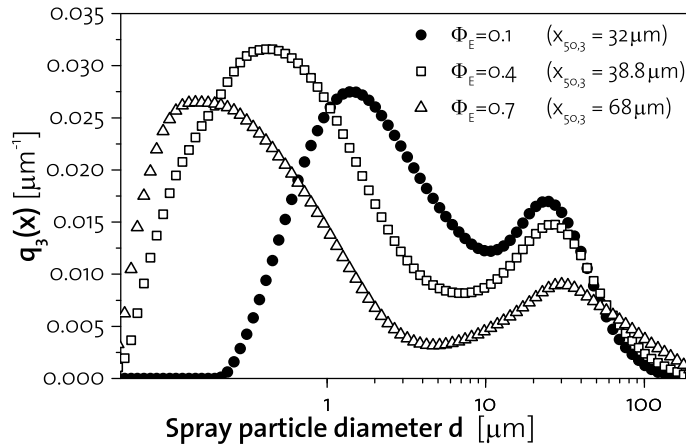


Figure 6.9.: Viscosity of emulsions with different disperse fraction Φ_E . Viscosity of liquid emulsions was measured at a temperature of 70°C .

and $W_{total,baseline}$ both increase significantly in the same magnitude with increasing Φ_E . This is in line with the observations made in figure 6.8 as described earlier. Obvious is also a decreasing tendency in $\Delta_{W_{total}}$ for increasing Φ_E ; with increasing Φ_E , $W_{total,baseline}$ increases at a higher rate compared to $W_{total,forcepeaks}$. The increasing force peaks can be explained, as mentioned earlier, by the increasing particle size distributions and mean particle sizes of powder fat containing increased intra-particle disperse mass fractions Φ_E . The numeric data underlying figure 6.11 is listed in table C.1.

It is concluded, that particle size distributions and mean particle sizes of powder fat have to be monitored closely, when working with powder fat containing increased intra-particle disperse mass fractions Φ_E .

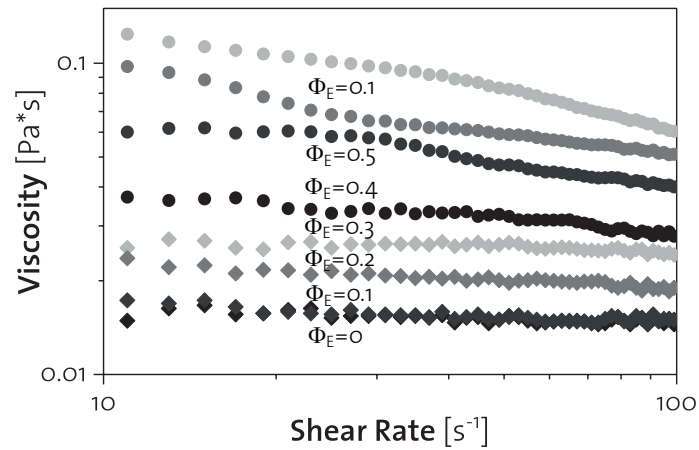


Figure 6.10.: Viscosity of emulsions with different disperse fraction Φ_E . Viscosity of liquid emulsions was measured at a temperature of 70°C .

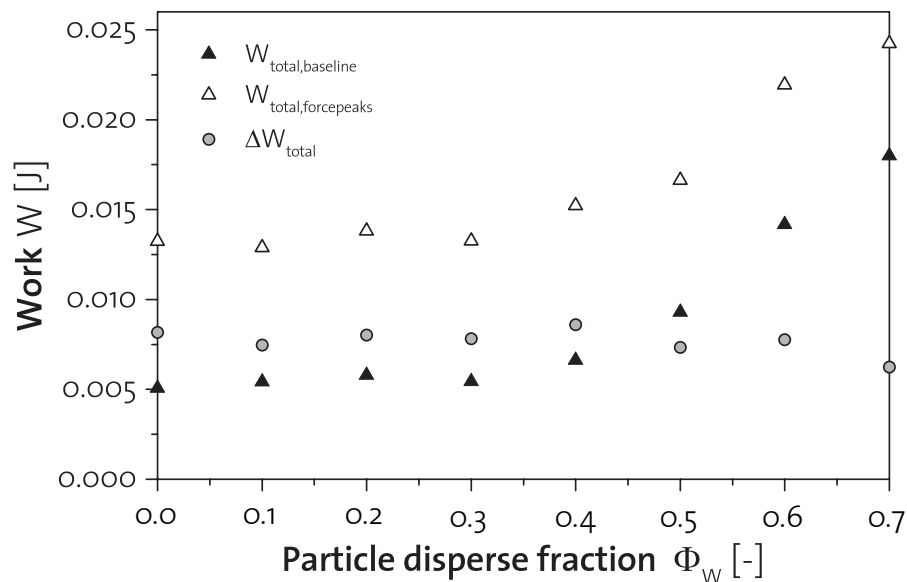


Figure 6.11.: Total work needed for confinement of fat particles with different particle disperse fraction Φ_E .

6.7. Emulsion based fat particles: The impact of temperature

The influence of temperature on micro-rheology of fat particles was investigated by SCR measurements at temperatures of 4°C and 30°C . In section 6.6, a pronounced impact of the particle disperse fraction Φ_E on the micro rheology and the normal

force exhibited by fat particles was observed. As the large normal forces exerted by powder fat containing elevated disperse mass fractions Φ_E and therefore increased particle size distributions might have a severe impact on dough layers during pastry production, another parameter was used to further tailor the particles properties: temperature.

Figure 6.12 shows three different particle systems: As observed in section 6.6, fat particles with a $\Phi_E = 0.7$ and an mean particle size $x_{50,3} = 68.08\mu m$ exhibit large normal forces at conventional pastry dough processing conditions $4^\circ C$. Working at higher temperatures of $30^\circ C$, lead to a significant reduction in normal forces for $\Phi_E = 0.7$ particles, which could lead to a reduction of ruptured dough layers during pastry production. As illustrated by figure 6.12, particle fat systems with $\Phi_E = 0.7$ exhibit similar normal forces at $30^\circ C$ as systems with $\Phi_E = 0.0$ and a mean particle size $x_{50,3} = 31.59\mu m$ at $4^\circ C$.

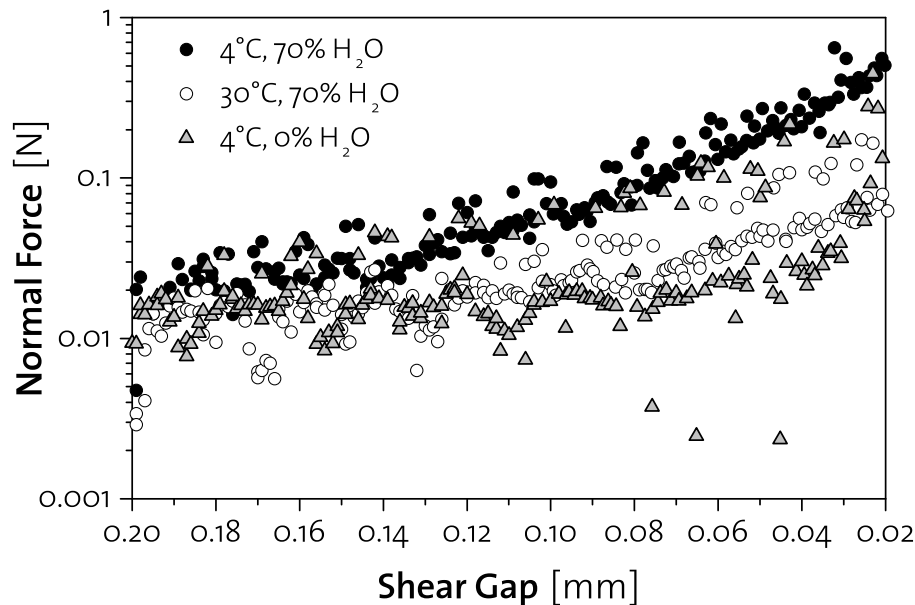


Figure 6.12.: SCR measurement for fat powders with a water content $\Phi_E = 0.7$ and $\Phi_E = 0.0$ at temperatures of $4^\circ C$ and $30^\circ C$

In 6.13, the work required to confine particles at different Φ_E is shown. At a temperature of $4^\circ C$, confinement of powder particles is influenced by the particle disperse fraction Φ_E to a large extent. Increasing the temperature to $30^\circ C$ leads to a far less pronounced dependence of Φ_E .

Therefore, when applying high Φ_E powder fat system in puff pastry production, an increased working temperature of up to $30^\circ C$ might be beneficial.

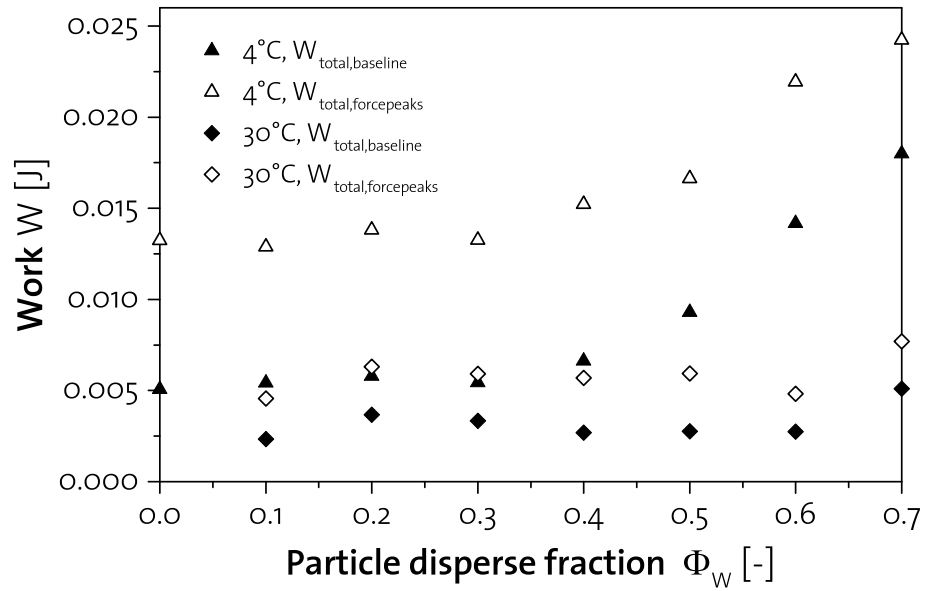


Figure 6.13.: Total work needed for confinement of fat particles with different particle disperse fraction Φ_E at two different temperatures of 4°C and 30°C.

6.8. Significance for Puff Pastry Dough Systems

Combining oscillatory thermo rheology (OTR) and shear confinement rheology (SCR) measurements facilitates a more fundamental understanding of forces exhibited by particulate fat on the macro and micro scale.

Fats are used in puff pastry dough to separate layers⁶⁴. In order to achieve homogenous alternating dough and fat layers, fat with a viscosity matching the viscosity of dough is required. Thereby, similar flowing properties can be achieved leading to homogeneous co-flowing of fat and dough resulting in the desired layered microstructure. McGill described the required properties of lamination fat: A too low viscous fat will break down in the lamination process leading to ruptured fat layers and will subsequently be absorbed by the dough leading to a loss of the layered structure. In opposite thereto, too high fat viscosities will lead to fat penetrating the dough layers leading to dough layer ruptures and a loss of the layered structure. Therefore, the viscosity of the powder fat was adjusted in the same magnitude as conventional puff pastry margarine as described in section 6.3. By using a specific fat blend and mixing powder at an optimized ratio with oil, the thermo-rheological properties of conventional puff pastry margarine could be matched with the novel powder fat.

To further understand micro rheological properties, SCR measurements were performed for powder fat using different particle sizes, fat melting properties and particle water contents in order to estimate normal forces exhibited by the powder fat on dough layers. In opposite to conventional puff pastry margarine consisting of a fat crystal network, where viscous and normal forces stay constant upon confinement, significant differences in normal forces could be measured for different fat powder properties. As described in section 6.4 and 6.6, significantly increased normal forces were exhibited by larger fat particles. In section 6.7 it was shown, that working at larger temperatures of 30°C instead of the conventionally used 4°C, leads to a significant decrease in normal forces exhibited by particles with larger mean particle size. Therefore, working at elevated temperatures could effectively decrease the damage caused by particle fat on the layering of puff pastry dough during lamination process.

6.9. Conclusions

NFPC was rheologically characterized in order to find optimal system characteristics for application in laminated dough products. Working with the same fat blend as applied in conventional puff pastry margarine at a particle disperse fraction $\Phi_P = 0.675$ lead to a matching complex viscosity and thermo-rheological properties of NFPC and conventional puff pastry margarine. It can be concluded, that the bulk rheology of NFPC can be easily tuned by varying the temperature dependent solid fat content

(SFC) curve and the particle fat phase and the hard fat powder disperse fraction. Thereby, NFPC can be adjusted to the dough.

As the hard fat powder particles exhibit significant normal forces on dough layers during lamination, the micro rheology characteristics for different hard fat powders were characterized. The normal forces increased with particle size and intra-particle disperse mass fractions Φ_E . Working at elevated temperatures could also effectively decrease normal forces exhibited by hard fat particles and lead to a decrease of dough layer rupturing probabilities when working at high particle disperse fractions.

From this one can summarize, that for optimal rheological and thermally stable NFPCs, the hard fat particles should be kept smaller than the resulting fat layer thickness in the laminated dough systems.

7. Mimicking the Baking Process

After the lamination process puff pastry is obtained by baking. The process of lamination is governed by the thermal- and microrheological properties of the applied fat system and dough. After lamination, the dough is ready to get baked. Baking in the controlled environment of an oven applies a specific temperature and humidity profile resulting in a preferably finely layered pastry dough product.

The mechanics underlying the expansion during baking of the layered dough/fat system have yet to be further understood. Therefore, thermo-rheological properties of layered dough were investigated in the following to gain a more fundamental mechanistic insight into the thermally induced expansion of puff pastry products.

Moisture in puff pastry dough turns into steam during baking¹⁰⁰. In conventional pastry dough, fat layers form a steam barrier hindering steam exiting the dough. The increasing steam pressure built up in the layered product, forces the dough layers to separate from each other and lift the pastry product. In general, it is assumed, that steam generated in composite dough mainly originates from the moisture contained in the dough layers, as conventional pastry fat does not contain significant amounts of water to be responsible for the expansion. The NFPC, in opposite, has a big influence on the leavening force generated by baking. At total water contents $m_{w,tot}$, which can be up to 4 times the water contained in conventional puff pastry fat, the potential for lift generated by thermal processing scales accordingly. The baking process and the impact on puff pastry is illustrated in figure 7.1.

As described in 8.1.1, the model puff pastry dough recipe during this thesis consisted of $m_d = 1908g$ dough and $m_f = 740g$ fat respectively adding up to a total dough weight of $m_{tot} = 2648g$. The dough mass m_d contains a total amount of 640g water, which is 24% of m_{tot} .

Conventional margarine contains 16.9% water, which translates to 125g or 4.7% water relative to the total dough weight m_{tot} . Therefore, pastry dough produced with conventional pastry margarine contains a total of $m_{w,tot} = 24 + 4.7 = 28.7\%$ water.

NFPC contains up to 60% water, translating to 444g or 16.8% water relative to the total dough weight of m_{tot} . This leads to a total of $m_{w,tot} = 24 + 16.8 = 40.7\%$ water in puff pastry produced with NFPC.

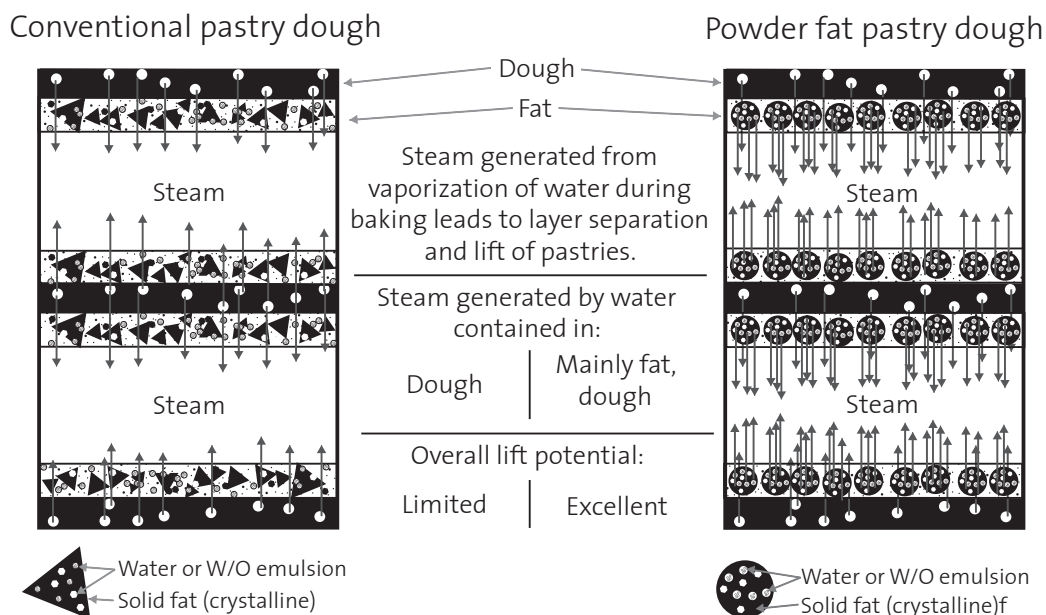


Figure 7.1.: Lift generated through physical leavening in the baking process of laminated dough.

As discussed earlier, the total water content of 40.7% contained in novel pastry dough compared to 28.7% contained in conventional dough leads to a significantly higher lifting potential. The goal of this chapter was gaining a fundamental understanding and quantification of the added lifting potential.

7.1. Materials and methods

The basic principles of the methods used during this chapter are described in 8.1.3. As the methods were used to mimic the baking process, detailed parameters and adaptations used are described as follows.

7.1.1. Thermogelling agents

In order to potentially influence evaporation of water during baking, two different thermogelling agents, methylcellulose (MC) and hydroxypropyl-methylcellulose (HPMC) were investigated. MC and HPMC and the underlying thermogelling mechanism described in section 2.7. The thermogelling agents provided by Dow Chemical Company (USA) are listed in table 7.1. The name of the listed MC and HPMC always consist of a letter followed by a number. The letter 'A' always stands for MC,

whereas 'E' and 'K' specifies HPMC type systems. 'SG' denotes a specific MC blend exhibiting extreme supergelling behavior. The number after the first letter stands for the viscosity of a MC or HPMC solution at a concentration of 2%(w/w) at a temperature of 20°C. Finally, the letter 'C' after the number stands for a multiplier of *100 (4C stands for 4000).

Table 7.1.: Specification of a 2% methylcellulose solution of the respective type

Name	Product Names (METHOCEL Type)	Gelation temperature [°C]	Viscosity [mPa·s]
Methylcellulose	A15	50-55	15
	A15C	50-55	1500
	SGA7C	38-45	700
Hydroxypropyl	E19	58-64	19
Methylcellulose	K99	70-90	99

7.1.2. Baking

Baking has been simulated by thermal analysis in literature^{16;33;14}. However, the oven rise due to steam formed during baking was not directly correlated to thermal measurements. In this section, baking was simulated by differential scanning calorimetry (DSC) and thermo gravimetric analysis (TGA).

the temperature profile of bread during baking at different spatial locations (crust, center) has been previously measured and mathematically described^{106;98;70}. For all measurements performed in this chapter, the conditions used during the baking trials performed in the course of this thesis (220°C for 25 minutes) were applied. Product core and crust temperatures of 100°C and 160°C respectively can be expected. Therefore, the baking process was mimicked by DSC, TGA and Thermo-Rheology with a temperature profile of 20°C - 150°C and a heating rate of 10°C/min..

7.1.3. Differential Scanning Calorimetry (DSC) and Thermogravimetry Analysis (TGA)

For DSC and TGA measurements, a sample of approximately 7mg was placed in an aluminum sample pan. Measurements were performed with open sample pan (no lid was applied to close the sample pan), in order to reassure unhindered evaporation of water contained in the sample. Combined DSC/TGA measurements were used to

correlate the heat flux measured by DSC (indirect measurement of evaporation) with the weight loss measured by TGA (direct measurement of evaporation).

7.2. Contribution of water contained in dough and fat towards total lift force

In order to assess the contributions towards the total lifting force generated during the baking process, dough and emulsion based fat systems were in a first step both measured by combined DSC/TGA analysis. Thereby, as described before, DSC and TGA curves can be correlated in order to reassure observed peaks can be linked to evaporation phenomena.

Figure 7.2 shows dough (composition see section 8.1.1) and fat (NFPC with $\Phi_E = 0.5$) portion of laminated pastry dough measured by combined DSC/TGA.

The dough shows a relatively broad heat flux peak between 50–110°C, which is caused by starch gelatinization, dissociation of amylose-lipid complexes and to a lesser extent evaporation of water^{32;16}. The second heat flux peak observed between 120 – 140°C can be linked to evaporation of water from the dough samples. These observations are also in line with the weight loss measured by TGA; between low temperatures of 20 – 120°C, a constant, relatively linear decrease of the total weight of the dough sample could be observed. Starting at 120 – 140°C a more pronounced water loss becomes apparent which is also in line with the heat flux peak observed in the same temperature range.

NFPC with $\Phi_E = 0.5$ in opposite, shows a first heat flux peak at 50 – 80°C, which can be explained by the melting enthalpy of the fat fraction. A second, considerable larger peak can be observed at 100 – 140°C, which is clearly related to evaporation of water. This is also in line with the TGA data, where the fat powder shows a constant weight loss until a temperature of 100°C. At 100°C, which is the boiling point of water, the weight loss increases rapidly, which is also in line with the DSC measurements.

The difference slope of the weight loss curve between 20 – 100°C of dough and NFPC, which is linked to the evaporation of water, is caused by the differences in total water contained in dough (contains a total of 24% water) and powder (total water content of 37.5%).

This data suggests, that the dough portion contributes to a lesser extent and at higher temperature to the total lift force generated compared to emulsion based powder fat.

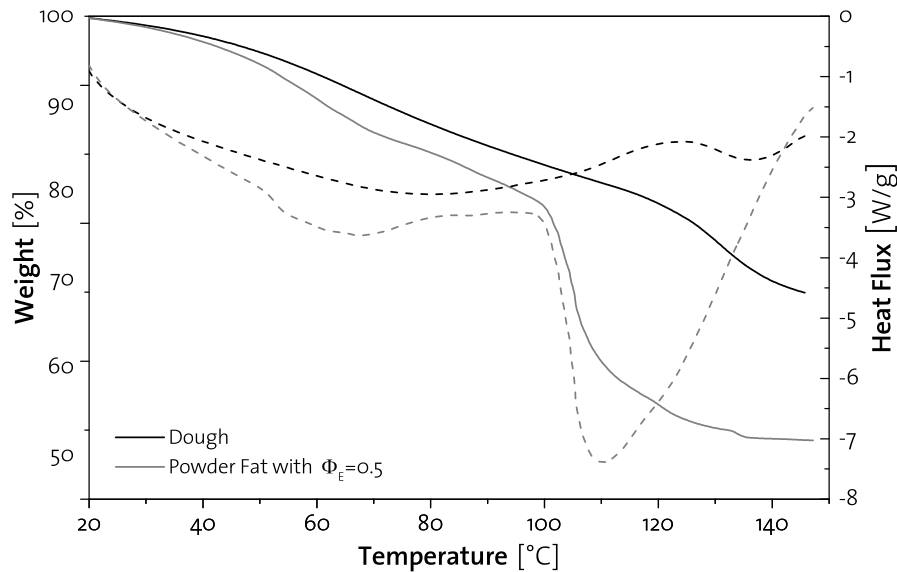


Figure 7.2.: Simulation of the Baking process the components of pastry dough by combined DSC/TGA measurement. The solid lines show the relative weight (TGA) and the dotted lines the heat flux (DSC) simultaneously measured for the two samples.

7.3. Thermal stability of emulsion based systems

Figure 7.3 compares DSC curves obtained from measuring pure water, stable and unstable emulsions ($\Phi_E = 0.5$) respectively. Pure water shows a very sharp, clear evaporation peak at a temperature of 100°C. For the stable and unstable emulsions, a bimodal melting peak of the fat fractions between 50 – 60°C was observed. Stable emulsions showed a delayed evaporation of water between 100 – 130°C. In opposite thereto, unstable emulsions followed the evaporation of pure water closely. It can be expected, that unstable emulsions phase separate quickly upon heating, leading to a binary system consisting of a water layer covered by a fat layer. Further heating of this binary system leads to evaporation kinetics closely resembling those of pure water. Fluctuations in the heat flux can be explained by local destabilization phenomena and the nature of the binary system, where the less dense oil layer covers the water layer. In these binary systems, evaporating water has to permeate the oil layer first, before unhindered evaporation. Due to the differences in total water contained in pure water and the emulsions, the integral of pure water and emulsions are not identical.

Therefore, we can characterize the stability of emulsions and emulsion based systems by DSC. Stable emulsions will show an evaporation peak at high temperatures (higher than the evaporation peak of pure water), whereas unstable emulsions will follow the

trend of pure water closely.

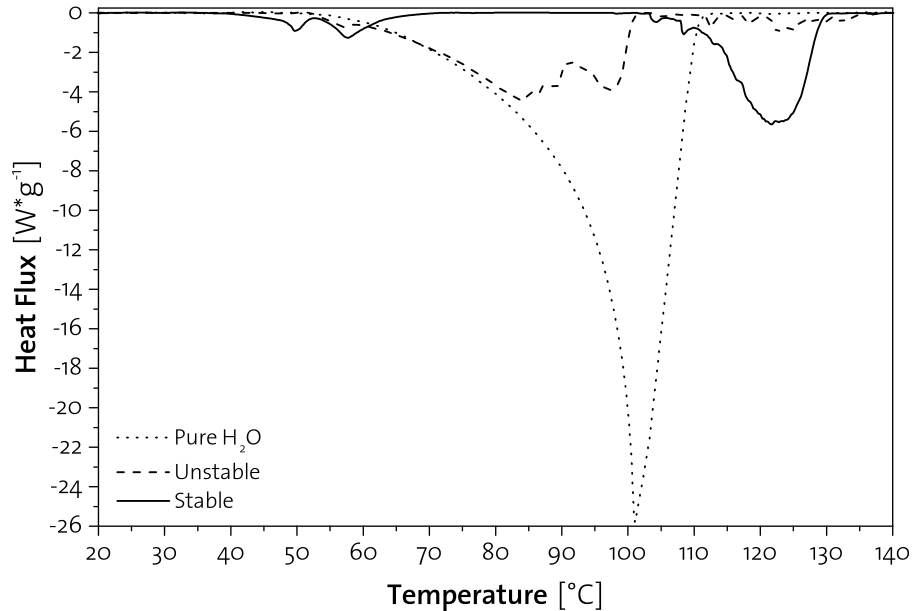


Figure 7.3.: Comparison of stable and unstable emulsion based fat systems compared with pure water.

7.4. Evaporation kinetics of emulsion based systems

After the assessment of emulsion stability, and evaporation behavior of pure DSC, the impact of different emulsion disperse fractions (Φ_E) were investigated. In figure 7.4, emulsion systems with $\Phi_E = 0.2 - 0.7$ are shown. The impact of an increased emulsion disperse fraction is twofold.

Firstly, as illustrated by T_{melt} , the onset and end of melting show a tendency to be shifted towards higher temperatures for higher Φ_E . This can be explained by the higher heat capacity of water ($c_p = 4.1813 J * g^{-1} * K^{-1}$) compared to fat ($c_p = 1.8 J * g^{-1} * K^{-1}$). Due to this, water acts as a heat buffer leading to a delayed heating of the sample and therefore to onset and offset of melting at higher temperatures for higher Φ_E .

Secondly, significant differences in the evaporation peak are obvious. At low $\Phi_E = 0.2 - 0.3$, only a small peak could be observed. At higher $\Phi_E = 0.4 - 0.7$, the evaporation peak progressively increases finally showing a very pronounced peak for $\Phi_E = 0.7$ could be observed. With increasing depth of the peak, the width of the

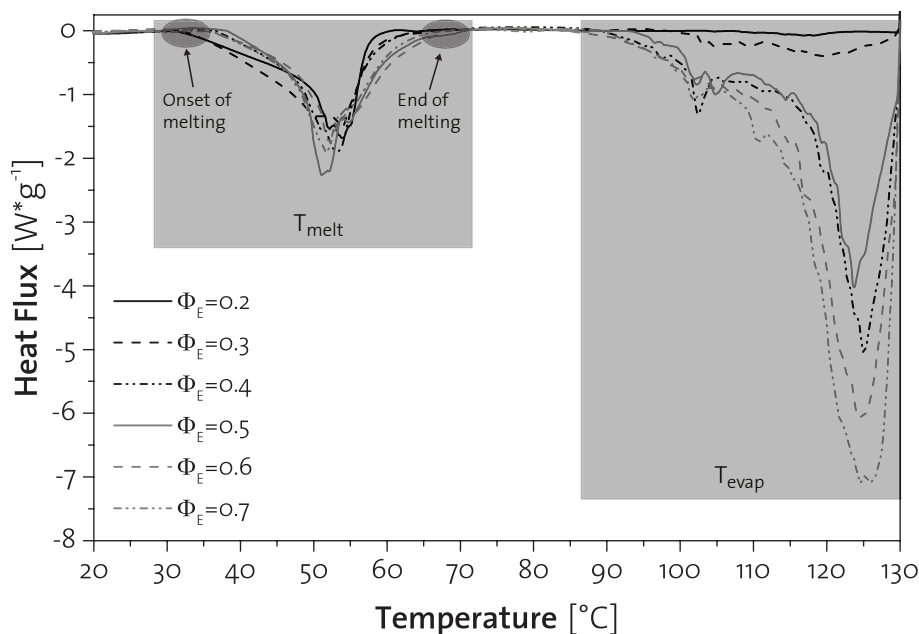


Figure 7.4.: Evaporation kinetics of emulsion based systems.

peak also increases slightly. A trend towards an earlier onset of the evaporation peak could be observed for higher Φ_E values.

It can be concluded, that as expected elevated water contents generate more steam and thereby possess a higher pastry lift potential.

7.5. Modulating the evaporation of water during baking

As the pronounced, relatively sharp evaporation peak observed for high Φ_E values (see figure 7.4) might be connected to a very rapid, uncontrolled water release during baking, possibilities to influence the water release from emulsion based NFPC were investigated. Possible starting points for influencing the water release are modifying either the fat or the water fraction of the powder fat.

Baking simulation measurements performed by DSC showed, that using fat fractions with different melting range has no influence on the evaporation kinetics during baking. This can be explained by the thermal properties of fat and the mechanics of water evaporation. At water evaporation temperatures ($> 100^\circ\text{C}$), all investigated fat fractions (different fractions of palm fat) are completely liquefied. Therefore, the

mobility of the water droplet emulsion substructure at elevated temperatures is not influenced by the melting point of fat.

Altering the water phase of the emulsion based fat particle disperse substructure, in opposite, was much more promising. As illustrated by figure 7.5, enrichment of water with methyl cellulose (MC) and hydroxypropyl methylcellulose (HPMC) has a significant influence on the evaporation properties compared to pure, unmodified water. Pure water exhibits a sharp evaporation peak at 100°C. In comparison thereto, application of MC and HPMC shifts the evaporation peak towards higher temperatures. For all different MC (A4C, SGA7C) and HPMC (E19, K99) investigated, evaporation peaks were observed at approximately 113°C.

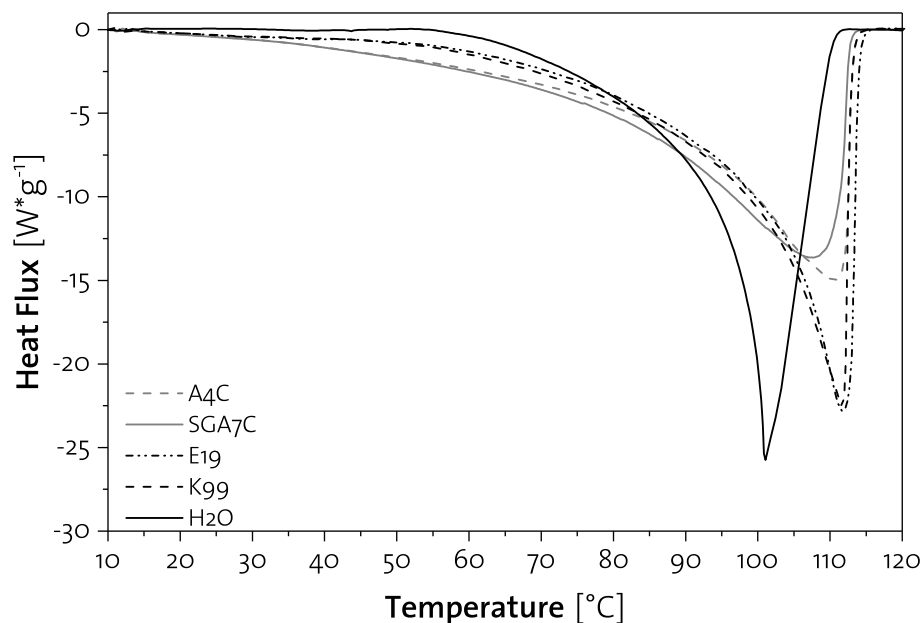


Figure 7.5.: Evaporation kinetics of emulsion based systems.

This behavior can be explained by the thermo-gelling properties of cellulose. The complex viscosity at increasing temperatures was measured by OTR with the goal to mimick the baking process by rheometry similarly as described earlier for thermal analysis methods. OTR measurements were performed in a temperature range of 50 – 120°C at a heating rate of 10°C/*minute* in order to simulate the baking process. This slightly altered temperature profile was caused by the instrumentation setup. The same water phase as measured by DSC in chapter 7.5 was measured by OTR.

Pure water without cellulose showed a relatively flat complex viscosity curve with a slightly declining slope (figure 7.6). This is in line with the expectations, as a higher temperature is linked to a higher mobility of water molecules and therefore a declining complex viscosity measured.

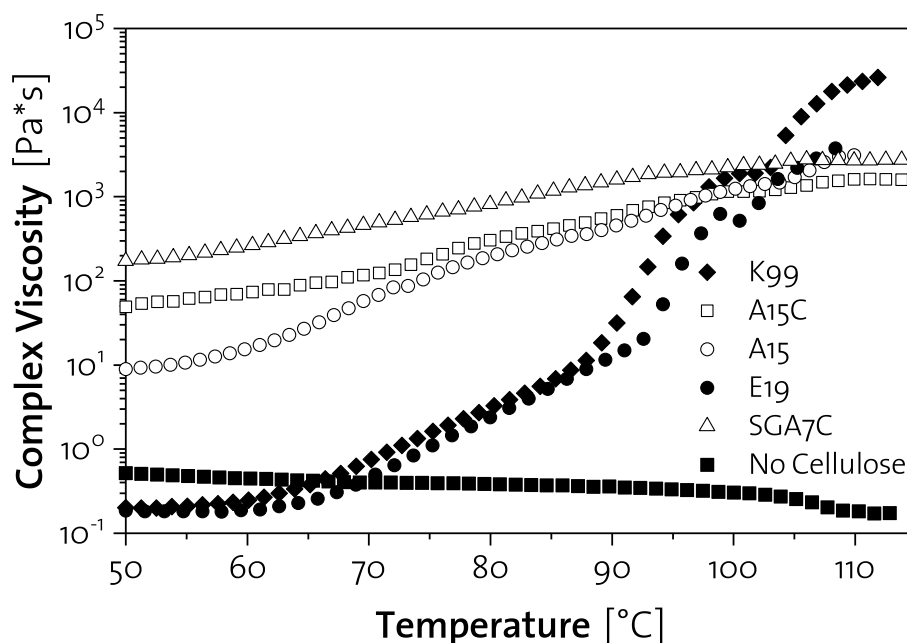


Figure 7.6.: Evaporation kinetics of emulsion based systems.

A different trend could be observed for MC and HPMC. Methylcellulose of the type A15, A15C and SGA7C have gelling points in the range of 38 – 55°C as listed in table 7.1 and form strong networks in the whole temperature range observed. In opposite thereto, hydroxypropyl methyl cellulose of the type E19 and K99 form strong thermogels at elevated temperatures with a gelling point of 58 – 90°C. Therefore a strong increase in complex viscosity could be observed at elevated temperatures starting at approximately 70°C.

The thermorheologic measurements shown in figure 7.6 are in line with trends shown in literature, where OTR measurements in the range of 20–80°C were performed^{48;52;57;20}.

These observations made by OTR and DSC lead to the conclusion, that MC and HPMC could be powerful modifiers allowing tailored gelling of emulsion water droplets and modified water release. By OTR it was shown, that MC and HPMC form strong networks at elevated temperature due to their thermo-gelling properties; the hypothesis, that MC and HPMC influence the evaporation of water through thermo-gelling was confirmed by DSC measurements, where the evaporation peak was effectively shifted by cellulose.

7.5.1. The impact of the methyl cellulose concentration

After the proof-of-concept shown before, the optimum (hydroxypropyl-) methyl cellulose concentration to be applied to the fat system had to be determined. Figure 7.7 illustrates the impact of different methylcellulose concentrations on baking simulated by DSC. The properties of methylcellulose gels not only depend on the degree of substitution of the methylcellulose gel, but also on the concentration applied to the solution²⁰.

Increasing the methylcellulose concentration lead to slightly broader, more fluctuating evaporation peaks. However, the impact on evaporation appears to be small. Therefore, methylcellulose was applied at a concentration of 1% in future trials.

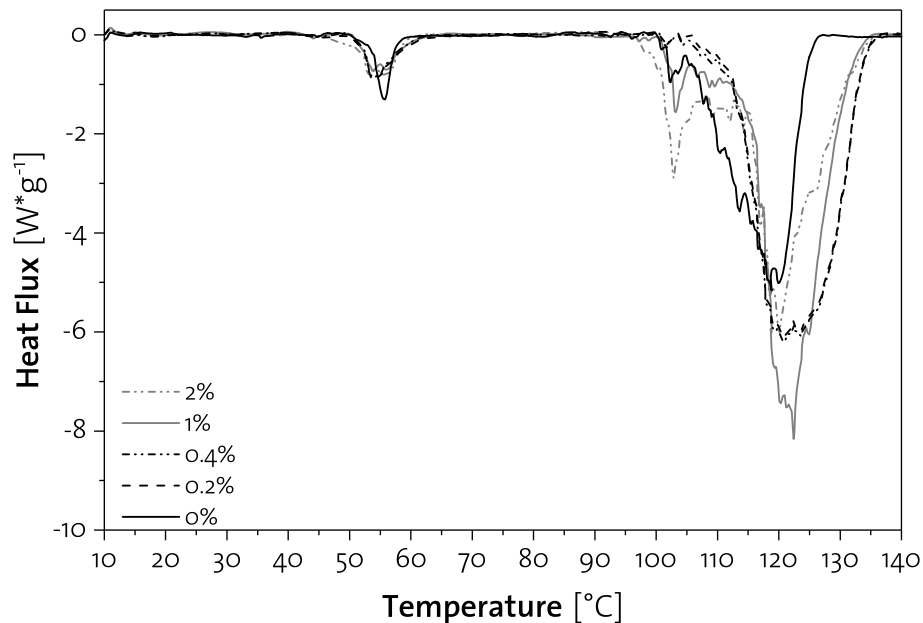


Figure 7.7.: Evaporation kinetics of emulsion based systems.

7.5.2. The evaporation kinetics of HPMC based systems

Figure 7.8 shows the impact of two different HPMC at 1% concentration in the emulsion dispersed water phase on evaporation kinetics. When no HPMC is present in the water phase, a relatively sharp evaporation peak at 120°C with an onset at 102°C and an offset at 130°C was observed. The two HPMC, E19 and K99 applied showed a similar onset of evaporation at 102°C and a similar peak location at 120°C. The offset of evaporation appeared to be slightly shifted towards higher temperatures

of 135 for the HPMC systems. Therefore the impact of HPMC on the evaporation kinetics from novel powdered fats seems to be negligible.

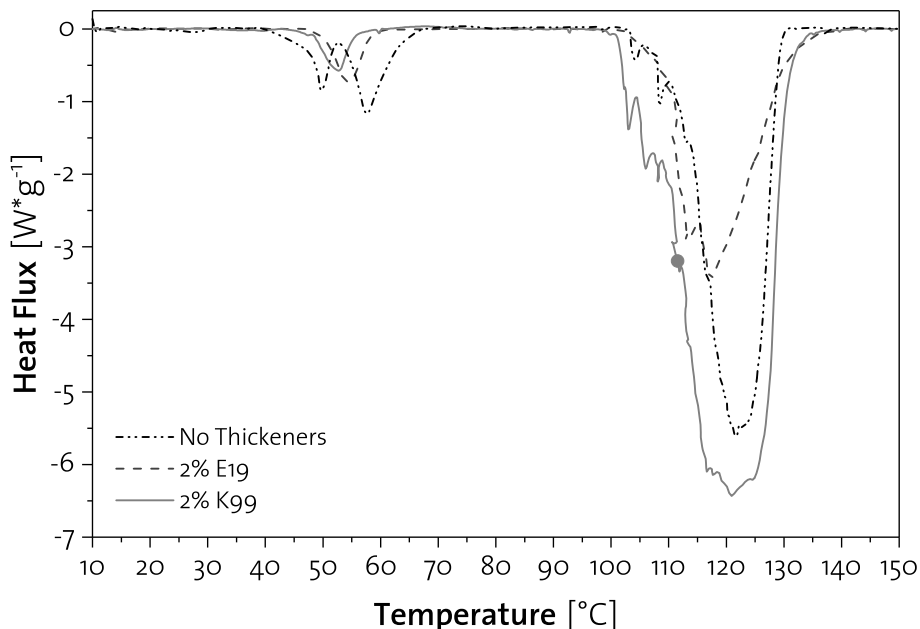


Figure 7.8.: Evaporation kinetics of emulsion based systems.

7.5.3. The evaporation kinetics of MC based systems

The evaporation from systems enriched with MC at 1% concentration is shown in figure 7.9. The impact of MC seems to be much more pronounced compared to HPMC. All MC systems have evaporation peaks which are spread over a relatively large temperature range. Onset of evaporation for all systems is similar at around 100°C. However, the evaporation peak for MC systems is less pronounced for all MC systems compared to standard. Additionally, the endset of evaporation is shifted towards significantly higher temperatures, especially for the SGA7C, which is the methyl cellulose which forms the strongest gel networks. Endset of evaporation for MC systems is in the range of 140 – 150°C for all observed MC systems.

The broad (less sharp) evaporation peaks with a much higher offset of evaporation lead to the conclusion, that evaporation, and thereby lift force generated during baking, can be significantly impacted by MC. MC should thus lead to a more controlled evaporation over a broader temperature range in puff pastry and in general dough systems which rely on physical leavening instead of leavening by yeast.

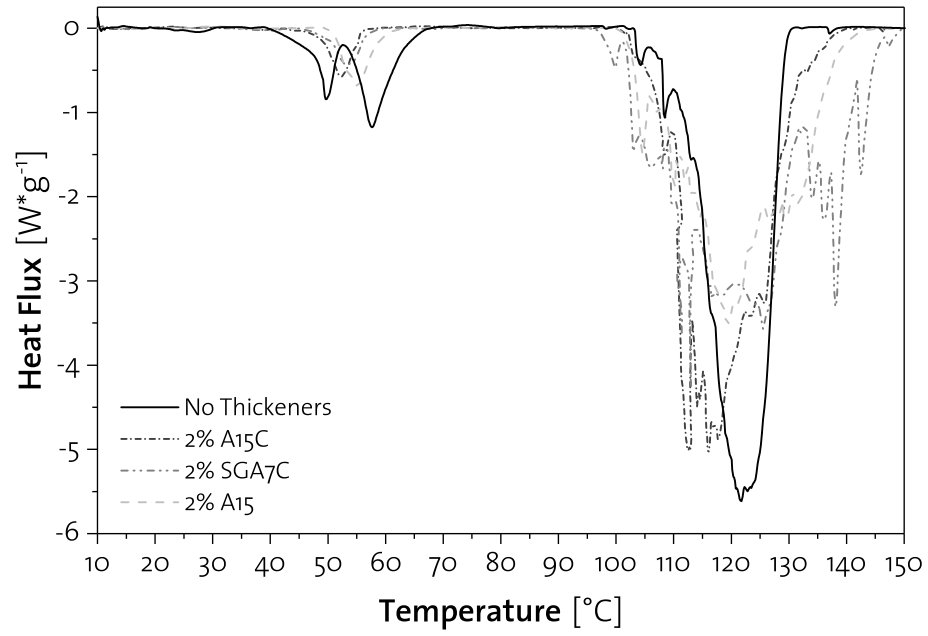


Figure 7.9.: Evaporation kinetics of emulsion based systems.

7.5.4. The impact on low temperature gelling agents (sodium alginate)

In opposite to MC and HPMC type thickening agents, which act at elevated temperatures, the conventional low temperature thickener sodium alginate was applied to the water phase of the fat particles. The resulting system was investigated by DSC as shown in figure 7.10; no clear impact of sodium alginate on the evaporation of water could be observed. The onset, peak and endset of evaporation was in the same range as the standard system.

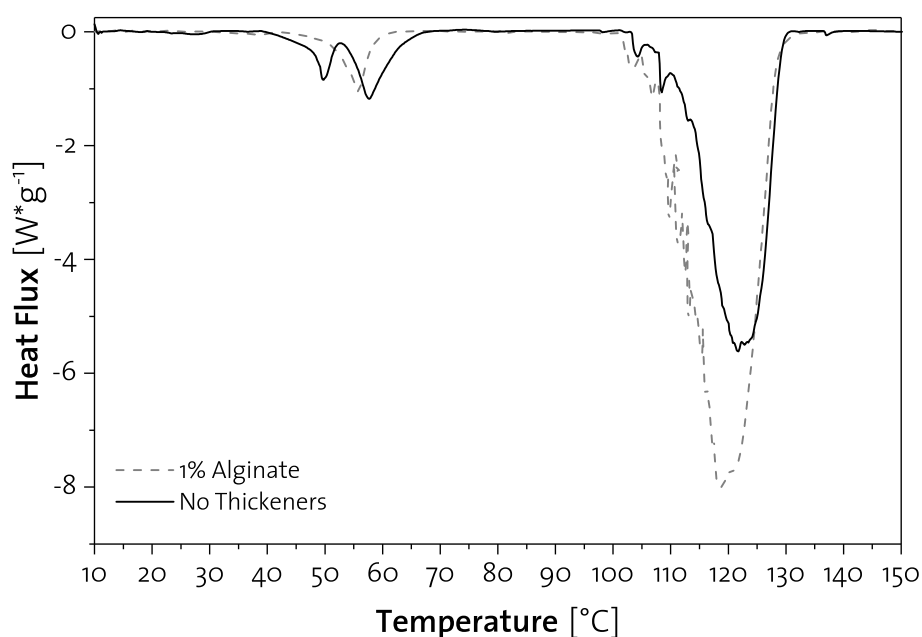


Figure 7.10.: Evaporation kinetics of emulsion based systems.

7.6. Significance for Puff Pastry Dough Systems

Rise in puff pastry products is mainly driven by physical leavening forces caused by steam pressure built up through evaporated water. For gaining a deeper understanding of baking and underlying driving forces, it therefore is crucial to quantify leavening forces generated in laminated dough. As water contained in dough and fat can both significantly impact the rise generated by baking, dough and different fat systems were characterized by thermal analysis.

In conventional puff pastry dough produced with puff pastry margarine, rising forces originate mainly from water contained in the dough. When NFPC containing elev-

ated water contents is applied during baking, a strong impact on the leavening forces can be expected. As shown in figure 7.4, elevated water contents show significant peaks during DSC baking simulation. It was also shown, that water release from powder shows strong peaks. The formation of large leavening forces from powder fat containing elevated water contents in combination with the relatively narrow temperature frame where the leavening forces are to be expected, might be problematic. It is hypothesized, that evaporation of water over a larger temperature frame might be beneficial, as the laminated dough system might be able to better hold steam formed over a longer time compared to relatively quick evaporation as seen in figure 7.4.

Therefore, different thermogelling agents (MC and HPMC) were applied to the water phase of the powder fat system. It could be shown, that water evaporation can be significantly delayed and spread over a broader temperature frame.

7.7. Conclusions

The baking process of puff pastry products was simulated by thermal analysis (DSC, TGA). Using thermal analysis to simulate baking allows the observation of evaporation of water from emulsion based fat systems. Application of thermogelling agents allowed a modification of the water released by evaporation from emulsion based systems. Methylcellulose (Types A15, A4C, A15C, SGA7C) and hydroxypropyl methylcellulose (Types E19, F50, K99) were analyzed which differ in their form and degree of substitution.

It can be concluded, that DSC is an adequate method for predicting the thermal behavior of emulsion based fat systems. Melting of fat and evaporation of water could be observed precisely by their respective peaks. The evaporation peak of pure water based systems is located at a temperature of 100°C. Supplementing the emulsion water phase with methylcellulose allowed a broadening and shifting of the evaporation peaks towards higher temperatures; it is suggested, that this shift in evaporation peaks is caused by the mechanical stabilization caused by methylcellulose substructuring which have to be overcome for vaporization⁶⁸.

For all observed systems, methylcellulose had a larger impact on the evaporation of water than hydroxypropyl methylcellulose. A higher viscosity of the thickener resulted in a broader water evaporation peak with a smaller peak depth and more fluctuations. An increase in gel elasticity due to higher methylcellulose concentrations was reported⁵⁷. It is assumed that gel strengthening enforces a phase separation during baking simulation trials by DSC, leading to a dissociation of water from the gel network. This free water might evaporate earlier whereas water bound in the gel network retains in the sample longer. This mechanism could explain the earlier onset

of the water evaporation peak and its fluctuations above 130 °C occurring in some heating curves.

8. Application of powdered fat systems in laminated dough

After successful production of NFPC by spray-chilling (chapter 5) and its rheometric (chapter 6) and thermal (chapter 7) characterization, application trials were carried out in order to validate the theoretical insight gained. Powder fat systems were compared to conventional puff pastry fat (total water content of 16.9% (w/w)).

All runs displayed in the same graph in the following pages were performed on the same day. Due to temporal and processing variations (temperature of the refrigerator, temperature of the oven, exact setting of the laminating machine, daily variations in processing performed by the baker producing the dough), samples can only be compared intra-daily.

8.1. Materials and Methods

8.1.1. Dough

The dough phase of the composite puff pastry dough was produced using the ingredients listed in 8.1.

Table 8.1.: Ingredients of the puff pastry dough. All ingredients were stored in a refrigerated environment (10 °C) prior to dough preparation.

	Ingredient	Weight [g]
Dough	Wheat Flour Type 550	1200
	Puff Pastry Margarine	40
	Water	640
	Salt	24
Touring	Laminating fat	740
	Total weight	2648

8.1.2. Conventional puff pastry fat

The composition of conventional puff pastry fat (CPPF) with a total water content of 16.9% (w/w) is listed in table 8.2. This fat was produced by Mibelle AG, Switzerland through conventional processing (as described in 2.3) and is not a powder based, but a fat system stabilized by a fat crystal network substructure.

Table 8.2.: Composition of conventional puff pastry fat (CPPF).

Ingredient	Mass fraction [% (w/w)]
Palm stearin	39.75
Palm super stearin	13.25
Palm mid fraction	4.0
Canola oil	25.0
Danisco PS 404	1.0
Citric acid	0.1
Water	16.9

Powder fat

As described in section 2.4, NFPC was produced by simultaneous spray chilling as previously discussed in detail in section 5. For all fat system, the same hard fat blend matching the melting properties of CPPF was utilized. The composition of the hard fat blend (HFB) is listed in table 8.3.

The different powder fat systems utilized for the application trials discussed in this section are listed in table 8.4. Relevant parameters changed in the respective fat system are highlighted in **bold font**.

Table 8.3.: Composition of the hard fat blend (HFB) used in all powder fat systems.

Ingredient	Mass fraction % (w/w)
Palm stearin	57.8
Palm super stearin	36.4
Palm mid fraction	5.8

Table 8.4.: Composition of powder fat systems used in this section.

Powder fat system	HFB [% (w/w)]	Canola oil [% (w/w)]	PGPR 90 [% (w/w)]	Water [% (w/w)]	$x_{50,3}$ [μm]
P_R (Reference)	49.6	32.5	1	16.9	32
$P_{\Phi_P=0.75}$	57.1	25	1	16.9	32
$P_{\Phi_P=0.725}$	54.6	27.5	1	16.9	32
$P_{\Phi_P=0.70}$	52.1	30	1	16.9	32
$P_{\Phi_P=0.675}$	49.6	32.5	1	16.9	32
P_{large}	49.6	32.5	1	16.9	100
P_{small}	49.6	32.5	1	16.9	32
P_{30}	36.5	32.5	1	30	32
P_{40}	26.5	32.5	1	40	32
P_{50}	16.5	32.5	1	50	32

8.1.3. Preparation of the puff pastry dough samples

The basics of laminated dough are described in detail in section 2.5. For the application trials performed in this section, puff pastry dough was prepared according to the german method⁸⁴. Refrigerated wheat flour, puff pastry margarine, water and salt, as listed in table 8.1, were placed in a hook kneader and kneaded for 5 minutes until a dough temperature of $22^\circ C$ was reached. Then the dough was rested at $10^\circ C$ for 10 minutes.

Dough and fat used for touring were rolled out to a thickness of $1cm$. The fat layer was enclosed into the dough layer, and lamination steps (single and double tours as shown in figure 8.1 according to the german method of lamination, where fat is enclosed by dough) as listed in table 8.5 were applied. Depending on the number and combination of (single and double) tours applied to the dough, the desired number of fat layers in the composite dough could be controlled. The composite dough was always rested for 30 minutes after lamination and rolling out steps in order to let possible tensions in the dough relax and to reassure a homogeneous pastry product.

After the last touring step, the dough was rolled out to $3.2mm$ and cut into quadratic pieces measuring $80 \cdot 80mm$. After a resting time of 30 minutes, the dough was baked in a preheated oven at $230^\circ C$ after initial injection of steam for 25 minutes.

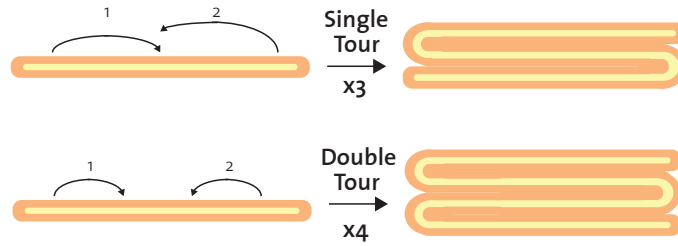


Figure 8.1.: Touring steps during lamination of puff pastry dough. Single tours result in a 3*-multiplier, double tours in a 4*-multiplier to the fat layers contained in the dough.

Table 8.5.: Number of fat layers obtained by lamination and the underlying program of lamination.

Total number of fat layers	Touring steps
27 (3 * 3 * 3)	single * single * single
48 (3 * 4 * 4)	single * double * double
144 (3 * 4 * 3 * 4)	single * double * double * single
192 (3 * 4 * 4 * 4)	single * double * double * double
256 (4 * 4 * 4 * 4)	double * double * double * double

8.1.4. Analysis of puff pastry dough structure by CLSM

Sample Preparation

CLSM is able to differentiate fat from dough layers in composite dough when combined with staining by fluorophores. CLSM microscopy has been used for qualitative analysis of composite dough⁵. Bousquieres *et al.* developed a method allowing quantitative study of layers in laminated dough. During this thesis, laminated dough was produced and examined according to this method. As shown in figure 8.2(a), puff pastry dough was rolled out to a final thickness of 3.2mm using a mechanical dough sheeter type Rondo Econom 4000 STM 5303 (Rondo, Switzerland).

A cubic sample measuring 5.5mm was cut out of the center of the rolled out dough and frozen in a cryo-microtome of the type CryostarTM NX70 (Thermo Fischer Scientific, USA). The samples were embedded in OCT medium and positioned in such a way, that the slicing direction was perpendicular to the sheeting direction as shown in 8.2(b). The cryo-microtome chamber was tempered to $T = -20^{\circ}C$ and the cutting blade was tempered to $T = -30^{\circ}C$, insuring clean, non destructive cutting of the samples. Slices measuring 20 μm were cut off each cube and transferred to microscopic slides.

Subsequently, slices were stained with Nile red (Sigma-Aldrich, USA) and crystal violet (Sigma-Aldrich, USA). Thereby, puff pastry dough microstructure can be visualized.

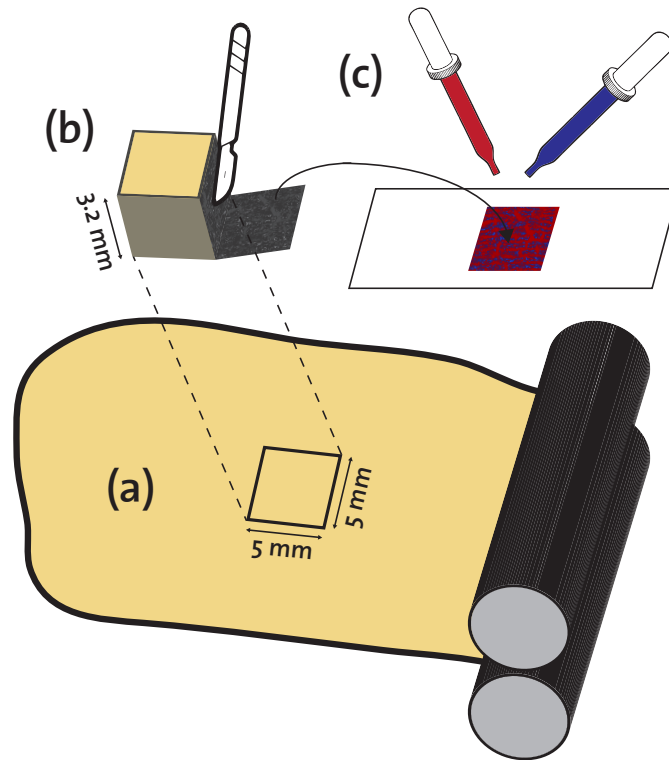


Figure 8.2.: Sample preparation for assessment of puff pastry dough by CLSM: (a) Puff pastry dough rolled out to a thickness of 3.2mm, (b) 5 · 5mm cube cut out of the dough. Sliced by Cryotome perpendicular to rolling out direction (c) slice transferred to slide and stained with Nile red and crystal violet dyes.

Image acquisition and analysis

Images of puff pastry dough were acquired by a 10x 0.3 EC Plan-Neofluar objective. Resolution was 0.6/pixel at an image size of 1355 x 1355 pixels. For each puff pastry dough sample, at least three pictures were acquired at random locations.

Limitations

Analyzing dough microstructure using this method requires stable laminated dough after rolling out and prior to freezing in the cryo-microtome. Puff pastry dough produced with laminating fat (conventional and powder fat) at a water content of $m_{w,tot} = 16.9\%$ lead to a product which showed excellent temporal stability.

Increasing the powder fat water content to $m_{w,tot} \geq 30\%$ lead to a decreased dough stability, especially after rolling out the dough to a final thickness of 3.2mm . Therefore application of this method is only suited for laminated dough produced with low water content laminating fat and was only used for characterization of puff pastry dough with laminating fat at a water content of $m_{w,tot} = 16.9\%$. For characterization of laminated dough produced with laminating fat containing high water contents, development of a new method or adapted sample preparation is required. Due to time restrictions, this was not done in the course of the experimental work underlying this thesis.

8.1.5. Volume measurement of the baked puff pastries by 3D scanning

A NextEngine 3D Scanner Ultra HD (NextEngine Inc., Canada) was used to measure the volume of the baked puff pastry samples. Samples of the same pastry dough were scanned in quadruplets and the mean volume was calculated.

8.2. The micro- and macrostructure of conventional puff pastry products

As a baseline, puff pastry using conventional puff pastry fat (CPPF, with a total water content $m_{w,tot} = 16.9\%$ as listed in 8.1.2) consisting of 144 alternating dough and fat layers was produced. An illustration of the obtained product is shown in figure 8.3.

Figure 8.3a shows the cross section of standard puff pastry dough with a layering of 144. The fine and undamaged, continuous layers of dough (dyed blue, with entrapped starch granules in black) and fat (black) are obvious. Thanks to this microstructure, evaporating water can be entrapped in the pastry product during baking leading to a large pastry volume with fine, well separated layers as illustrated in figure 8.3b.

In a next step, different layerings of 27, 48 and 144 were investigated for conventional puff pastry dough. A higher number of layers lead to a higher volume of the baked

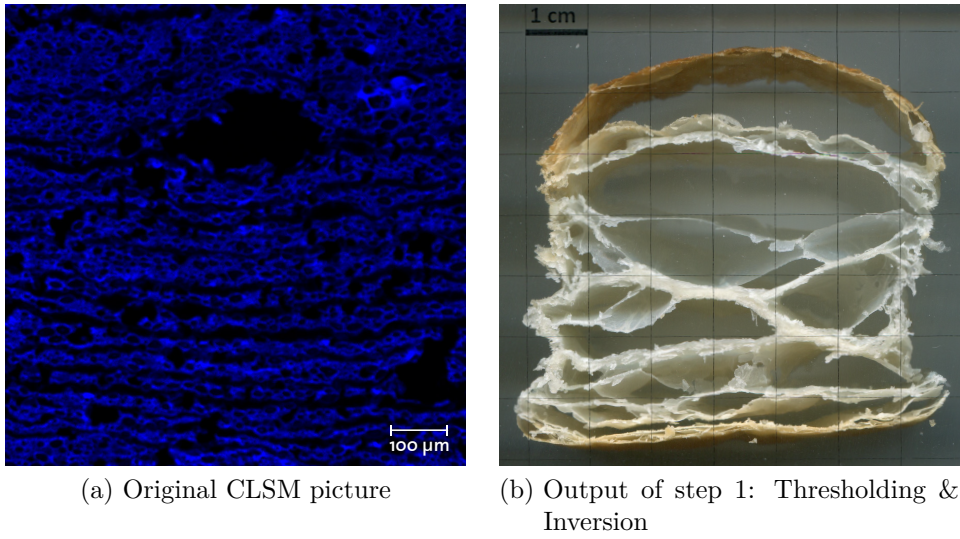


Figure 8.3.: The microstructure of conventional puff pastry dough.

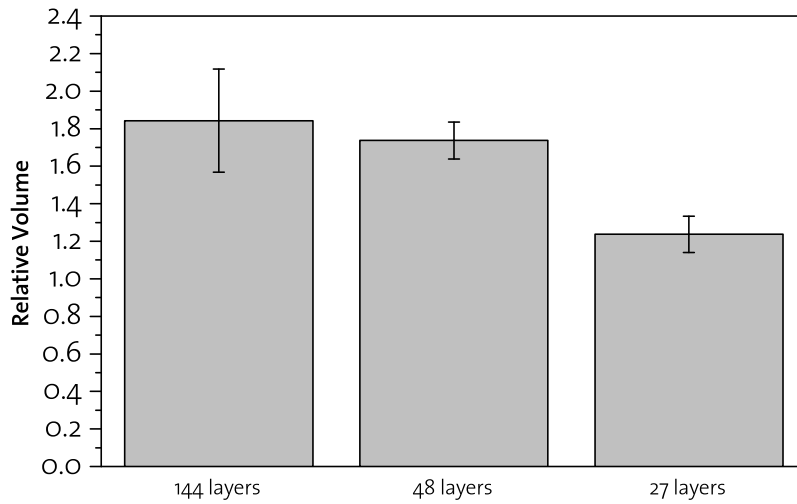


Figure 8.4.: Volume obtained from baking of conventional puff pastry dough using different layerings.

puff pastry. This is in line with the parameters used in bakery industry. Usually puff pastry dough is toured in such a way, that 144 layers are obtained.

8.3. The micro- and macrostructure of puff pastry products produced with powder fat at different powder in oil disperse ratios Φ_P

As described in 6.3, the powder in oil disperse ratio Φ_P is of crucial importance for the complex viscosity and the flowing behavior of the novel powder fat (NPF). An optimum viscoelasticity of NPF was found at $\Phi_P = 0.675$ for particles produced with the same fat blend as used in CPPF. To validate these rheometric results, powder fat with different Φ_P as listed in table 8.4 ($P_{\Phi_P=0.75}$, $P_{\Phi_P=0.725}$, $P_{\Phi_P=0.70}$ and $P_{\Phi_P=0.675}$) was used to investigate the impact of different fat flowing properties on the volume of the baked puff pastry product. All doughs were produced with powder fat containing the same water content as CPPF of $m_{w,tot} = 16.9\%$ and a layering of 144.

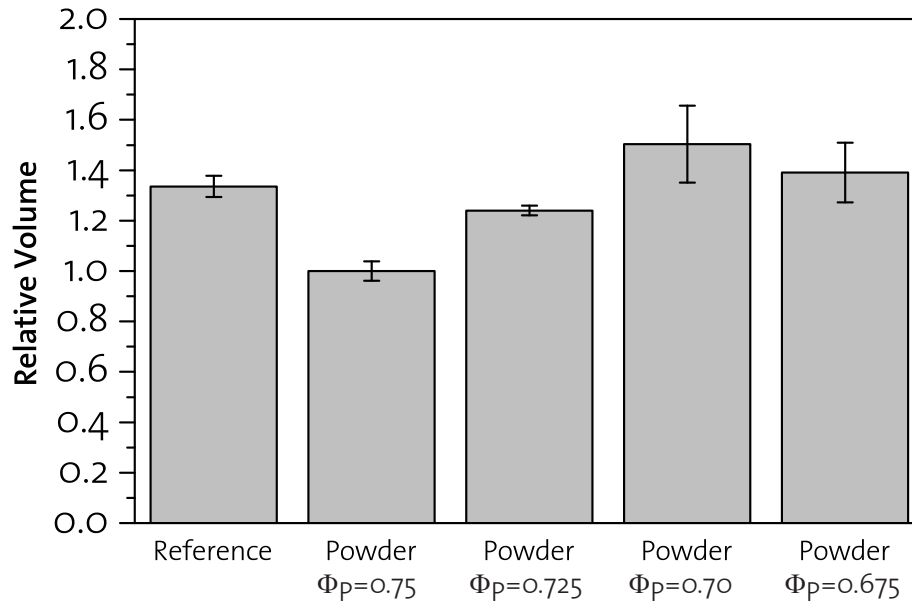


Figure 8.5.: Influence of the powder in oil disperse ratio Φ_P on the volume generated by baking.

Figure 8.5 shows the volume obtained after baking puff pastry dough samples with different powder in oil disperse ratios Φ_P . Higher Φ_P ratios are linked to higher viscosities as previously discussed and can thereby adversely impact the co-flowing of dough and fat layers during lamination. Application of powder fat $P_{\Phi_P=0.75}$ leads to the lowest (significantly lower than reference dough) volume after baking. The complex viscosity at processing temperature (10°C) of this powder fat is $\eta = 2 \cdot 10^4 \text{ Pa} \cdot \text{s}$. In powder fat $P_{\Phi_P=0.725}$ the complex viscosity decreases to $\eta = 1.6 \cdot 10^4 \text{ Pa} \cdot \text{s}$, which was linked to a higher volume generated after baking. At even lower powder to oil

8.3. The micro- and macrostructure of puff pastry products produced with powder fat at different powder

disperse ratios $P_{\Phi_P=0.70}$ and $P_{\Phi_P=0.675}$ complex viscosity decreased to $\eta = 1.2 \cdot 10^4 Pa \cdot s$ and $\eta = 1.1 \cdot 10^4 Pa \cdot s$ respectively. This further decrease in viscosity lead to an improved flowability of the powder fat between the dough layers during dough production and resulted in an improved volume generated after baking.

Powder fat $P_{\Phi_P=0.70}$ and $P_{\Phi_P=0.675}$ lead to similar, highest volume obtained after baking. The obtained volume was higher than the reference dough produced with conventionally produced puff pastry fat.

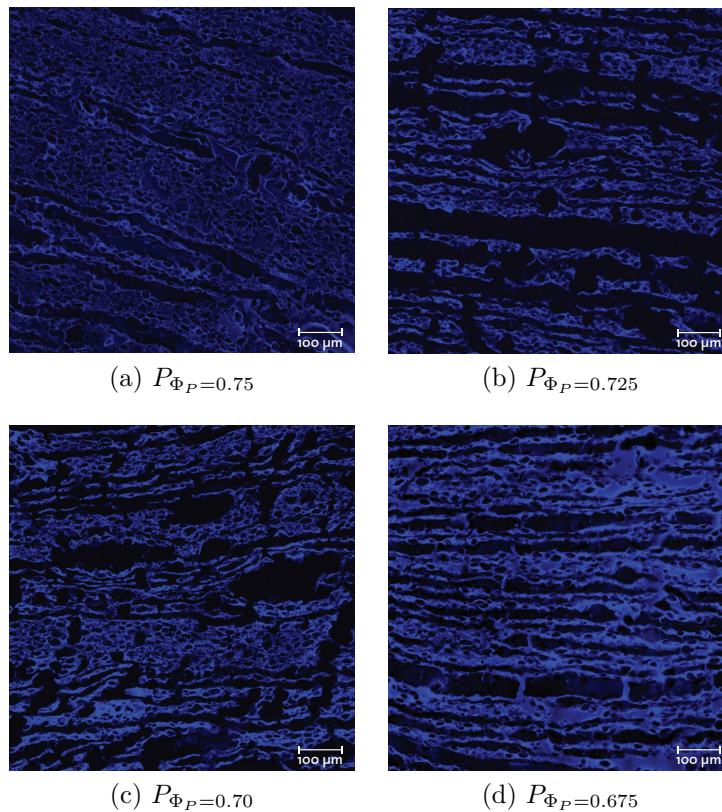


Figure 8.6.: Influence of the powder in oil disperse ratio Φ_P on the microstructure of puff pastry dough.

These observations are in line with dough micrographs obtained by CLSM as shown in figure 8.6. At a powder in oil disperse ratio $\Phi_P = 0.75$, few intact dough layers are visible. The low flowability of the powder fat lead to a partial disintegration of the dough microstructure. As a direct consequence, vapor released during baking could not be retained in the puff pastry product leading to a lower volume generated.

Powder in oil disperse ratios of $\Phi_P = 0.725, 0.70$ and 0.675 lead to clearly layered microstructured dough comparable to reference dough as shown earlier. Due to the fine, numerous layers steam could be hold back to a higher degree in the puff pastry

product during baking leading to a higher volume generated for these systems. Higher Φ_P ratios seem to preserve dough microstructure to a higher degree during puff pastry dough production, leading to higher volume obtained by baking. At $\Phi_P < 0.675$ a critical limit seems to be reached, where fat shows a too high flowability leading to loss of fat during lamination (puff pastry production).

Conclusions Decreased powder in oil disperse ratios lead to higher volumes obtained after baking puff pastry dough. An optimum seems to be reached at $\Phi_P = 0.70$ and 0.675 , leading to comparable or higher product volumes compared to reference dough after baking. Due to improved handling of dough with a lower viscosity and thereby better flow behavior, in the following application trials powder fat with $\Phi_P = 0.675$ was used.

8.4. Impact of the powder fat particle size and layering

As characterized in detail in section 6.4, the powder particle size distribution of the novel fat systems has a significant impact on the normal force generated upon confinement. The total confinement work required to confine large particles was approximately ten fold higher than the total confinement work required to confine small particles. It was also illustrated, that normal force generated during confinement increased as of a shear gap of $0.2mm$ for large particles, whereas for small particles the normal force increased starting at $0.08mm$. Forces exhibited by fat particles upon confinement through the touring process are therefore expected to be considerably higher for large particles compared to small particles.

Figure 8.7 shows the volume obtained after baking different laminated doughs using powder fat with the same water content as CPPF of $m_{w,tot} = 16.9\%$. From the rolling out layer thickness before baking of $3.2mm$ and the number of layers contained in the sample, the average single layer thickness d_L can be calculated. Puff pastry dough consisting of 144 layers has a $d_{L,144} = 3.2mm/144layers = 0.022mm = 22\mu m$. A dough consisting of 48 layers has a $d_{L,48} = 67\mu m$ and a dough consisting of 27 layer a $d_{L,27} = 119\mu m$ respectively.

Puff pastry dough consisting of 27 layers has the highest layer thickness $d_{L,27} = 119\mu m$. Application of powder fat with small (P_{small}) and large (P_{large}) particle size with mean particle sizes of $x_{50,3} = 32\mu m$ and $x_{50,3} = 100\mu m$ respectively as listed in 8.4, yields puff pastries with similar volume as shown in figure 8.7. This is also in line with the dough microstructure measurements obtained by CLSM as shown in figure 8.8. Subfigures 8.8a and 8.8d show the microstructure of puff pastry dough

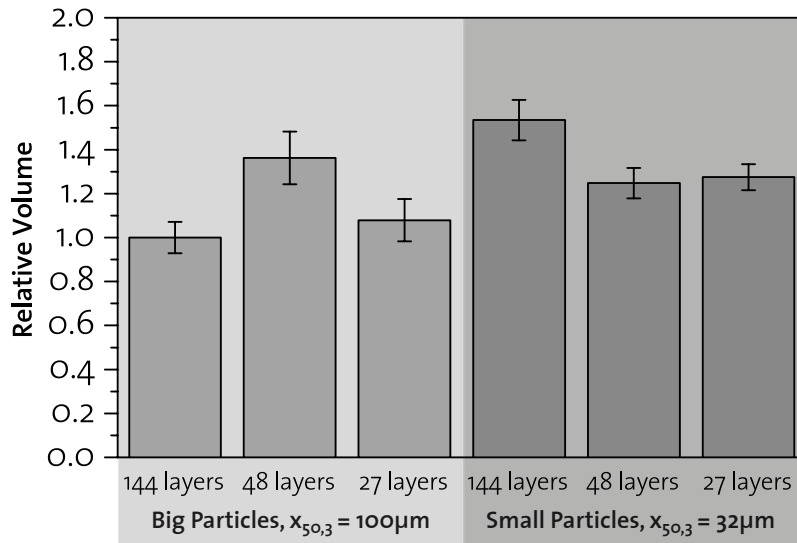


Figure 8.7.: Evaporation kinetics of emulsion based systems.

consisting of 27 layers (layer thickness $d_{L,27} = 119\mu\text{m}$). If small particles are applied (figure 8.8d), clearly separated undamaged fat (black) and dough (blue) layers can be observed. Small particles therefore do not lead to micro ruptures of dough layers. A different microstructure can be observed looking at the same system produced with large particles; a layering can partially still be observed, however, due to the presence of fat particles with a particle size distribution in the same magnitude as the layer thickness, partial rupture of dough layers can not be avoided. This can be explained by the mean particle size of the large particles ($x_{50,3} = 100\mu\text{m}$) and the only marginally larger layer size ($d_{L,27} = 119\mu\text{m}$). It is hypothesized, that layer ruptures in this system may also be amplified by the relatively broad particle size distribution of the fat particles applied, and the high probability of particles with a diameter $x_{50,3} > 100\mu\text{m}$.

Dough consisting of 48 layers with a layer thickness of $d_{L,48} = 67\mu\text{m}$ works similar for small and large particles by generating similar volumes in the baked product (see figure 8.7). The underlying microstructure is shown in figure 8.8. The layering is still predominantly intact when small particles are applied as can be seen in subfigure 8.8e. Due to the relatively broad particles size distribution, as discussed above, significantly larger particles than the mean particle size $x_{50,3} = 32\mu\text{m}$ are very likely to occur in the fat phase. Therefore partial layer ruptures can be observed in subfigure 8.8e. For large particles, a partially intact layering can be observed as shown in 8.8b. Dough systems consisting of 27 and 48 layers respectively (8.8a and 8.8b) show a very similar microstructure in the CLSM micrographs. It is suggested, that working with large particles at 27 and 48 layers leads to partially intact and partially coalesced layers and therefore a very similar, partially maintained puff pastry dough microstructure, which

8. Application of powdered fat systems in laminated dough

is also in line with the volume generated by the dough during baking as illustrated by 8.7.

A different outcome is obvious looking at dough consisting of 144 layers with a layer thickness $d_{L,144} = 22\mu\text{m}$. Small particles combined with the finest layering of 144 layers lead to the best overall baked product with the highest volume generated as shown in figure 8.7. In opposite thereto, applying large particles to the finest layering pastry consisting of 144 layers, leads to the worst overall baked product with the lowest volume obtained after baking. This behavior can be explained by the microstructure. As shown in figure 8.8f, a mostly intact layering was obtained using small particles and a layering of 144. Partial rupture of layers may be caused, as described before, by the relatively large particle size distribution of the fat particles. Large particles have a detrimental effect on a finely layered puff pastry dough consisting of 144 layers as shown in subfigure 8.8c, which is in line with the volume generated by baking this dough.

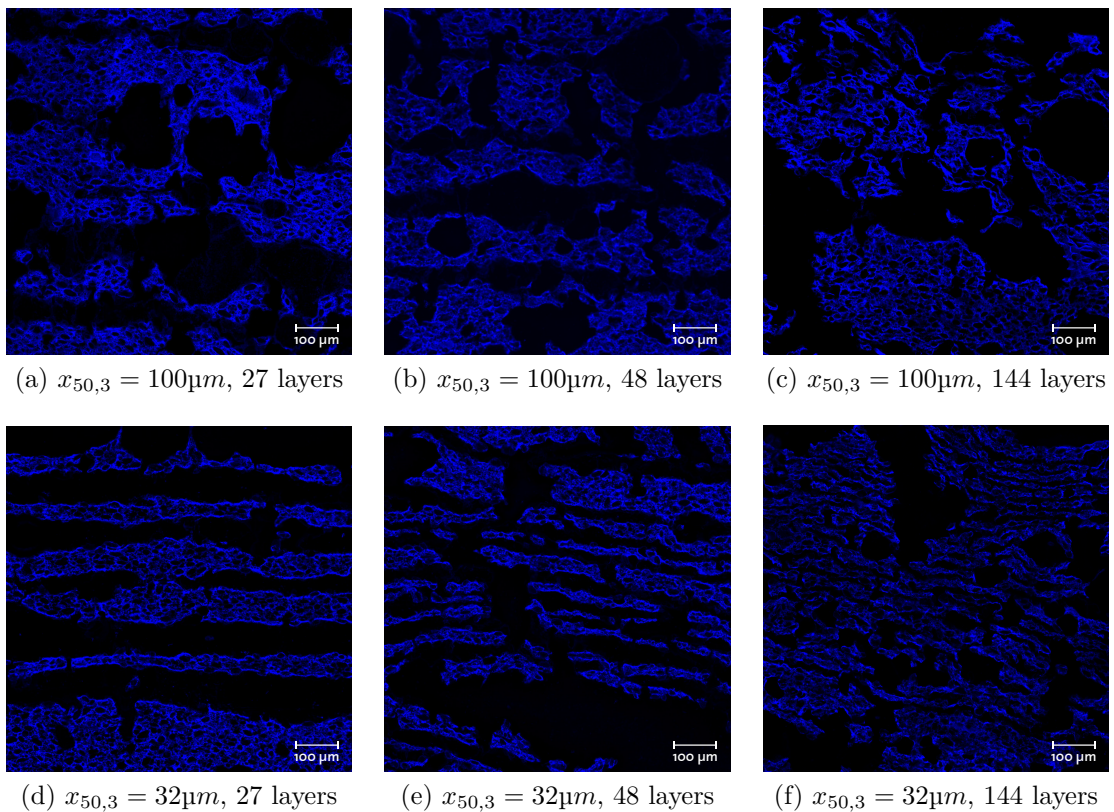


Figure 8.8.: Influence of particle size and layering on the microstructure of puff pastry dough.

Using a new, dimensionless number when working in confined layered systems might

Table 8.6.: Rupture number Ru for different composite dough systems.

	$x_{50,3} = 32\mu m$	$x_{50,3} = 100\mu m$
$d_L = 22\mu m$	0.67	0.26
$d_L = 67\mu m$	2.09	0.67
$d_L = 119\mu m$	3.72	1.19

be useful to predict the technological functionality of powder fat based on the mean particle size $x_{50,3}$ and the layer thickness d_L . The rupture number Ru is hereby defined as the quotient of layer thickness and mean particle size as shown in equation 8.1.

$$Ru = \frac{d_L}{x_{50,3}} \quad (8.1)$$

In table 8.6, rupture numbers for the dough systems used in this section (see figure 8.8) are listed. As described above, powder fat with a particle size $x_{50,3} = 32\mu m$ produced good results without excessive layer rupturing at all investigated d_L . Large ($x_{50,3} = 100\mu m$) particles, in opposite, lead to good results when used for composite dough with a layer thickness $d_L = 119\mu m$ and $d_L = 67\mu m$. At the thinnest layer thickness $d_L = 22\mu m$, large particles had a catastrophic impact on the fine layer microstructure and lead to a low volume of the baked product.

Therefore a critical rupture number in the range of $0.26 < Ru, crit._{x_{50,3}=100\mu m} < 0.67$ for particles with a size $x_{50,3} = 100\mu m$ leads to pronounced layer rupturing and a loss of the characteristics of puff pastry dough (finely layered microstructure) and the baked product (high volume and well separated multi-layered microstructure). For particles with a size $x_{50,3} = 32\mu m$ no critical rupture number could be determined, as all investigated systems lead to stable puff pastry dough and baked products.

It can be concluded, that the smallest obtainable particle size by spray chilling is desirable for application in laminated dough. Therefore, fat particles with a mean particle diameter of $x_{50,3} = 32\mu m$ were used in all further trials in this section.

8.5. The influence of an increased number of layers

As previously investigated in section 8.4, layerings of up to 144 improved the dough microstructure and the volume generated from baking the samples. In opposite to large particles, where a critical rupture number $0.26 < Ru, crit._{x_{50,3}=100\mu m} < 0.67$ was found, a $Ru, crit.$ for small particles could not be determined yet. Therefore, dough with layering of up to 192 are shown in figure 8.9. The upward trend as discussed

in 8.4 could be validated. Dough produced with powder fat P_R with a layering of 192 performed similar or slightly better than dough produced with conventional puff pastry fat (CPPF) consisting of 192 layers.

In 8.10, the microstructure of reference and powder fat dough consisting of 192 layers is compared. Fine layering can be observed for both, reference and powder dough. It can be concluded, that even at a layering of 192 with a layer thickness $d_L = 16.6\mu m$, no pronounced rupturing occurred for small particles as opposed to large particles. The critical rupture number for small particles therefore is $Ru, crit. x_{50,3} = 32\mu m < 0.52$.

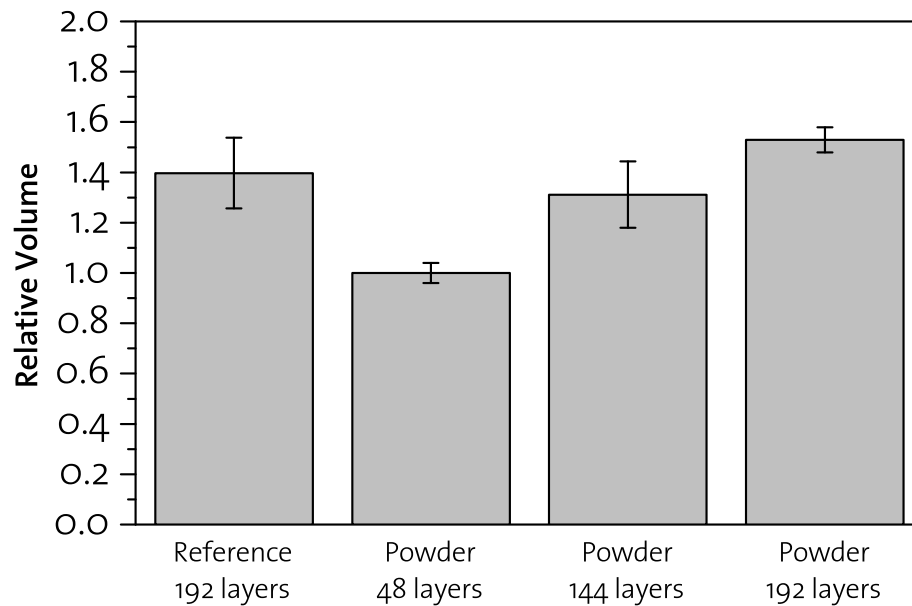


Figure 8.9.: The impact of high layer numbers on the volume obtained by baking puff pastry samples.

8.6. The impact of elevated water contents

In the last sections, optimum parameters for puff pastries produced with powder fat were determined. A dough layering of 192 for conventional as well as powder fat with a particle size $x_{50,3} = 32\mu m$ and a powder in oil disperse ratio $\Phi_P = 0.675$. The next trials were geared towards elevated powder fat water contents $m_{w,tot} \geq 25\%$. Figure 8.11 illustrates the volume generated by baking puff pastry dough produced with powder fat. Puff pastry dough produced with powder fat at the same water content ($m_{w,tot} = 16.9\%$) as conventional puff pastry fat performed similar as dough produced with very high water powder fat $m_{w,tot} = 40\%$ and 50% . Surprisingly, powder fat

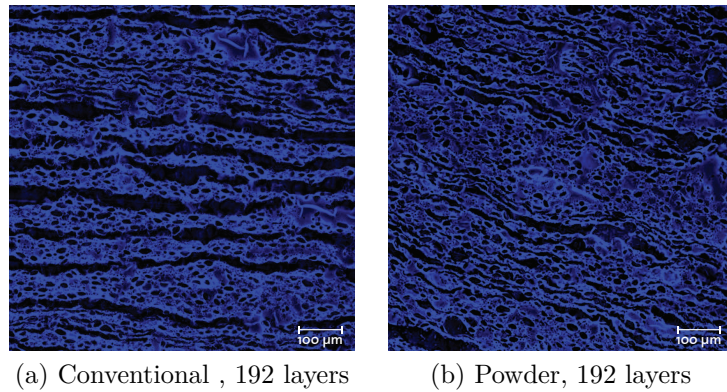


Figure 8.10.: Microstructure of puff pastry dough produced with conventional and powder fat at a layering of 192.

with a water content of $m_{w,tot} = 25\%$ performed significantly worse compared to low and very high water contents.

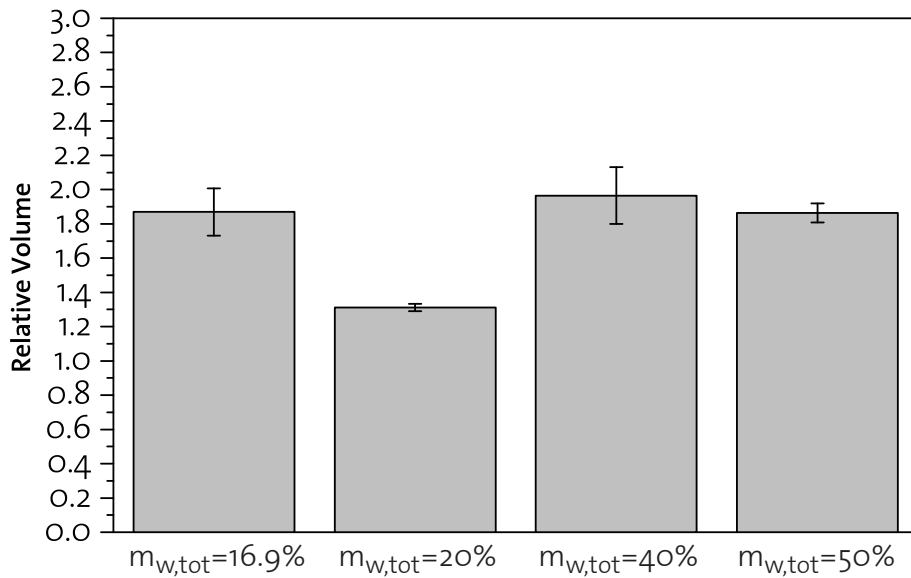


Figure 8.11.: The impact of elevated water contents on the volume obtained by baking puff pastry samples produced with NFPC.

This trend could be explained by two opposing mechanisms. As described in section 6.6, fat particles with higher water content exhibit higher normal force during confinement. Translated to the real system observed in this section, this increase in normal force could lead to more ruptures in fat and dough layers and thereby have a negative impact on the microstructure of dough. A second mechanism which has to

be considered is the raising potential for the generation of steam and thereby lifting force at elevated water contents as described in section 7.4.

The normal force generated by the fat particles upon confinement increase substantially starting at particle disperse fractions $\Phi_W \geq 0.3$ as shown in figure 6.8. As a particle disperse fraction $\Phi_W = 0.3$ translates to a water content of the composite powder fat system used in this section of $m_{w,tot} \approx 20.25\%$ (based on the particle in oil disperse ratio $\Phi_P = 0.675$), more pronounced layer rupturing can be expected for all elevated water contents $m_{w,tot} \geq 25\%$ listed in figure 8.11. Due to the increasing normal forces generated by particles with particle disperse fractions, higher water contents should lead to more pronounced rupturing and therefore a decrease in volume of the baked puff pastry, which is not in line with good baking result obtained in figure 8.11.

Therefore, the second mechanism, which is the raising potential for the generation of lifting forces at elevated water contents. As shown in figure 7.4, a substantial increase in potential lifting force generated can be expected as of a particle disperse fraction $\Phi_W \geq 0.4$ which translates to a total water content of the powder fat system used in this section of $m_{w,tot} \approx 27\%$. The lifting forces generated by elevated water contents contained in the fat system therefore start to substantially increase as of a water content of $m_{w,tot} \approx 27\%$. Therefore, increased lifting forces can be expected for all fat systems with water contents $m_{w,tot} \geq 27\%$.

It can be concluded, that a critical balance, where increasing lifting forces are starting to outweigh potential damage done by elevated normal forces generated by fat particles with increase disperse fractions, might lay between a total water content $m_{w,tot} = 25$ and 40% .

8.7. Influencing the consistency and baking volume of puff pastry dough with $m_{w,tot} \geq 40\%$

Applying powder fat containing elevated water contents $m_{w,tot} \geq 40\%$ to puff pastry dough lead to significantly decreased dough viscosities. It is suggested, that high mechanical forces exhibited by touring (as shown by^{65, 56} and others) on the particle fat containing high water contents lead to partial loss of water from the fat phase during touring and subsequent migration of water into the dough layers. As³⁰ and others have shown, additional water leads to a weakened gluten network and therefore a decreased viscosity of the puff pastry dough.

In order to decrease water lost from fat particles damaged by touring, and thereby limit thereby maintain a high dough viscosity as observed for low water puff pastry

doughs, resting time between touring and rolling out steps was adapted. The resting time applied in conventional puff pastry dough after each touring and rolling out step of 30 minutes was continuously shortened to 20, 15, 10 and 5 minutes. It is suggested, that reducing touring time leads to decreased water loss from fat particles and viscosity decrease in the composite dough, as water loss from fat particles and subsequent adsorption of water by the dough gluten network are highly time-dependent.

Figure 8.12 shows the volume obtained by baking puff dough with powder fat at a water content of $m_{w,tot} = 40\%$ and a layering of 192. A standard resting time of 30 minutes as applied during all trials so far was compared to resting times of 20, 15, 10 and 5 minutes. It can be seen, that resting the dough for 30 minutes as done in conventional puff pastry dough, leads to a significantly inferior volume compared to shortened resting times. An optimum resting time leading to a maximum volume in the final puff pastry product after baking seems to be reached at a resting time of 15 minutes. It is suggested, that water droplets can leak out from particles damaged during lamination at high resting times of 30 minutes, which could lead to a more pronounced networking between individual dough layer having a detrimental impact on layer separation during baking. Decreasing the resting time to 15 minutes lead to a higher volume generated during baking; this can be explained by a reduced time frame, during which water can leak from damaged fat particles and lead to networking of individual dough layer resulting in a better leavening of laminated dough at shorter resting times. Further reduction of the resting lead to decreased volumes obtained after baking the dough. It is suggested, that besides the anticipated reduced watering out from damaged fat particles and networking of individual dough layers at short resting times of 10 and 5 minutes, the dough might not have enough time to relax leading to detrimental impact of these tensions during baking as displayed in figure 8.12.

Therefore, high resting times of > 15 minutes (where pronounced networking between dough layers due to water leakage from damaged fat particles is expected) and low resting times of < 15 minutes (where the time frame for relaxation of the dough between individual touring steps might not be sufficient) are detrimental for a nicely separated, high volume puff pastry product after baking. For all following trials at water contents of $m_{w,tot} \geq 40\%$, a resting time of 15 minutes between touring and rolling out steps was used.

8.8. The influence of thickening agents

As previously discussed, elevated water contents can lead to substantially higher lifting forces through steam formed by baking. However, the water is released during a relatively short period (7.4). It was hypothesized, that this rapid water release

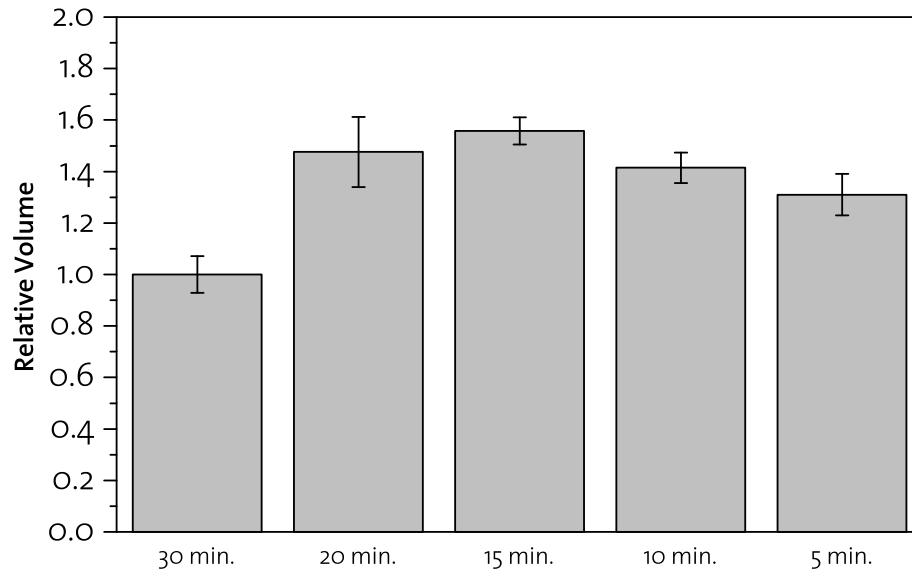


Figure 8.12.: The influence of dough resting time on the volume generated by baking.

could have a negative impact on the micro- and macrostructure of puff pastry dough as the puff pastry dough layers might not be able to hold back all the steam formed. Thus, this additional lifting forces could be lost during baking.

In figure 7.5, it was shown, that water release from emulsion based fat systems can be influenced by thermogelling agents such as methyl- and hydroxypropyl methylcellulose. A shift of the evaporation peak to higher temperatures as well as a delayed endset of evaporation was found.

A second thickener type with a potentially positive impact on puff pastry dough produced with powder fat containing elevated water contents $m_{w,tot} \geq 40\%$ is sodium alginate. Sodium alginate forms strong networks at processing (during puff pastry dough lamination) temperatures of 4 – 10°C. However, it does not show any thermo gelling behavior, leaving the viscosity at elevated temperatures unchanged. It is suggested, that forms a network in the emulsion droplets of the fat powder acting as a stabilizing agent counteracting the loss of water by shear forces applied by touring (as described in section 8.7).

Application of individual thickeners thereby could positively influence the volume generated by baking puff pastry dough by two mechanisms. Firstly, sodium alginate could enhance the mechanical stability of the powder fat during touring. Secondly, the lift generated during baking by steam formed from evaporation of water contained in fat particles, could be positively influence through tailoring (shifting to higher temperatures and releasing over a broader temperature range) the water release kinetics through thermogelling agents.

Figure 8.13 shows the impact of different thickeners applied to the disperse phase of the fat ($\Phi_W = 0.5$) particles for puff pastry dough produced with a resting time of 15 minutes at a layering of 192. Sodium alginate as well as MC A15 and HPMC E19 clearly showed a positive impact on the volume obtained after baking. Therefore, the influence of a combination of sodium alginate and thermogelling agent to enhance mechanical and thermal properties of the fat system, were further investigated.

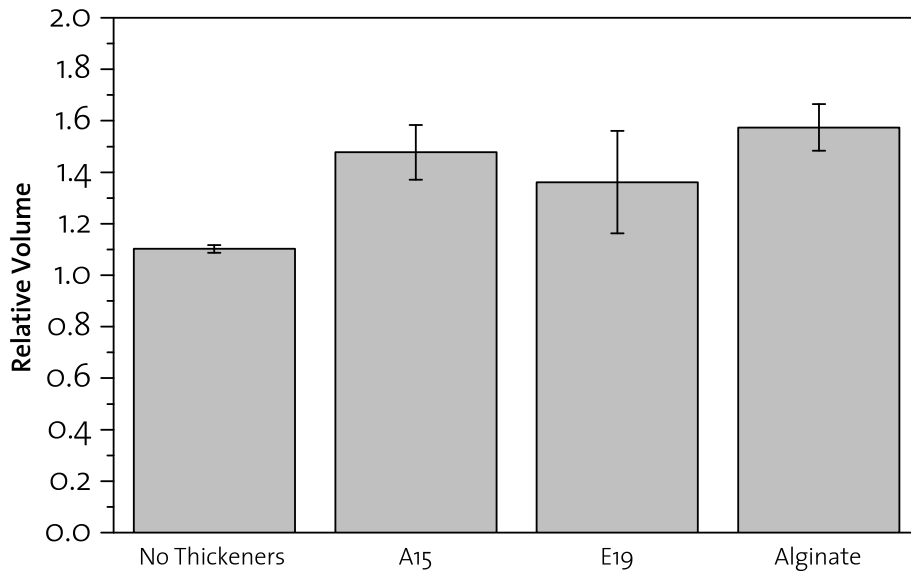


Figure 8.13.: Evaporation kinetics of emulsion based systems.

In figure 8.14, puff pastry dough produced with powder fat ($\Phi_W = 0.5$) with disperse phases supplemented by either sodium alginate, sodium alginate + MC A15 and sodium alginate + HPMC E19 produced with a resting time of 15 minutes at a layering of 192 is shown. Dough produced with sodium alginate was used as a reference and compared to the two other composite systems. A clear benefit of applying sodium alginate with either MC A15 or HPMC E19 was observed.

8.9. Conclusions

The influence of various product and process parameters was investigated in baking trials in order to validate rheometric and thermal measurements. Applying a powder in oil disperse ratio $\Phi_P = 0.675$ and particles with the smallest achievable mean particle diameter $x_{50,3} = 32$ were found to be optimal. This is in line with the theoretical measurements. The bulk viscosity of powder fat at $\Phi_P = 0.675$ was comparable to the viscosity of reference fat and small particles exhibited the smallest observed normal forces during SCR micro rheometric measurements.

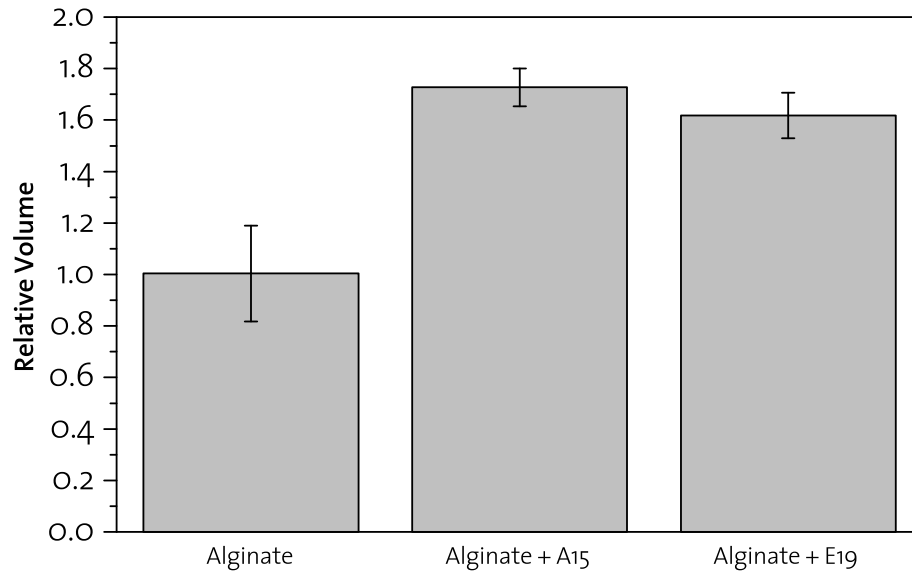


Figure 8.14.: Evaporation kinetics of emulsion based systems.

Increasing the number of layers of laminated dough lead to continuously improved baking results. Even at a maximum number of layers of 192, no pronounced layer rupturing could be observed by CLSM. Increasing the water contained in powder fat lead to improved baking results; an optimum leavening of laminated dough products during baking was found for water contents $m_{w,tot} = 40\%$. Further trials investigated the resting time between touring steps. An optimum was found at a resting time of 15 minutes.

Application of different gelling agents had a positive effect on the volume obtained by baking of puff pastry dough. Individual application of sodium alginate, MC or HPMC showed comparable effects on the volume obtained by baking of puff pastry dough with supplemented disperse phases. This might be due to two different mechanisms. Sodium alginate is expected to mechanically stabilize water contained in fat particles and therefore potentially decrease the water lost during touring by mechanically induced leakage. MC and HPMC is expected to directly positively affect the evaporation of water by modulating the water release.

Combining the two thickener types further symbiotically influenced the baking volume obtained by baking. Therefore, application of a combination of sodium alginate and MC or HPMC type thickeners for NPF containing elevated water contents ($m_{w,tot} \geq 40\%$) is suggested.

9. Concluding remarks and outlook

The aim of this thesis was the development of a process to produce a novel, powder based fat system for application in laminated dough systems and to gain a more systematic understanding into the mechanisms underlying the novel fat systems, its mechanical properties and the impact of the novel microstructure during baking of laminated dough.

During the initial phase of this thesis, a novel process allowing simultaneous spray chilling and mixing in the spray tower of two different melting fat phases resulting in a fat system consisting of solid, emulsion based fat particles suspended in liquid oil (concentrated suspension type system) was developed. Stability of emulsions was investigated on ultra-short time scales of 0 – 240 seconds, which was the relevant time frame of stability of the emulsions between emulsification and being stabilized by the crystalline networks in the fat particles upon solidification through spray chilling. Optimum emulsifier concentrations and combinations and their impact on the emulsion droplet size distribution and microstructure was determined. Thermodynamics underlying the simultaneous spray chilling process were modeled according to the three-stage solidification model developed by³¹. Thereby, an optimal injection location of the two (high melting, emulsions based and liquid oil) phases was determined based on the ambient temperature of the spray chilling tower. The particle size distribution and morphology of the powder fat system produced by simultaneous spray chilling was characterized depending on process and product parameters. In order to generate a most polymorphically stable fat crystal system, polymorphism of the powder fat system in dependence of different ambient spray tower temperatures (and relating chilling rates) were determined.

Bulk- and microrheological measurements were applied to characterize the thermo- and microrheological properties of the novel powder fat system. Using bulk rheology, factors influencing the bulk flow behavior of powder based fat systems were investigated and powder fat system matching the flowing properties of conventional lamination fats were determined. Microrheology lead to a fundamental understanding of forces acting during confinement of powder fat systems and forces exhibited by confined fat particles during lamination. Thereby, a systematic understanding of particulate fat systems and their properties on the micro scale during confinement allowed identification of optimum particulate fat properties for application in laminated dough.

Furthermore, thermal methods (DSC, TGA) were used to gain a sound understanding of the mechanics on the micro scale leading to leavening of the dough during baking. The expected leavening forces developed during baking could be quantified and the evaporation could be influenced and controlled by thermogelling agents such as MC and HPMC.

The fundamental understanding of the lamination and the baking process of laminated dough developed during this thesis was applied during the final stage of this work to puff pastry products. Theoretical results could be translated to real systems and used to fundamentally understand the products obtained when baking laminated dough using powder fat with different properties.

During this thesis a new simultaneous spray chilling process for production of novel, powder based suspension based composite fat systems was developed. Powder fat was systematically characterized and understood and the gained knowledge was successfully translated to applied systems. However, the dough phase of the composite dough was left unchanged and the fat system was optimized for one reference composite dough. Through adaptation of process and product parameters, the properties of the fat system can be tuned to match the properties of the dough phase and thus be applied to an extremely broad range of different products. The contribution and tailoring of the dough phase of composite dough should be systematically characterized in order to generate novel fat systems and to exploit the full potential of the powder fat system. Furthermore, application of microwaves or high frequency ovens might be of further interest, as it allows more direct heating of powder fat containing elevated water contents.

Finally, the application of the novel fat system should not be limited to laminated dough. Powder fat could potentially be beneficial in yeast leavened composite dough (croissants) but also conventional bakery products such as bread or fried dough batter. Additionally, tailored release of water and / or functional compounds encapsulated in powder fat could be beneficial in various applications, such as mechanical processing, where certain compounds could be released upon rupture of powder fat or applications, where unstable compounds could be encapsulated and supplemented through powder fat in shelf life stable form.

Bibliography

- [1] *Technical handbook*. Dow Chemical Company, Midland, Michigan, USA, 1997.
- [2] Acevedo, N. C. and A. G. Marangoni: *Nanostructured fat crystal systems*. Annual review of food science and technology, 6:71–96, 2015.
- [3] Atiemo-Obeng, V. A. and R. V. Calabrese: *Rotor–stator mixing devices*. Handbook of industrial mixing: Science and practice, pp. 479–505, 2004.
- [4] Bibette, J., F. L. Calderon, and P. Poulin: *Emulsions: basic principles*. Reports on Progress in Physics, 62(6):969, 1999.
- [5] Blonk, J. C. G.: *Viewing Food Microstructure*. Engineering and Food for the 21st Century, 2002.
- [6] Bodvik, R., A. Dedinaite, and P. M. Claesson: *Aggregation and network formation of aqueous methylcellulose and hydroxypropylmethylcellulose solutions*. Colloids and Surfaces A: Physicochemical and Engineering Aspects, 354(1-3):162–171, feb 2010.
- [7] Bottom, R.: *Thermogravimetric Analysis*. Principles and Applications of Thermal Analysis, pp. 87–118, 2007.
- [8] Bousquieres, J., C. Deligny, A. Riaublanc, and T. Lucas: *CLSM study of layers in laminated dough: Roll out of layers and elastic recoil*. Journal of Cereal Science, 60(1):82–91, jul 2014.
- [9] Braipson-Danthine, S. and V. Gibon: *Comparative analysis of triacylglycerol composition, melting properties and polymorphic behavior of palm oil and fractions*. European Journal of Lipid Science and Technology, 109(4):359–372, apr 2007.
- [10] Braun, O. and A. Naumovets: *Nanotribology: Microscopic mechanisms of friction*. Surface Science Reports, 60(6-7):79–158, feb 2006.
- [11] Breitschuh, B. and E. J. Windhab: *The effects of defined shear on the crystallization kinetics of fat systems and the crystal structure*. Food Rheology and Structure. Proc. 1st Int. Symp. EJ Windhab and B. Wolf, eds. Vincentz Verlag: Hanover, Germany, pp. 274–278, 1997.

- [12] Brown, E., H. Zhang, N. A. Forman, B. W. Maynor, D. E. Betts, J. M. DeSimone, and H. M. Jaeger: *Shear thickening in densely packed suspensions of spheres and rods confined to few layers*. Journal of Rheology, 54(5):1023–1046, 2010.
- [13] Bueschelberger, H.-G.: *Lecithins*. In *Emulsifiers in Food Technology*, pp. 1–39. Blackwell Publishing Ltd, 2004.
- [14] Bushuk, W. and V. K. Mehrotra: *Studies of water binding by differential thermal-analysis 1. Dough studies using boiling mode*. Cereal Chemistry, 54(2):311–320, 1977.
- [15] Campos, R., S. Narine, and A. Marangoni: *Effect of cooling rate on the structure and mechanical properties of milk fat and lard*. Food Research International, 35(10):971–981, jan 2002.
- [16] Chevallier, S., G. D. Valle, D. Lourdin, and P. Colonna: *Study of (SSD) Biscuit Baking by Dynamic Thermal Analyses (DMTA, DSC, TGA)*. Progress and Trends in Rheology V: Proceedings of the Fifth European Rheology Conference Portorož, Slovenia, September 6–11, 1998, pp. 185–186, 1998.
- [17] Clusel, M., E. I. Corwin, A. O. N. Siemens, and J. Brujic: *A 'granocentric' model for random packing of jammed emulsions*. Nature, 460(7255):611, 2009.
- [18] Collaboration, A.: *ATLAS detector and physics performance: Technical Design Report, 2*. ATLAS-TDR-15 ; CERN-LHCC-99-015, (Technical Design Report ATLAS 15), 1999.
- [19] Dalgleish, D. G.: *Food emulsions: their structures and properties*. Food emulsions, pp. 1–44, 2004.
- [20] Desbrières, J., M. Hirrien, and S. B. Ross-Murphy: *Thermogelation of methylcellulose: Rheological considerations*. Polymer, 41(7):2451–2461, 2000.
- [21] Desmond, K. W. and E. R. Weeks: *Influence of particle size distribution on random close packing of spheres*. Physical Review E, 90(2):22204, 2014.
- [22] Donev, A., I. Cisse, D. Sachs, E. A. Variano, F. H. Stillinger, R. Connelly, S. Torquato, and P. M. Chaikin: *Improving the density of jammed disordered packings using ellipsoids*. Science, 303(5660):990–993, 2004.
- [23] Dopierala, K., A. Javadi, J. Krägel, K.-H. Schano, E. Kalogianni, M. Leser, and R. Miller: *Dynamic interfacial tensions of dietary oils*. Colloids and Surfaces A: Physicochemical and Engineering Aspects, 382(1-3):261–265, jun 2011.
- [24] D'Souza, V., J. M. DeMan, and L. DeMan: *Short spacings and polymorphic forms of natural and commercial solid fats: A review*. Journal of the American Oil Chemists' Society, 67(11):835–843, 1990.

-
- [25] Dumouchel, C.: *On the experimental investigation on primary atomization of liquid streams*. Experiments in Fluids, 45(3):371–422, sep 2008.
- [26] Dürrenberger, M. B., S. Handschin, B. Conde-Petit, and F. Escher: *Visualization of food structure by confocal laser scanning microscopy (CLSM)*. LWT-Food Science and Technology, 34(1):11–17, 2001.
- [27] E., B.: *Monoglycerides in food systems: current and future uses*. Food technology (USA), 51, 1997.
- [28] Eisner, V.: *Emulsion processing with a rotating membrane (ROME)*. 2007.
- [29] Faeth, G., L.-P. Hisang, and P.-K. Wu: *Structure and Breakup Properties of Sprays*. International Journal of Multiphase Flow, 21:99–127, 1995.
- [30] Farahnaky, A. and S. Hill: *The effect of salt, water and temperatur on wheat dough rheology*. Journal of Texture Studies, 38(4):499–510, aug 2007.
- [31] Feigl, K. and T. Althaus: *Development of a Solidification Model for Food Sprays*. (August), 2009.
- [32] Fessas, D. and A. Schiraldi: *Starch Gelatinization Kinetics in Bread Dough. DSC investigations on 'simulated' baking processes*. Journal of Thermal Analysis and Calorimetry, 61(2):411, 2000.
- [33] Fessas, D. and A. Schiraldi: *Water properties in wheat flour dough I: classical thermogravimetry approach*. Food Chemistry, 72(2):237–244, feb 2001.
- [34] Fischer, K.: *Neues Verfahren zur maanalytischen Bestimmung des Wassergehaltes von Flssigkeiten und festen Krpern*. Angewandte Chemie, 48(26):394–396, jun 1935.
- [35] Fligner, K., M. Fligner, and M. Mangino: *The effects of compositional factors on the short-term physical stability of a concentrated infant formula*. Food Hydrocolloids, 4(2):95–104, jun 1990.
- [36] Garti, N.: *Crystallization and Polymorphism of Fats and Fatty Acids*. 1988.
- [37] Garti, N. and K. Sato: *Crystallization Processes in Fats and Lipid Systems*. 2001.
- [38] Ghotra, B. S., S. D. Dyal, and S. S. Narine: *Lipid shortenings: a review*. Food Research International, 35(10):1015–1048, jan 2002.
- [39] Gilbert, E. P., A. Lopez-Rubio, and M. J. Gidley: *Characterisation Techniques in Food Materials Science*. In *Food Materials Science and Engineering*, pp. 52–93. Wiley-Blackwell, 2012.

- [40] Graber, M.: *Transport phenomena in rotating membrane processed W/O/W emulsions*. 2010.
- [41] Grace, H. P.: *Dispersion phenomena in high viscosity immiscible fluid systems and application of static mixers as dispersion devices in such systems*. Chemical Engineering Communications, 14(3-6):225–277, 1982.
- [42] Griffin, W. C.: *Classification of surface-active agents by "HLB"*. J Soc Cosmetic Chemists, 1:311–326, 1949.
- [43] Haque, A. and E. R. Morris: *Thermogelation of methylcellulose. Part I: molecular structures and processes*. Carbohydrate Polymers, 22(3):161–173, 1993.
- [44] Hartel, R. W.: *Crystallization in foods*. p. 325 p., 2001.
- [45] Hasenhuettl, G. and R. Hartel: *Food Emulsifiers and their applications*. 2008.
- [46] Hiemenz, P. C. and P. C. Hiemenz: *Principles of colloid and surface chemistry*, volume 9. M. Dekker New York, 1986.
- [47] Himawan, C., V. Starov, and A. Stapley: *Thermodynamic and kinetic aspects of fat crystallization*. Advances in Colloid and Interface Science, 122(1-3):3–33, sep 2006.
- [48] Hirrien, M., C. Chevillard, J. Desbrieres, M. A. V. Axelos, and M. Rinaudo: *Thermogelation of methylcelluloses: new evidence for understanding the gelation mechanism*. Polymer, 39(25):6251–6259, 1998.
- [49] Hussain, S.: *A thermorheological investigation into the gelation and phase separation of hydroxypropyl methylcellulose aqueous systems*. Polymer, 43(21):5623–5628, oct 2002.
- [50] Jacobsberg, B. and O. C. Ho: *Studies in palm oil crystallization*. Journal of the American Oil Chemists' Society, 53(10):609–617, oct 1976.
- [51] Janssen, J. M. H. and H. E. H. Meijer: *Droplet breakup mechanisms: Stepwise equilibrium versus transient dispersion*. Journal of Rheology, 37(4):597–608, 1993.
- [52] Kimura, S.-i., H. Kusano, M. Kitagawa, and H. Kobayashi: *Layer-by-layer characterization of cellulose Langmuir–Blodgett monolayer films*. Applied surface science, 142(1):585–590, 1999.
- [53] Kloek, W., T. van Vliet, and P. Walstra: *Mechanical properties of fat dispersions prepared in a mechanical crystallizer*. Journal of Texture Studies, 36(5-6):544–568, dec 2005.
- [54] Lawler, P. J.: *Crystallization and polymorphism of fats*. Food Lipids: Chemistry, Nutrition, and . . . , pp. 275–300, 2002.

-
- [55] Lefebvre, A. H.: *Properties of Sprays*. Particle & Particle Systems Characterization, 6(1-4):176–186, jan 1989.
- [56] Levine, L. and B. A. Drew: *Rheological and Engineering Aspects of the Sheeting and Laminating of Doughs*, pp. 513–555. Springer US, Boston, MA, 1990.
- [57] Li, L., P. M. Thangamathesvaran, C. Y. Yue, K. C. Tam, X. Hu, and Y. C. Lam: *Gel network structure of methylcellulose in water*. Langmuir, 17(26):8062–8068, 2001.
- [58] Loglio, G., P. Pandolfini, R. Miller, A. Makievski, F. Ravera, M. Ferrari, and L. Liggieri: *Drop And Bubble Shape Analysis As A Tool For Dilatational Rheological Studies Of Interfacial Layers*. Novel Methods to Study Interfacial Layers, p. 439, 2001.
- [59] Lott, J. R., J. W. McAllister, S. A. Arvidson, F. S. Bates, and T. P. Lodge: *Fibrillar structure of methylcellulose hydrogels*. Biomacromolecules, 14(8):2484–2488, 2013.
- [60] Marangoni, A. G.: *Fat crystal networks*. Fat crystal networks: microstructure, 140:Online–Ressource, 2005.
- [61] Marangoni, A.: *Crystallography*. In *Fat Crystal Networks*, Food Science and Technology, pp. 1–20. CRC Press, dec 2004.
- [62] Martini, S.: *Differential scanning calorimetry : Application in fat and oil technology*. Differential scanning calorimetry : Application in fat and oil technology, pp. 164–190, 2015.
- [63] Mazzanti, G., A. G. Marangoni, and S. H. J. Idziak: *Modeling phase transitions during the crystallization of a multicomponent fat under shear*. PHYSICAL REVIEW E, 71(4, 1), apr 2005.
- [64] McGill, E. A.: *Puff pastry production*. Baker’s Dig, 49:28–38, 1975.
- [65] Mitsoulis, E., S. Sofou, E. B. Muliawan, and S. G. Hatzikiriakos: *Calendering and Rolling of Viscoplastic Materials: Theory and Experiments*. AIP Conference Proceedings, 907(1):830–834, 2007.
- [66] Miyawaki, O., T. Abe, and T. Yano: *A numerical model to describe freezing of foods when supercooling occurs*. Journal of Food Engineering, 9(2):143–151, jan 1989.
- [67] Moonen, H. and H. Bas: *Mono- and diglycerides*. 2004.
- [68] Mura, E., C. Josset, K. Loubar, J. Bellettre, and P. Massoli: *Experimental study of the water in oil emulsions features by differential scanning calorimetry analysis*. Applied energy, 97:834–840, 2012.

- [69] Narine, S. and A. Marangoni: *Relating structure of fat crystal networks to mechanical properties: a review*. Food Research International, 32(4):227–248, 1999.
- [70] Nicolas, V., P. Glouannec, J.-P. Ploteau, P. Salagnac, and V. Jury: *Experiment and multiphysic simulation of dough baking by convection, infrared radiation and direct conduction*. International Journal of Thermal Sciences, 115:65–78, 2017.
- [71] Norton, I. T., F. Spyropoulos, and P. Cox: *Practical Food Rheology: An Interpretive Approach*. Practical Food Rheology: An Interpretive Approach, 2010.
- [72] Ohnesorge, W. V.: *Die bildung von tropfen an d{ü}sen und die aufl{ö}sung fl{ü}ssiger strahlen*. ZAMM-Journal of Applied Mathematics and Mechanics/Zeitschrift f{ü}r Angewandte Mathematik und Mechanik, 16(6):355–358, 1936.
- [73] Omar, Z., E. Hishamuddin, M. M. Sahri, and S. H. Mohamad: *Palm oil crystallisation: A review*. Journal of Oil Palm Research, 27(2):97–106, 2015.
- [74] Pecharsky, V. and P. Zavaliy: *Fundamentals of Powder Diffraction and Structural Characterization of Materials*. Springer ebook collection / Chemistry and Materials Science 2005-2008. Springer US, 2005.
- [75] Piacentini, E., L. Giorno, M. M. Dragosavac, G. T. Vladisavljević, and R. G. Holdich: *Microencapsulation of oil droplets using cold water fish gelatine/gum arabic complex coacervation by membrane emulsification*. Food research international, 53(1):362–372, 2013.
- [76] Rosen, M. J.: *Emulsification by surfactants*. In *Surfactants and Interfacial Phenomena, Fourth Edition*, pp. 336–367. Wiley Online Library, 2012.
- [77] Rosen, M. J. and J. T. Kunjappu: *Surfactants and interfacial phenomena*. 2012.
- [78] Rousset, P.: *Modeling Crystallization Kinetics of Triacylglycerols*. Physical Properties of Lipids, mar 2002.
- [79] Saffman, P. G. and G. Taylor: *The penetration of a fluid into a porous medium or Hele-Shaw cell containing a more viscous liquid*. Proceedings of the Royal Society of London A: Mathematical, Physical and Engineering Sciences, 245 (1242):312–329, 1958.
- [80] Sarkar, N.: *Thermal gelation properties of methyl and hydroxypropyl methylcellulose*. Journal of Applied Polymer Science, 24(4):1073–1087, aug 1979.
- [81] Sarkar, N. and L. C. Walker: *Hydration—dehydration properties of methylcellulose and hydroxypropylmethylcellulose*. Carbohydrate polymers, 27(3):177–185, 1995.

-
- [82] Sato, K.: *Crystallization behaviour of fats and lipids — a review*. Chemical Engineering Science, 56(7):2255–2265, apr 2001.
- [83] Scheuble, N.: *Controlling Satiety by Tailored Interfaces*. 2016.
- [84] Schünemann, C.: *Lernfelder der Bäckerei - Produktion: Praxis-Theorie-Lehrwerk für die Berufsausbildung zum Bäcker, zur Bäckerin*. Gildebuchverl., 2005.
- [85] Schupper, N., Y. Rabin, and M. Rosenbluh: *Multiple Stages in the Aging of a Physical Polymer Gel*. Macromolecules, 41(11):3983–3994, 2008.
- [86] Seeck, O.: *Overview of X-Ray Scattering and Diffraction Theory and Techniques*. X-Ray Diffraction, pp. 1–28, feb 2015.
- [87] Shi, H. and C. Kleinstreuer: *Simulation and analysis of high-speed droplet spray dynamics*. Journal of fluids engineering, 129(5):621–633, 2007.
- [88] Simovic, D. S., B. Pajin, Z. Seres, and N. Filipovic: *Effect of low- trans margarine on physicochemical and sensory properties of puff pastry*. International Journal of Food Science & Technology, 44(6):1235–1244, jun 2009.
- [89] Srinivasan, S and Tanner, F X and Feigl T O and Althaus, T O and Windhab, E. W.: *Development of a freezing model for food sprays*. Proceedings of the 8th World Congress of Chemical Engineering, 2009.
- [90] Tadros, T. F.: *Emulsion Formation, Stability, and Rheology*. Emulsion Formation and Stability, pp. 1–75, 2013.
- [91] Tanner, F. X.: *Handbook of Atomization and Sprays*. pp. 327–338, 2011.
- [92] Tanner, F. X., K. Feigl, and E. J. Windhab: *Modeling and Validation of a Three-Stage Solidification Model for Sprays*. AIP Conference Proceedings, 1700(1):1700–1703, 2010.
- [93] Tcholakova, S.: *Evaluation of short-term and long-term stability of emulsions by centrifugation and NMR*. Bulg. J. Phys, 31:96, 2004.
- [94] Tcholakova, S., N. D. Denkov, D. Sidzhakova, and B. Campbell: *Effect of Thermal Treatment, Ionic Strength, and pH on the Short-Term and Long-Term Coalescence Stability of β -Lactoglobulin Emulsions*. Langmuir, 22(14):6042–6052, 2006.
- [95] Torquato, S. and F. H. Stillinger: *Jammed hard-particle packings: From Kepler to Bernal and beyond*. Reviews of modern physics, 82(3):2633, 2010.
- [96] Turnbull, D.: *Formation of Crystal Nuclei in Liquid Metals*. Journal of Applied Physics, 21(10):1022–1028, 1950.

- [97] Turnbull, D. and J. C. Fisher: *Rate of Nucleation in Condensed Systems*. The Journal of Chemical Physics, 17(1):71–73, 1949.
- [98] Ureta, M. M., D. F. Olivera, and V. O. Salvadori: *Baking of Sponge Cake: Experimental Characterization and Mathematical Modelling*. Food and Bioprocess Technology, 9(4):664–674, 2016.
- [99] Whitehurst, R. J.: *Appendix 1: Hydrophile Lipophile Balance*. In *Emulsifiers in Food Technology*, p. 237. Blackwell Publishing Ltd, 2004.
- [100] Wickramarachchi, K. S., M. J. Sissons, and S. P. Cauvain: *Puff pastry and trends in fat reduction: an update*. International Journal of Food Science & Technology, (MAY):n/a–n/a, 2015.
- [101] Wildmoser, H., J. Scheiwiller, and E. J. Windhab: *Impact of disperse microstructure on rheology and quality aspects of ice cream*. Food Science and Technology, 37(8):881–891, 2004.
- [102] Windhab, E. J.: *Fette/Oele*. Rheologie der Lebensmittel, pp. 543–561, 1993.
- [103] Yap, P. H., J. M. De Man, and L. De Man: *Polymorphism of palm oil and palm oil products*. Journal of the American Oil Chemists’ Society, 66(5):693–697, 1989.
- [104] Young, N. W. G.: *Emulsifiers and stabilisers*. Fats in Food Technology 2e, pp. 253–287, 2014.
- [105] Zhang, C., C. B. O’Donovan, E. I. Corwin, F. Cardinaux, T. G. Mason, M. E. Möbius, and F. Scheffold: *Structure of marginally jammed polydisperse packings of frictionless spheres*. Physical Review E, 91(3):32302, 2015.
- [106] Zhang, J. and A. Datta: *Mathematical modeling of bread baking process*. Journal of Food Engineering, 75(1):78–89, jul 2006.
- [107] Zusatzstoffverordnung: *Verordnung des edi über fremd- und inhaltsstoffe in lebensmitteln*. 1:1–208, 2014.

Appendix

A. First appendix: Short-term emulsion stability

Table A.1.: Average mean diameter $D_{50,3}$ for emulsions shown in 4.6.

Emulsifier	Φ	$D_{50,3}$	$\sigma_{D_{50,3}}$
0.3% PGPR		5.87	0.79
0.3% PGPR & 0.3% Dimodan U/J	0.9	-	-
0.3% PGPR & 0.3% Lecithin		-	-
0.3% PGPR		6.09	0.46
0.3% PGPR & 0.3% Dimodan U/J	0.85	4.73	0.20
0.3% PGPR & 0.3% Lecithin		-	-
0.3% PGPR		5.31	0.40
0.3% PGPR & 0.3% Dimodan U/J	0.8	5.03	0.33
0.3% PGPR & 0.3% Lecithin		4.74	0.30
0.3% PGPR		5.33	0.49
0.3% PGPR & 0.3% Dimodan U/J	0.75	3.66	0.45
0.3% PGPR & 0.3% Lecithin		5.44	0.47
0.3% PGPR		5.15	0.15
0.3% PGPR & 0.3% Dimodan U/J	0.7	4.56	0.18
0.3% PGPR & 0.3% Lecithin		5.70	0.45

A. First appendix: Short-term emulsion stability

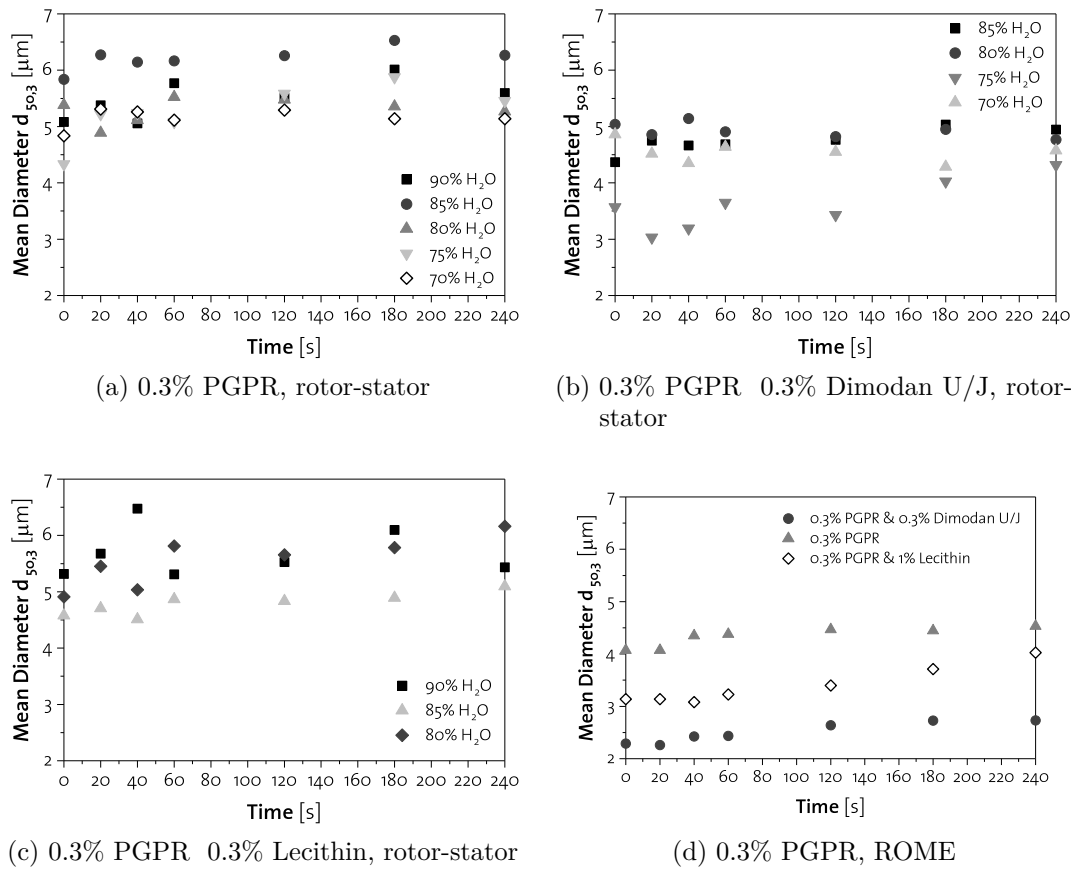


Figure A.1.: Temporal stability of selected emulsions stabilized by different emulsifiers.

B. Second appendix: Simultaneous Spray-Chilling

Table B.1.: Parameters used for simulation of simultaneous spray-chilling.

Parameter		Value
Droplet diameter	d	32 μm
Droplet density	ρ_d	894 kg/m^3
Initial droplet temperature	T_d	343 K
Freezing temperature	T_f	330 K
Ambient gas temperature	T_g	277 K
Ambient gas pressure	p_a	1 bar
Ambient gas thermal conductivity	K_g	0.024 $\text{W}/\text{m}\cdot\text{K}$
Ambient gas density	ρ_g	1.29 kg/m^3
Ambient gas viscosity	μ_g	$1.81 \cdot 10^{-5} \text{Pas}$
Droplet-gas velocity at nozzle tip	v_0	1 m/s
Maximum droplet-gas velocity	v_∞	6.88 m/s
Latent heat (onset of crystallization)	L_f	135 J/kg
Liquid droplet specific heat capacity	C_l	2.2 $\text{kJ}/\text{kg K}$
Solid droplet specific heat capacity	C_s	1.25 $\text{kJ}/\text{kg K}$
Model constant	k	0.789
Droplet drag coefficient	c_w	0.47

C. Third appendix: Rheology

Table C.1.: Integration $\int \tau_N(d_s) dd_s$ resulted in the total work needed W_{total} to confine particles at different Φ_W .

Φ_W	$W_{total,baseline}$	$W_{total,forcepeaks}$	ΔW_{total}
0.0	0.00505	0.01324	0.00818
0.1	0.00542	0.01289	0.00747
0.2	0.00579	0.01381	0.00802
0.3	0.00543	0.01326	0.00783
0.4	0.00663	0.01523	0.00861
0.5	0.00928	0.01664	0.00735
0.6	0.01417	0.02193	0.00777
0.7	0.0180	0.02424	0.00624

Curriculum Vitae

Pascal Jonas Guillet



Personal Data

date of birth 30th July 1986
place of birth Zürich
citizen of Switzerland

Education and Stages

- 05/2013 – 09/2017 PhD in Food Process Engineering, ETH Zurich
Thesis: Development of a new technology to generate low-calorie food systems with dispersed solid, fluid and gas fractions and tailored properties
May 2015: Best student paper presentation award “Production of Substructured Fat Systems by Co-Spraying of Two Different Fat(-Emulsions) with very low Emulsifier Concentrations & Controlled Fat Polymorphism” at ILASS Americas Conference, Raleigh, USA
- 09/2011 – 04/2013 MSc in Food Science, ETH Zürich, Zurich
- 01/2012 – 06/2012 Exchange Semester, University of Georgia, Athens (USA)
- 09/2007 – 08/2011 BSc in Food Science, ETH Zürich, Zurich